学位論文（要約）

Ultrasensitive analysis of halogens in mantle xenoliths: Implications for volatile transportation into the mantle

（マントル捕獲岩の超高感度ハロゲン分析：揮発性物質の沈み込み過程の解明）

平成２８年１２月博士（理学）申請

東京大学大学院理学系研究科

化学専攻

小林　真大

Abstract

Volatiles are transported from the Earth's surface into the mantle carried by subducting slabs. However, the detailed mechanism of volatile transportation into the mantle has been still enigmatic. Halogens are potentially powerful tracers of volatile transportation from the Earth's surface into the mantle because of (i) their high incompatibilities in mineral phases, (ii) the large contrast in concentrations between the surface and interior of the Earth, (iii) their distinct compositions in each reservoir. In order to gain a better understanding of volatile transportation mechanism into the mantle and its impact on the volatile compositions in the mantle, I analyzed halogens in mantle xenoliths, which are expected to provide direct evidence of volatile signatures in the mantle.

Studied mantle xenoliths are from various geological settings: volcanic fronts, rear-arc regions, and intraplate settings. Because mantle xenoliths contain only trace amounts of halogens, I applied an ultrasensitive analytical technique using neutron irradiation in a nuclear reactor and noble gas mass spectrometry. Most of the neutron irradiated samples were analyzed using an analytical system that I had improved. I also analyzed compositions of major and trace elements, and fluid inclusions.

Because of their geochemical characteristics, halogen/^{40}Ar* ratios (^{40}Ar* is excess ^{40}Ar from air) are expected to reflect the extent of subduction influence. I found that the halogen/^{40}Ar* ratios of the mantle xenoliths decrease toward the depleted mantle (DM) values in the order of volcanic fronts > rear-arc regions > intraplate settings, indicating that the extent of subduction influence decreases in this order.

Halogen and noble gas elemental ratios obtained from the volcanic front samples are similar to those of sedimentary pore fluids and serpentinites. The consistency between halogen and noble gas signatures is strong evidence that the halogen and noble gas signatures derived from sedimentary pore fluid have been preserved during the subduction processes without significant fractionation. This indicates that subducted volatiles significantly extend into the mantle beneath volcanic front. On the other hand, Cl/H_2O and ^{36}Ar/H_2O ratios of the studied samples are higher than those in sedimentary pore fluids and serpentine. Based on the halogen-noble gas-H_2O systematics, I propose

subduction mechanism of sedimentary pore fluid-derived volatiles: (i) water derived from sedimentary pore fluid is incorporated into serpentine in a closed system formed along fracture zones developed at the outer rise, where oceanic plates bend prior to entering subduction zones, (ii) dehydration-hydration process within the oceanic lithospheric mantle maintains the closed system until the final stage of serpentine dehydration, which is a stepwise process accompanied with elemental fractionation of halogens, (iii) a portion of the fluids released at the final stage of serpentine dehydration hydrates the overlying slab whereas sedimentary pore fluid-like halogen and noble gas signatures are preserved in the remainder fluids due to highly channelized fluid flow.

The samples from rear-arc regions showed a wide range of Br/Cl and I/Cl ratios. All data can be explained by mixing among three components: sedimentary pore fluid-like high I/Cl halogens, high Br/Cl halogens, and DM-like halogens. Trace element patterns and Sr-Nd isotopic ratios are different among samples with different halogen signatures, indicating that these components derived from different sources. Whereas the high I/Cl and Br/Cl halogens are slab-derived, the DM-like halogens are expected to be those inherent in the mantle. This indicates that subducted halogens are not overwhelming in rear-arc regions, whereas they are overwhelming in the mantle beneath volcanic fronts

I/Cl and Br/Cl ratios obtained from the intraplate samples show two correlation trends extending from the DM-like values. Because arc-type signatures are not observed in trace element signatures, which are coupled with those of halogens, the influence of subducted halogens is considered not to extend into the SCLM (subcontinental lithospheric mantle) beneath the studied localities. Halogen and trace element signatures suggest that one trend would result from elemental fractionation during partial melting and the other would be formed by mixing between DM-like halogens and melt-derived halogens. The geochemical signatures obtained from the intraplate samples suggest that the SCLM in the studied localities, which has been isolated from the mantle convection since about 1.6 Ga, had similar halogen signatures to those of the present-day DM before fractionation and mixing processes. This indicates that halogen signatures in the convecting mantle has been constant at least for 1.6 Gyrs.

I applied a box model to estimate the halogen subduction fluxes required to have maintained the I/Cl ratio in the mantle in a global scale over the past 1.6 Gyr. The box model calculation indicates (i) that the I/Cl ratio in the mantle is sensitive to their subduction fluxes and mechanism, (ii) halogen subduction fluxes estimated from chemical compositions of subducting materials are too high to have maintained the I/Cl ratio in the mantle over the past 1.6 Gyr, (iii) halogens are subducted into greater depth than noble gases, which have been thought to be expelled from subducting slabs at upper mantle depths due to their high volatilities, and not incorporated into the mantle convection.

Contents

1. Introduction

1.1. Structure of the Earth's interior and plate tectonics

The structure of the Earth's interior has been investigated by seismological studies (e.g., Dziewonski and Anderson, 1981; Kennett and Engdahl, 1991). The Earth has a layered structure (Figure 1.1a): the outer part (<2900 km depth) consists of silicates whereas the inner part (>2900 km depth) consists of Fe-Ni alloy. The Fe-Ni alloy layer, the core, is divided into two parts at 5100 km depth: the outer core and inner core, which are molten and solid metal, respectively. The silicate part consists of the crust and mantle. The thickness of the crust, which is the outermost shell of the Earth, differs in the continental (about 30 km) and oceanic crust (<10 km), which constitute the continent and seafloor, respectively. The mantle is divided into three layers: the upper mantle (<410 km depth), transition zone (410–660 km depth), and lower mantle (>660 km depth). Transformation of olivine, which is the most abundant mineral in the upper mantle, and its polymorphs is thought to be responsible for the layer boundaries in the mantle (Figure 1.1b).

The surface of the Earth is covered by tectonic plates, which is composed of the crust and uppermost part of the mantle (about 100 km thick). At mid-ocean ridges, which are divergent boundaries of tectonic plates, the oceanic crust is continuously produced and diverges. At a subduction zone, which is a convergent boundary of tectonic plates (Figure 1.2), the tectonic plate collides with and subducts (sinks) beneath another plate due to the relative density difference. The subducting plates are called as slabs or subducting slabs.

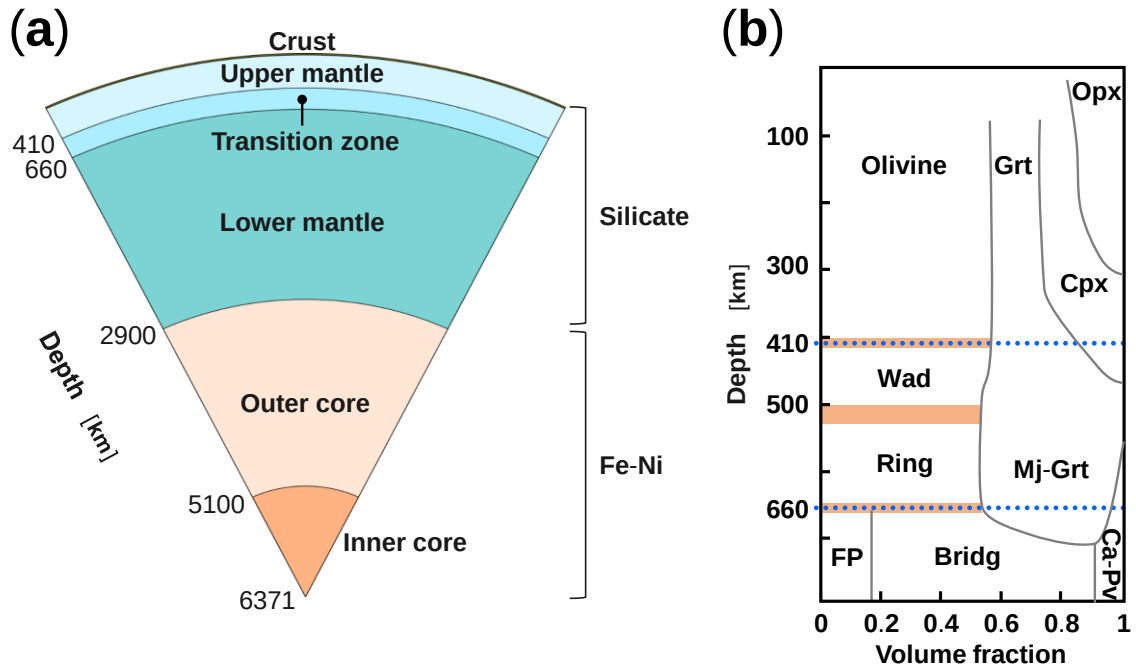

Figure 1.1. (a) The structure of the Earth's interior. (b) The mineral constitution of the mantle (modified after Stachel et al., 2005). Dashed blue lines represent the upper mantle-transition zone and transition zone-lower mantle boundaries. Light brown bars represent the depth where olivine and its polymorphs transform to high-pressure phases. Bridg: bridgmanite, Ca-Pv: CaSi-perovslite; Cpx: clinopyroxene; FP: ferropericlase; Grt: garnet; Mj-Grt: majorite-garnet; Opx: orthopyroxene; Ring: ringwoodite; Wad: wadsleyite.

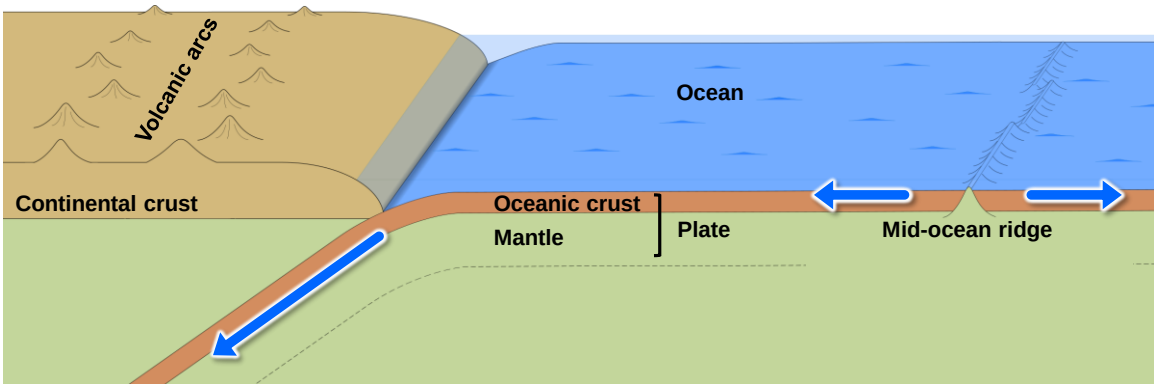

Figure 1.2. A cartoon of a subduction zone. Allows represent motion of the oceanic plate. Figure is not to scale.

1.2. Volatile in geoscience

Volatiles are species which pass readily into a gaseous phase, such as hydrogen (H_2O), carbon (CO_2), nitrogen, halogen, and noble gas. Elemental and isotopic compositions of volatiles have provided key information on the formation and evolution history of the Earth, such as ingredients of the Earth, formation and evolution of the atmosphere and ocean, differentiation of the mantle, and so on (e.g., Caracausi et al., 2016; Coltice et al., 2009; Marty, 2012; Marty et al., 2016; Mukhopadhyay, 2012; Porcelli and Ballentine, 2002).

Because of their high volatilities and incompatibilities in mineral phases, volatiles concentrate on the Earth's surface while their concentrations are low in the mantle (Marty, 2012). Volatiles are continuously expelled from the mantle via volcanic activities at mid-ocean ridges, hot spots, and arcs. They are also transported from the Earth's surface into the mantle via subduction processes. Volatile subduction is important in geoscience because even relatively small amounts of volatiles may result in major changes to the chemical and physical properties of rocks, transporting elements and influencing mineral phase assemblages, melting temperatures, viscosities, seismic wave velocities, and electrical conductivities (Bolfan-Casanova, 2005; Kawamoto et al., 2015). The subduction flux of a free fluid phase trapped within pore spaces in subducting slabs is insignificant at least after forearc depth because the pore spaces collapse at shallow subduction levels due to compaction (Hyndmann and Peacock, 2003; Jarrard, 2003). Hydrous minerals in subducting slabs are thought to be one of the main carriers of subducted volatiles. Volcanism and seismicity associated with subduction zones are linked to the dehydration of those minerals and water released from the subducting slabs (Mitsui and Hirahara, 2009; Tatsumi, 1989). However, the detail mechanism of volatile transportation into the mantle, for example the detail of hydrous mineral and volatile release mass balance in subduction zones, is still enigmatic.

It is also uncertain how large amounts of the volatiles are transported into the deep mantle, i.e., not returned to the surface of the Earth, and how large impact on volatile compositions in the mantle the subduction has. Based on water concentration in the altered oceanic crust and water outgas flux from arc volcanoes, Ito et al. (1983) argued

that only about 10% of subducted water is returned to the surface through arc volcanisms and that significant amount of water is transported into the mantle. On the other hand, Wallace (2005) estimated that subducted water and Cl are efficiently returned to the surface. Noble gases are often assumed to be returned to the surface and little transferred into the deep mantle (Staudacher and Allègre, 1988). However, despite this "subduction barrier", the ratios of non-radiogenic isotopes of heavy noble gases (Ar, Kr, and Xe) in the convecting mantle are similar to those of seawater, suggesting that seawater-derived noble gases are subducted into the mantle (Holland and Ballentine, 2006). Evidence of halogen transportation into the deep mantle has also been found in plume related volcanic rocks (Halldórsson et al., 2016; John et al., 2010).

Although some studies considered only volatiles transported by the oceanic crust and sediment, the importance of the hydrated oceanic lithospheric mantle as carriers of volatiles has been pronounced (e.g., Kerrick, 2002; Kendrick et al., 2011; Rüpke et al., 2004). Hacker (2008) and van Keken et al. (2011) estimated that the amount of water within the hydrated mantle transported into the deep mantle is comparable with or larger than that within the oceanic crust and sediment. Serpentine, which contains 13 wt.% of H_2O, is a major hydrous phase in the oceanic lithospheric mantle. This mineral transforms into high-pressure hydrous phases in cold subducting slabs, suggesting that significant amounts of water can be transported into the deep mantle by the hydrated mantle (e.g., Ohtani, 2005, 2015).

Serpentine is mainly formed through hydration of the oceanic lithospheric mantle at transform faults and fracture zones at the outer rise, where oceanic plates bend prior to entering subduction zones (Kerrick, 2002). The direct evidence of the presence of serpentine has been obtained from only relatively shallow depth, because the Earth's surface is covered by the crust, which has more than a few km thickness. However, seismological studies have suggested the presence of this hydrous mineral in the oceanic lithospheric mantle (Ranero et al., 2003; Peacock, 2001). The depth of serpentinization is estimated to vary from few km to about 20 km (Faccenda, 2014).

1.3. Halogen and noble gas as tracers of volatile transportation into the mantle

Halogens and noble gases are expected to be powerful traces of volatile transportation into the mantle because of their high affinities to gas- and fluid-phases relative to mineral (Bernini et al., 2013; Bureau et al., 2000, 2016; Fabbrizio et al., 2013; Ozima and Podosek, 2002; Porcelli et al., 2002), and the large contrast in concentrations between the surface and interior of the Earth (Figure 1.3). Furthermore, because of the distinct elemental and/or isotopic compositions of halogens and noble gases (Figures 1.3–1.7), these groups of elements can be used to reveal the origin and subduction path of subducted volatiles.

1.3.1. Halogen

Halogens (F, Cl, Br, I, At) comprise of Group 17 of the periodic table. All isotopes of At are radioactive and only trace amount of At exists in nature within the decay chains of the ^{235}U and ^{238}U decay series. Therefore, I do not discuss this element in this study. Halogens mainly exist as halides in salts, solutions, and gases. Because of its large size, the mantle is the largest reservoir of halogens (Figure 1.3). However, due to their high volatilities and incompatibilities in mineral phases, their concentrations are up to several orders of magnitude higher in the Earth's surface (Figure 1.3a).

Although the geochemical behaviors of halogens are different in each element, the behavior of F is distinct from other halogens. Whereas heavy halogens (Cl, Br, and I) are strongly partitioned into aqueous fluids, F is more partitioned into silicate melts than aqueous fluids (Bureau et al., 2000). Fluorine, which has the smallest ionic radius (Table 1.1), can substitute for OH in minerals (e.g., Pyle and Mather, 2009). As a consequence, F exists in the crust with relatively high concentration rather than the ocean (Figure 1.3). Although Cl can also substitute for OH in minerals due to its relatively small ionic radius, Cl and Br concentrate in the ocean. On the other hand, iodine concentrate in marine sediment. This is because of its biophilic nature. Some planktons incorporate iodine, resulting in high iodine concentration in organic materials in sediment (Elderfield and Truesdale, 1980; Kennedy and Elderfield, 1987ab; Muramatsu and Wedepohl, 1998). The I/Cl ratios in sedimentary pore fluids, which originate as seawater trapped in the pores of

marine sediment, are up to several thousand times higher than that in seawater (Figure 1.4). This has been attributed to iodine supply from organic materials through their decomposition (Fehn et al., 2006; Martin et al., 1993; Muramatsu et al., 2007). Because Br also has small biophilic nature, the Br/Cl ratios in sedimentary pore fluids are slightly higher than that in seawater (Figure 1.4).

Halogen compositions in the mantle have been investigated from MORB (mid-ocean ridge basalt) glass, melt inclusions hosted by olivine in MORB, and diamonds (Burgess et al., 2002; Jambon et al., 1995; Kendrick et al., 2012a; Saal et al., 2002). The F and Cl concentrations in the depleted mantle have been estimated to be 11–16 ppm and 0.5–6 ppm, respectively (Burgess et al., 2002; Jambon et al., 1995; Saal et al., 2002; Salters and Stracke, 2004). The Br/Cl ratio of the MORB glass are constant in a wide range of concentration (Jambon et al., 1995; Kendrick et al., 2012a). Although small variation was observed, most of MORB glass also showed similar I/Cl ratio (Kendrick et al., 2012a). Using the revised values of their halogen standard materials (Kendrick 2012; Kendrick et al., 2013a), the Br/Cl and I/Cl ratios reported by Kendrick et al. (2012a) are revised to $(1.19 \pm 0.04) \times 10^{-3}$ and $(20 \pm 8) \times 10^{-6}$ mol/mol, respectively. From these ratios and Cl concentration, Br and I concentrations in the depleted mantle are obtained to be 1.3–16 ppb and 0.035–0.42 ppb, respectively.

Elemental ratios of heavy halogens in terrestrial reservoirs are shown in Figure 1.4. The I/Cl ratios vary up to several orders of magnitude among different reservoirs, whereas the variation in the Br/Cl ratio is relatively small. As mentioned above, marine sedimentary pore fluids showed high I/Cl ratio caused by decomposition of organic materials (Fehn et al., 2006; Kastner et al., 1990; Martin et al., 1993; Muramatsu et al., 2007). Serpentinites showed similar I/Cl ratio and Br/Cl ratios to sedimentary pore fluids, suggesting that they incorporate sedimentary pore fluid-derived halogens (John et al., 2011; Kendrick et al., 2011, 2013b). On the other hand, the altered oceanic crust (seafloor basalts and meta gabbros) showed low Br/Cl and I/Cl ratios (Chavrit et al., 2016; Kendrick et al., 2015a). This relative enrichment in Cl has been attributed to amphibole, which show low I/Cl and Br/Cl ratios (Chavrit et al., 2016; Kendrick et al., 2015a).

Table 1.1. Halogen characteristics.

	F	Cl	Br	I
Ionic radius [pm]	133	181	196	220
Concentration in CI chondrite [ppm]	60	690	3.4	0.8
Concentration in the primitive mantle [ppm]	25	30	0.075	0.007
Concentration in the depleted mantle [ppm]	11–16	0.5–6	0.0013–0.016	0.000035–0.00042
$D_{\text{fluid/albitic melts}}$	0.18	8.1	17.5	104

Data sources: Ionic radius (Shannon and Prewitt, 1969), concentrations in CI chondrite (Dreibus et al., 1979; Lodders and Fegley, 1998), concentrations in the primitive mantle (Palme and O'Neil, 2014), concentrations in the depleted mantle (see text), and partition coefficients between aqueous fluids and albitic melts (Bureau et al., 2000).

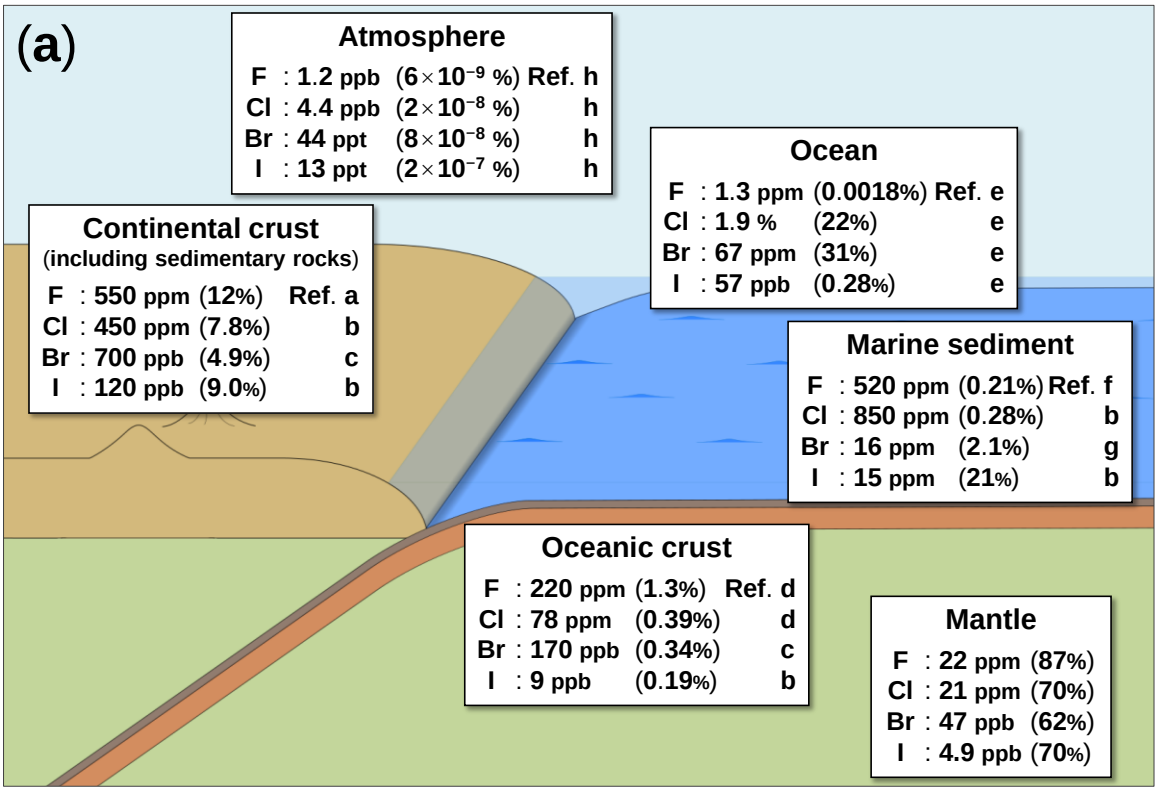

Figure 1.3.

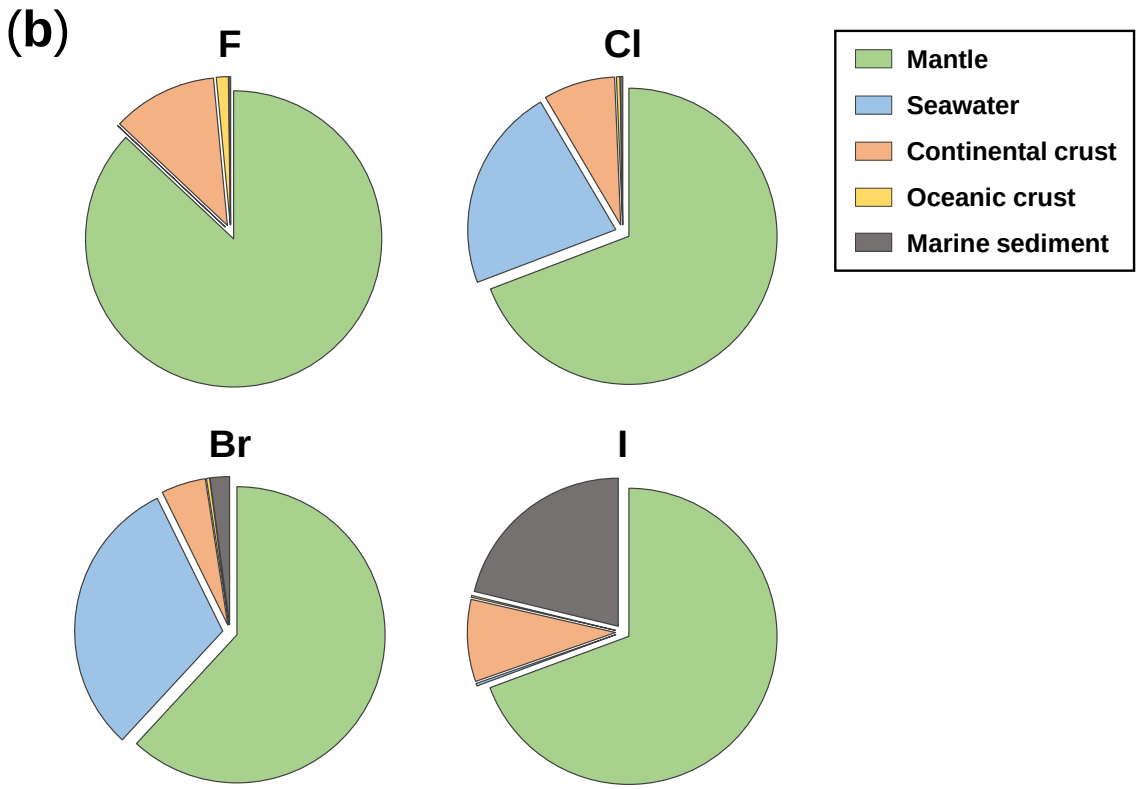

Figure 1.3. (a) Concentrations and relative abundances of halogens in terrestrial reservoirs. Relative abundances are given in brackets. (b) Relative abundances of halogens in terrestrial reservoirs shown in pie charts. Atmosphere is not shown because of its small halogen budget. The abundances in the mantle are obtained by subtracting abundances in surface reservoirs from terrestrial halogen budgets estimated from concentrations in the primitive mantle (1.0×10^{20}, 1.2×10^{20}, 3.0×10^{17}, and 2.8×10^{16} kg for F, C, Br, and I, respectively; see Table 1.1 for the concentrations in the primitive mantle). The concentrations in the mantle are the average in the whole mantle. Data sources: a (Rudnick and Gao, 2014), b (Muramatsu and Wedepohl, 1998), c (Schilling et al., 1978), d (Straub and Layne, 2003), e (Bruland and Lohan, 2014), f (Carpenter, 1969), g (Muramatsu et al., 2007), and h (Pyle and Mather, 2009).

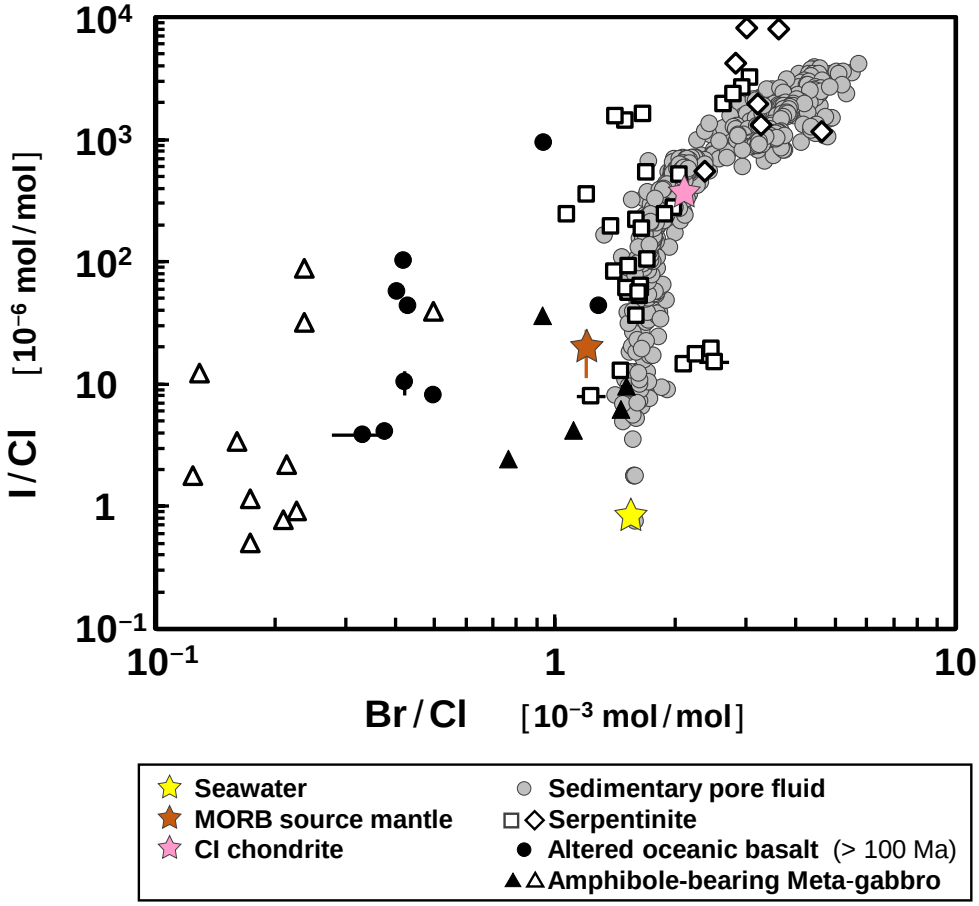

Figure 1.4. Elemental ratios of heavy halogens in terrestrial reservoirs. Errors are 1σ. Data sources: serpentinites from the oceanic lithosphere (open squares) and forearc (open diamonds) (John et al., 2011; Kendrick et al., 2011, 2013b), sedimentary pore fluid (Fehn et al., 2006; Kastner et al., 1990; Martin et al., 1993; Muramatsu et al., 2007), seawater (Bruland and Lohan, 2014), MORB source mantle (Kendrick et al., 2012a), altered oceanic crust older than 100 Ma (Chavrit et al., 2016), amphiboles in meta-gabbros (open triangles) and relict minerals and quartz-epidote veins in meta-gabbros (black triangles) (Kendrick et al., 2015a), and CI chondrite (Dreibus et al., 1979; Lodders and Fegley, 1998) The halogen ratios reported by Kendrick et al. (2011, 2012a, 2013b) were recalculated using revised values for scapolite monitors (Kendrick et al., 2013a).

1.3.2. Noble gas

Noble gases (He, Ne, Ar, Kr, Xe, and Rn) comprise of Group 18 of the periodic table. All isotopes of Rn are radioactive and only trace amount of ^{222}Rn exists in nature within the decay chain of the ^{238}U decay series. Therefore, I do not discuss Rn in this study. Because of their strong atmophile characteristics, most of noble gases in the Earth are thought to reside in the atmosphere (Marty, 2012; Ozima and Podosek, 2002; Porcelli et al., 2002). The abundance and isotopic compositions in the atmosphere are given in Tables 1.2 and 1.3, respectively. Because He is light, this element escapes from the atmosphere to space and is depleted in the atmosphere compared to other noble gases (Ozima and Podosek, 2002; Porcelli et al., 2002).

Noble gases are chemically inert and therefore the variations in their isotopic and elemental ratios are mainly controlled by addition of radiogenic, nucleogenic, cosmogenic, and fissiogenic isotopes, and physical processes such as mixing and diffusion (Ozima and Podosek, 2002; Porcelli et al., 2002; Sumino et al., 2005). As shown in Figure 1.5, ^{3}He/^{4}He and ^{40}Ar/^{36}Ar ratios in the terrestrial reservoirs show distinct ratios. All reservoirs show higher ^{40}Ar/^{36}Ar and lower ^{3}He/^{4}He ratios than primordial values in the solar system (^{40}Ar/^{36}Ar = 1.63 × 10^{-3} and ^{3}He/^{4}He ~ 100 Ra; Wieler, 2002a) This is because of accumulation of ^{40}Ar and ^{4}He produced from radioactive decay of ^{40}K and decay series of U and Th, respectively. The relatively low ^{40}Ar/^{36}Ar ratio in the atmosphere results from degassing from the mantle at early history of the Earth (e.g., Ozima, 1975). The crust and mantle have low ^{36}Ar/K ratio and accumulate ^{40}Ar produced form ^{40}K, resulting in higher ^{40}Ar/^{36}Ar ratio than atmospheric value. ^{3}He/^{4}He ratio of MORB is globally uniform (8 ± 1 Ra, Moreira and Kurz, 2013; 1 Ra = atmospheric ratio of 1.399 × 10^{-6}, Table 1.3). The plume source mantle has higher, i.e., more primordial, ^{3}He/^{4}He ratio (Figure 1.5), suggesting the presence of the less degassed deep mantle reservoir. This is consistent with lower ^{40}Ar/^{36}Ar ratio in the plume source mantle than the MORB source mantle. OIB (oceanic island basalt) has lower ratio of ^{129}Xe, which is produced from the radioactive decay of extinct ^{129}I ($T_{1/2}$ = 15.7 Ma; Porcelli et al., 2002), to non-radiogenic ^{130}Xe than MORB (e.g., Graham, 2002). Based on the differences in elemental and ^{20}Ne/^{22}Ne ratios between OIB and MORB, Mukhopadhyay (2012) showed

that the lower $^{129}Xe/^{130}Xe$ in OIB is attributed to lower I/Xe ratio in the OIB source mantle rather than mixing between MORB-like Xe and subducted atmospheric Xe. The lower I/Xe ratio in OIB also requires the less degassed deep mantle reservoir. Mukhopadhyay (2012) argued that the OIB and MORB sources had differentiated before ^{129}I became extinct (about 4.45 Gyrs ago), and that mixing between these sources have been limited.

Because of the large contrast in noble gas abundances between the atmosphere and solid materials, atmospheric noble gases are often incorporated into and/or adsorbed on samples before and/or during experiments. As shown in Figure 1.6, Ne isotopic ratios in the volatile-rich MORB glass, popping rock, clearly showed a linear relationship extending from atmospheric ratios toward high $^{20}Ne/^{22}Ne$ and $^{21}Ne/^{22}Ne$ ratio (Kunz, 1999; Moreira et al., 1998; Sarda et al., 1988). However, it is still debated whether the endmember of this trend extends toward solar $^{20}Ne/^{22}Ne$ ratio (13.6; Honda et al., 1991) or not (12.5; Trieloff et al., 2000). Holland and Ballentine (2006) studied noble gases in CO_2 gas from a CO_2 natural gas field and reported that the Ne isotopic compositions are explained by mixing between mantle-derived Ne and pre-mixed atmospheric and crustal Ne (Figure 1.6). They argued that the intersection of the (air-crust)-mantle mixing line and air-MORB mixing line represents Ne isotopic ratio in the convecting mantle. In 3D plots of $i/^{22}Ne$, $^{20}Ne/^{22}Ne$, and $^{21}Ne/^{22}Ne$ ratios, where i is any noble gas isotope, the data of the CO_2 gas fall on single plane, indicating the data are explained by three endmembers, the air, crust, and mantle (Holland and Ballentine, 2006). From the mantle Ne compositions (Figure 1.6), they obtained $i/^{22}Ne$ ratio in the convecting mantle. Because the obtained ratio of non-radiogenic isotopes of heavy noble gases (Ar, Kr, and Xe) in the convecting mantle are similar to that of seawater and distinct from other materials (Figure 1.7), it has been argued that subducted noble gases account for almost 100% of non-radiogenic Ar and Kr and 80% of Xe in the convecting mantle, and that subduction of seawater-derived noble gases controls the heavy noble gas compositions in the mantle (Ballentine and Holland, 2008; Holland and Ballentine, 2006).

Table 1.2. Noble gas abundances in the atmosphere.

	Volume ratio	Total inventory [ccSTP]
Dry air	≡ 1	3.961×10^{24}
He	5.24×10^{-6}	2.076×10^{19}
Ne	1.818×10^{-5}	7.202×10^{19}
Ar	9.34×10^{-3}	3.700×10^{22}
Kr	1.14×10^{-6}	4.516×10^{18}
Xe	8.7×10^{-8}	3.446×10^{17}

Data source: Porcelli et al., 2002.

Table 1.3. Noble gas isotope compositions of the atmosphere.

$^{3}He/^{4}He$	$^{20}Ne/^{22}Ne$	$^{21}Ne/^{22}Ne$	$^{38}Ar/^{36}Ar$	$^{40}Ar/^{36}Ar$
1.399×10^{-6}	9.80	0.0290	0.1880	296
$^{78}Kr/^{84}Kr$	$^{80}Kr/^{84}Kr$	$^{82}Kr/^{84}Kr$	$^{83}Kr/^{84}Kr$	$^{86}Kr/^{84}Kr$
0.006087	0.039599	0.20217	0.20136	0.30524
$^{124}Xe/^{132}Xe$	$^{126}Xe/^{132}Xe$	$^{128}Xe/^{132}Xe$	$^{129}Xe/^{132}Xe$	
0.003537	0.003299	0.07136	0.9832	
$^{130}Xe/^{132}Xe$	$^{131}Xe/^{132}Xe$	$^{134}Xe/^{132}Xe$	$^{136}Xe/^{132}Xe$	
0.1513	0.7891	0.3879	0.3293	

Data sources: Nier (1950), Porcelli et al. (2002), and Ozima and Podosek (2002).

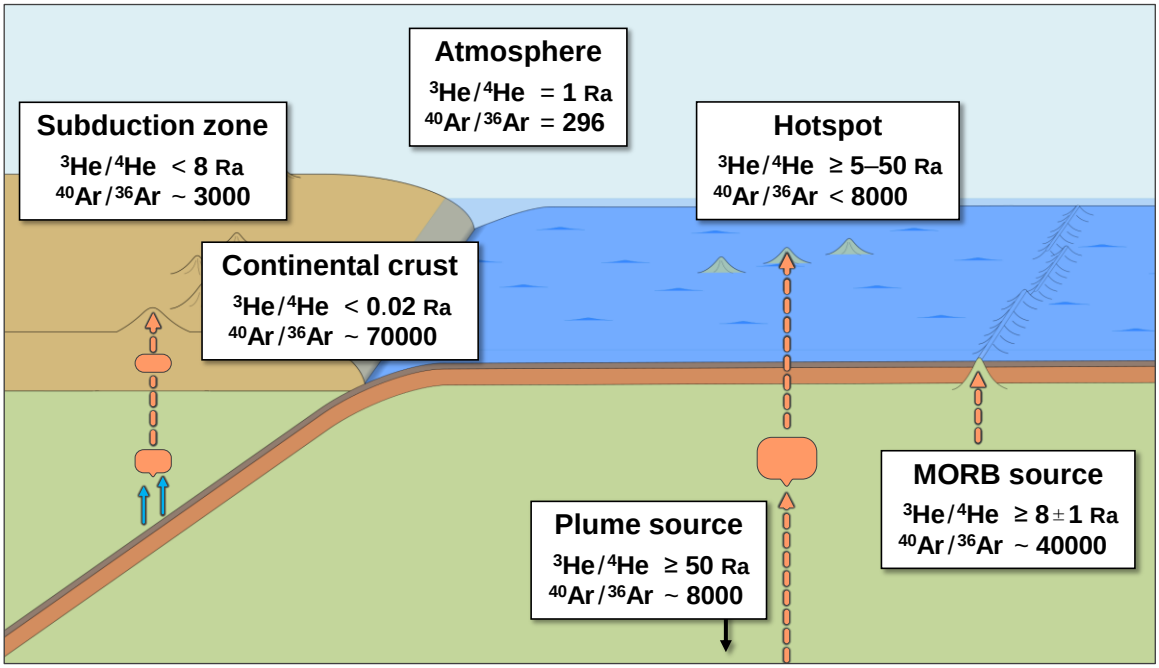

Figure 1.5. $^{3}He/^{4}He$ and $^{40}Ar/^{36}Ar$ ratio in the Earth (modified after Sumino et al., 2005). 1 Ra = atmospheric ratio of 1.399×10^{-6} (Table 1.3)

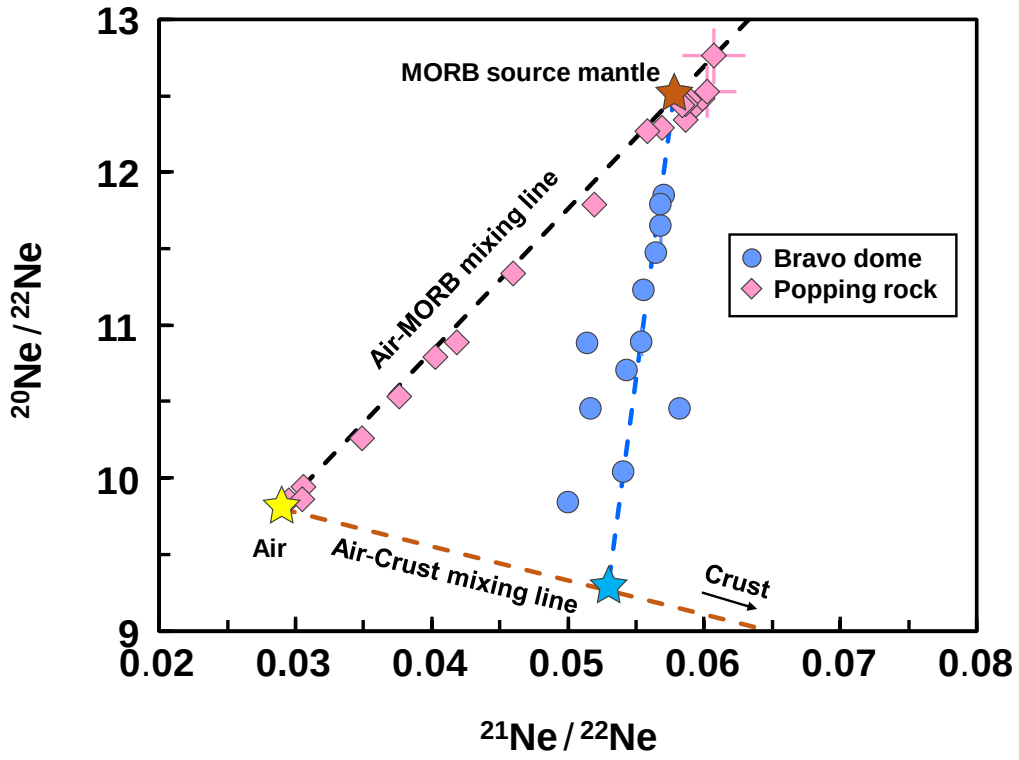

Figure 1.6. $^{20}Ne/^{22}Ne$ versus $^{21}Ne/^{22}Ne$ for popping rock and CO_2 gas from Bravo dome (modified after Sumino, 2012). The Baravo dome data are explained by mixing between mantle-derived Ne and pre-mixed atmospheric and crustal Ne (blue star) (Holland and Ballentine, 2006). Errors are 1σ. Data sources: air-MORB mixing line (Sarda et al., 1988), popping rock (Kunz, 1999; Moreira et al., 1998), and CO_2 gas from Bravo dome (Holland and Ballentine, 2006).

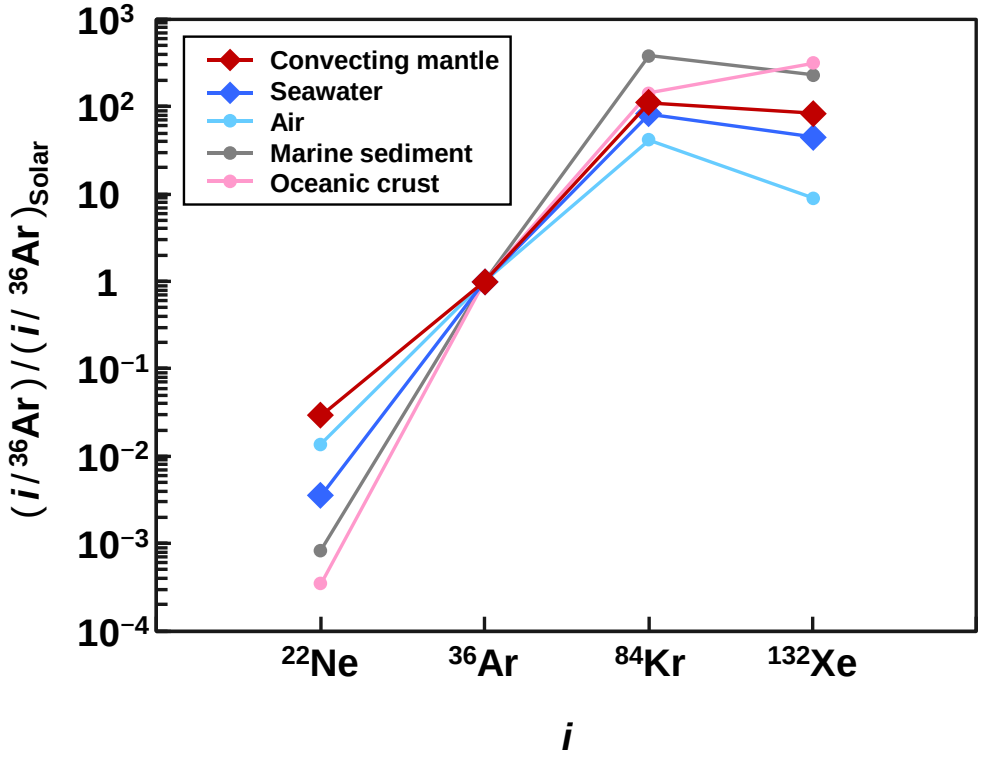

Figure 1.7. Elemental ratios of noble gases normalized to the solar abundance. Data sources: the convecting mantle (Holland and Ballentine, 2006), solar noble gas (Wieler, 2002a), air and seawater (Ozima and Podosek, 2002), marine sediment (Matsuda and Nagao, 1986), and oceanic crust (Staudacher and Allègre, 1988).

1.3.3. Subduction of halogen and noble gas

Isotopic compositions of noble gases in mantle-derived materials from subduction zones show a large contribution from atmospheric noble gases except for He (e.g., Hilton, 2002). Hereafter, I refer to atmospheric noble gases as those that show isotopic ratios similar to the air (elemental ratios can vary from those in the air). The atmospheric noble gases have been attributed to slab-derived atmospheric noble gases. However, because noble gases, especially Ar, are relatively abundant in the atmosphere and seawater, atmospheric noble gases can contaminate to samples during and/or after eruption, which cannot be distinguished from noble gases present in the samples before contamination (Ballentine and Barfod, 2000).

Matsumoto et al. (2001) studied noble gases in mantle peridotites from the Horoman peridotite massif, which represents a portion of the mantle wedge infiltrated with slab-derived fluids, and reported atmospheric $^{40}Ar/^{36}Ar$ ratios (≤450). They found that the amount of ^{36}Ar in the samples correlate with those of ^{3}He. Because ^{3}He can be regarded as mantle-derived due to its relative abundance in the Earth, they argued that the clear correlation is evidence that the low $^{40}Ar/^{36}Ar$ ratios result from slab-derived atmospheric Ar present in the mantle wedge and not from shallow-level contamination. Hopp and Ionov (2011) studied fluid inclusions in mantle xenoliths from the Avacha volcano, which is located in the subduction zone in the Kamchatka peninsula and also reported low $^{40}Ar/^{36}Ar$ ratios (<400). They analyzed the noble gases using stepwise crushing extraction, which enables extraction of noble gases mainly from fluid inclusions (Kurz, 1986) and obtained identical ratios during the stepwise crushing. Because the extent of the contribution from contamination can vary, Hopp and Ionov (2011) argued that the low $^{40}Ar/^{36}Ar$ ratios are not consequences of air contamination.

Compared to noble gases, halogens may be less affected by contamination, at least that from air. However, it is difficult to estimate primary halogen compositions in the mantle from volcanic rocks and fumaroles. Their elemental ratios can be fractionated during various processes such as differentiation of magma and degassing, in which halogen behaviors are not well constrained (e.g., Aiuppa et al., 2009). As shown in Figure 1.8, halogen elemental ratios in volcanic rocks and fumaroles from subduction zones show a wide range of values and it is difficult to interpret.

Because Cl and F are retained in magma until relatively shallow depth (e.g., Spilliaert et al., 2006) and able to be analyzed in μm scale using EPMA (electron probe microanalysis) or SIMS (secondary ion mass spectrometry), Cl and F in melt inclusions hosted by olivine in volcanic rocks have been intensively studied in recent 15 years (e.g., Benjamin et al., 2007; Le Voyer et al., 2010; Portnyagin et al., 2007; Sadofsky et al., 2008; Straub and Layne, 2003; Wade et al., 2006; Wysoczanski et al., 2006). The melt inclusions show higher Cl and F concentrations than MORB and F/Cl ratio between MORB and seawater values (Figure 1.9). Their halogen concentrations correlate with other fluid-mobile elements such as U. Based on these signatures, they have concluded that F and Cl

are supplied from the subducting slabs to the mantle wedge. Addition of halogens from subducting slabs to the mantel wedge has been also supported by the studies using $^{37}Cl/^{35}Cl$ and $^{129}I/^{127}I$ ratios (e.g., Barnes et al., 2008, 2009; Snyder and Fehn, 2002; Snyder et al., 2002; Tomaru et al., 2007).

High-pressure and high-temperature experiments have shown the importance of the presence of halogens in slab-derived fluids (Kawamoto et al., 2014; Keppler, 1996; Tsay et al., 2014). They have shown that the presence of Cl enhances solibilities of LILE (large-ion lithophile elements) and REE (rare earth elements) into aqueous fluids. The Cl-bearing slab-derived fluids are invoked to explain the relative enrichment of LILE in arc magmas compared to MORB source magmas (Kawamoto et al., 2014; Keppler, 1996). Moreover, the presence of Cl can fractionate the ratio of light/heavy REE as observed in arc magmas (Tsay et al., 2014).

As mentioned above, evidence of subducted halogens and its importance have been pronounced. However relatively few studies have reported Br and iodine in mantle-derived materials. This is mainly because few analytical techniques can determine ppb or sub-ppb level of Br and iodine in mantle-derived samples. Recently, an ultrasensitive halogen analytical technique using neutron irradiation and noble gas mass spectrometry (section 2.3) has been applied to geochemical samples.

Sumino et al. (2010) studied noble gases and heavy halogens (Cl, Br, and I) in mantle peridotites from the Higashi-akaishi peridotite body in the Sanbagawa metamorphic belt, Japan, which is a sliver of the former mantle wedge. The peridotites trapped slab-derived H_2O-rich fluids just above the subducting slab at ≥100km depth (Mizukami et al., 2004). The noble gas signatures are similar to those of seawater: however, the halogen signatures are similar to those of marine sedimentary pore fluids (Figure 1.10). John et al. (2011) and Kendrick et al. (2011, 2013b) have shown that serpentinites in the oceanic lithosphere contain substantial amounts of sedimentary pore fluid-like halogens and noble gases, suggesting that serpentinites may transport sedimentary pore fluid-derived volatiles into the mantle. However, halogens can be fractionated even among heavy halogens during subduction processes (John et al., 2011; Kendrick et al., 2011; Pagé et al., 2016; Svensen et al., 2001). Dehydration of serpentine is a stepwise process, and John et al. (2011) and

Kendrick et al. (2011) have shown that Br and iodine are preferentially released during first dehydration step, resulting in low I/Cl and Br/Cl ratios in the residue phase. Broadely et al. (2016) studied heavy halogens and noble gases in mantle xenoliths from the Western Antarctica, where subduction ceased around 105 Ma. The mantle xenoliths are enriched in halogens, especially iodine, with I/Cl ratio significantly higher than the sedimentary pore fluid trend (Figure 1.10). Although the SCLM (subcontinental lithospheric mantle) is likely to have been metasomatized by asthenospheric fluids and/or melts during rifting and continental thinning, the extremely high I/Cl ratios and iodine concentrations up to 1 ppm suggest that fluids with high I/Cl ratio were supplied from the subducting slab (Broadley et al., 2016). They attributed high I/Cl ratio to continuous release of fractionated I-rich halogens from the subducting slab into the SCLM, and argued that the SCLM is a potentially important reservoir for subducted volatiles.

As such, halogens and noble gases have been provided various information on volatile transportation into the mantle. However, the detailed mechanism of volatile transportation including that of halogens and noble gases has been still uncertain. This is, at least partly, because there are few data set of heavy halogens in mantle-derived materials, which are important tracers of volatile transportation. Mantle xenoliths, which are unmolten fragments from the upper mantle, can provide direct evidence of volatile signatures in the mantle, because they are rapidly brought to the Earth's surface by ascending magma. Especially, fluid inclusions in mantle xenoliths from subduction zones provide an opportunity to directly characterize the nature of slab-derived fluids. However, there is no report of heavy halogens in mantle xenoliths from modern subduction zones. Moreover, comprehensive studies of halogens in mantle xenoliths from various geological settings are required in order to discuss their transportation into the mantle.

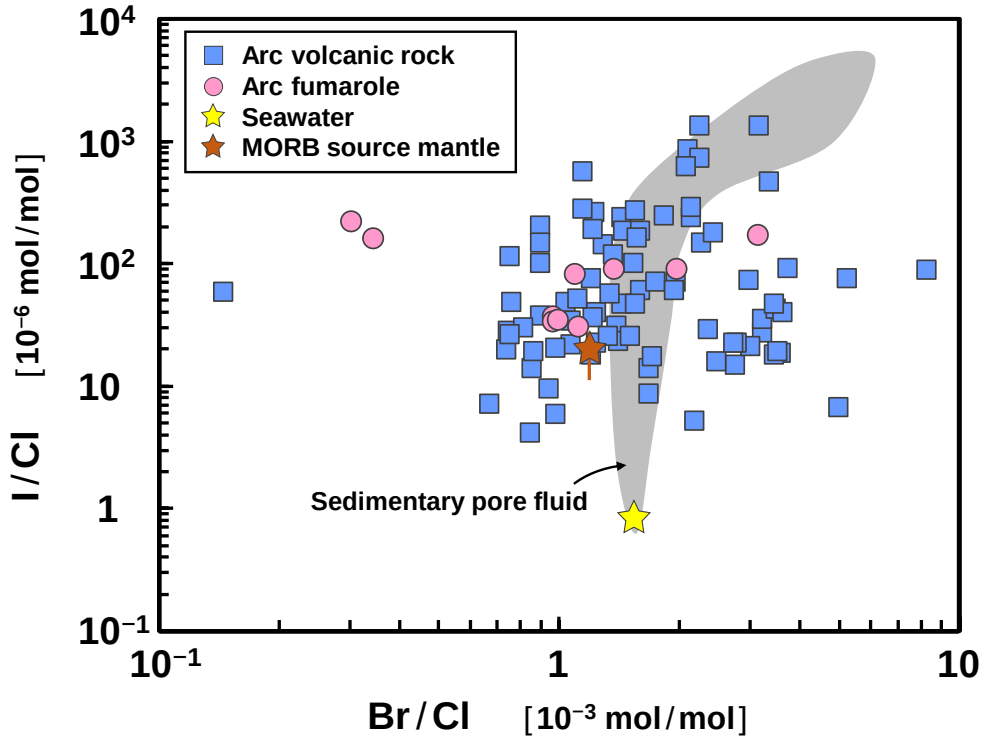

Figure 1.8. I/Cl versus Br/Cl for volcanic rocks and fumaroles from subduction zones. Area shown by grey is the ranges of sedimentary pore fluids. Data sources: volcanic rocks (Ebihara et al., 1997; Michel and Villemant, 2003; Shinonaga et al., 1994; Villemant et al., 2008; Yoshida et al., 1971), fumaroles (Snyder et al., 2002; Taran et al., 1995; Tomaru et al., 2007), and the MORB source mantle, seawater, and sedimentary pore fluids (see Figure 1.4).

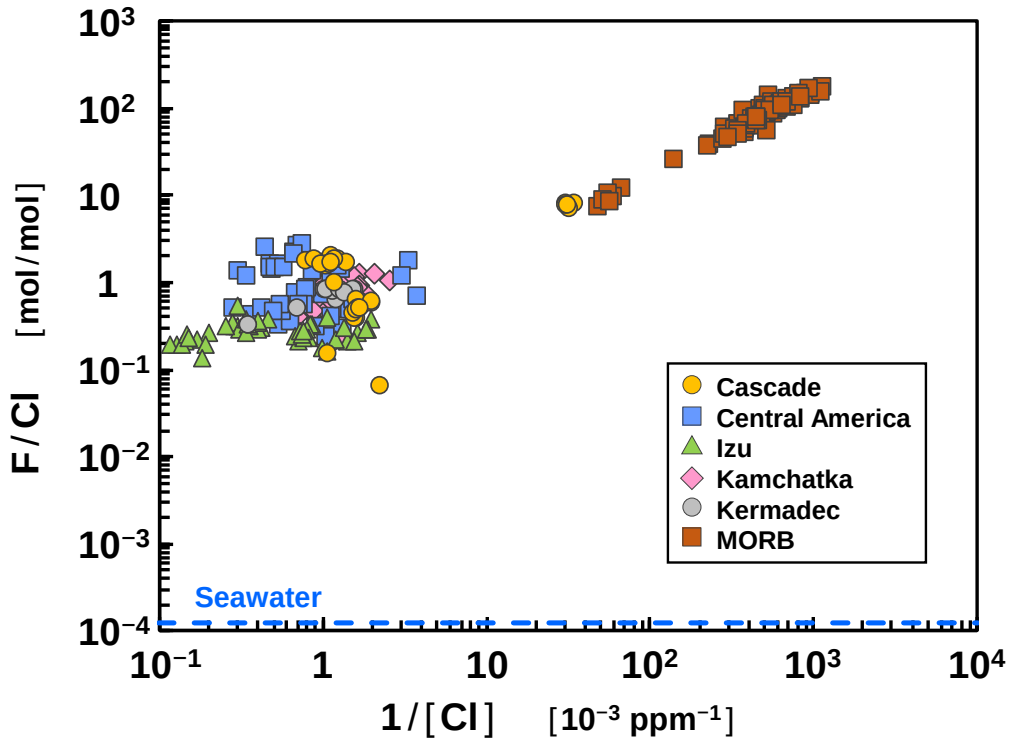

Figure 1.9. F/Cl versus Cl concentration for melt inclusions hosted by olivine in arc volcanic rocks and MORB (glasses and melt inclusions hosted by olivine). A blue dashed line represents F/Cl ratio in seawater. Data sources: Cascade (Levoyer et al., 2010), Central America (Benjamin et al., 2007; Sadofsky et al., 2008; Wade et al., 2006), Izu (Straub and Layne, 2003); Kamchatka (Portynyagin et al., 2007), Kermadec (Wyscozanski et al., 2006), MORB (Saal et al., 2002), and seawater (Bruland and Lohan, 2014).

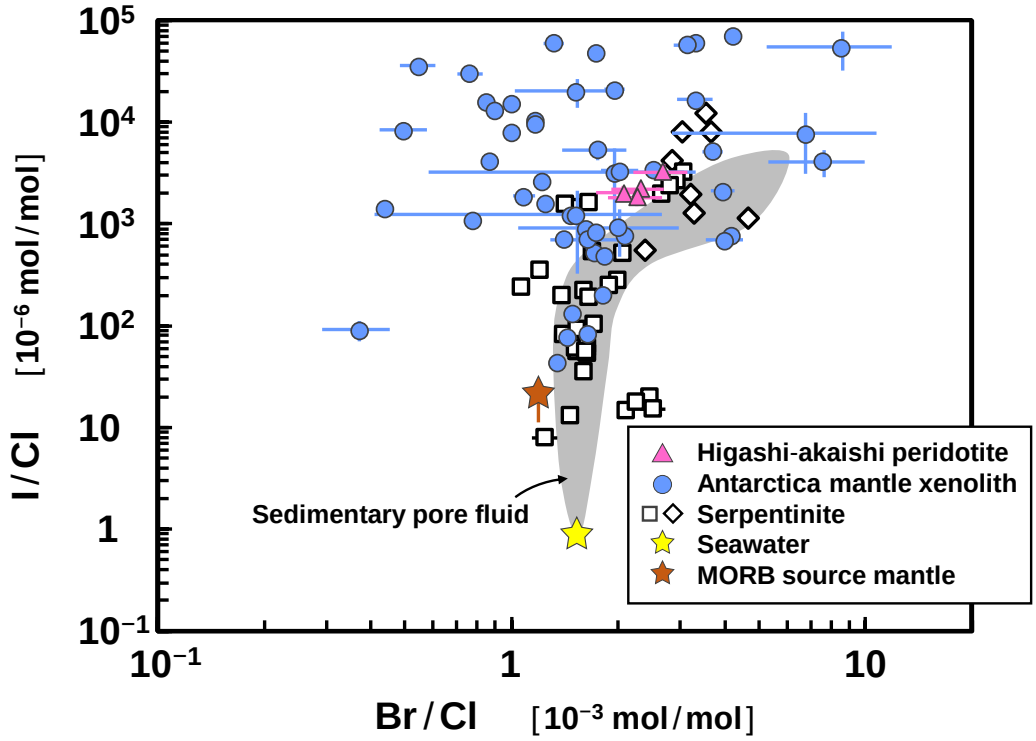

Figure 1.10. I/Cl versus Br/Cl for mantle peridotites and mantle xenoliths. Area shown by grey are the ranges of sedimentary pore fluids. Errors are 1σ. Data sources: Higashi-akaishi peridotites (Sumino et al., 2010), Antarctica mantle xenoliths (Broadley et al., 2016), serpentinites from the oceanic lithosphere (open squares) and forearc (open diamonds) (John et al., 2011; Kendrick et al., 2011, 2013b), sedimentary pore fluid (Fehn et al., 2006; Kastner et al., 1990; Martin et al., 1993; Muramatsu et al., 2007), seawater (Bruland and Lohan, 2014), and MORB source mantle (Kendrick et al., 2012a).

1.4. Aim of this study

The aim of this study is to gain a better understanding of volatile transportation mechanism into the mantle and its impact on the volatile compositions in the mantle. In order to reveal these topics, I analyzed halogens in mantle xenoliths from various geological settings: (i) volcanic front, which is a trenchward boundary of volcanic chains (arcs), (ii) rear-arc region, which is the behind the volcanic front, (iii) intraplate setting, of which volcanic activity occurs within the tectonic plate. Because of low halogen abundances in mantle-derived materials, I applied an ultrasensitive analytical technique using neutron irradiation and noble gas mass spectrometry (section 2.3), for which I had improved an analytical system. In order to interpret halogen signatures better, I also analyzed compositions of noble gases, major and trace elements, and fluid inclusions.

2. Samples and experimental methods

2.1. Samples

Mantle xenolith samples used in this study are listed in Table 2.1 and location maps of the samples are shown in Figure 2.1. The studied samples from volcanic fronts, rear-arc regions, and intraplate settings, and their geological backgrounds are described more in detail in sections 4.1, 5.1, and 6.1, respectively.

Table 2.1. Studied samples.

Locality	Sample ID
Volcanic front	
Avacha	#10, #122, #187, #203, #629, Avx1 C-part, Avx1 F-part, Avx33, F1
Pinatubo	P2, P2 (olivine), P3, P3 (olivine)
Rear-arc region	
Ichinomegata	ICH-MP-1, ICH-MP-1 (olivine), ICH-MP-5, ICH-MP-5 (olivine), ICH-MP-7, ICH-MP-7 (olivine), ICH-MP-9, ICH-MP-9 (olivine), ICH-MP-11, Ichinome olivine, Ich-30
Jeju	CHJ9901 (olivine), CHJ9901 (opx), CHJ9902 (olivine), CHJ9902 (opx), CHJ9903 (olivine), CHJ9903 (opx)
Oki	KRB-102, OKD-101, OKR010701
Sikhote-Alin	Ilc-1, Sv-1
Takashima	TKD1120, TKS-01, TKS602
Intraplate setting	
Eifel	MF-07-1, MF-07-2, MF-07-4, DW-07-3, DW-07-4
Hawaii	Hualalai
Kilbourne Hole	KLB-Lhz-11, KLB-Lhz-12, KLB-Lhz-14, KLB-Lhz-16
San Carlos	SC-1, SC-2

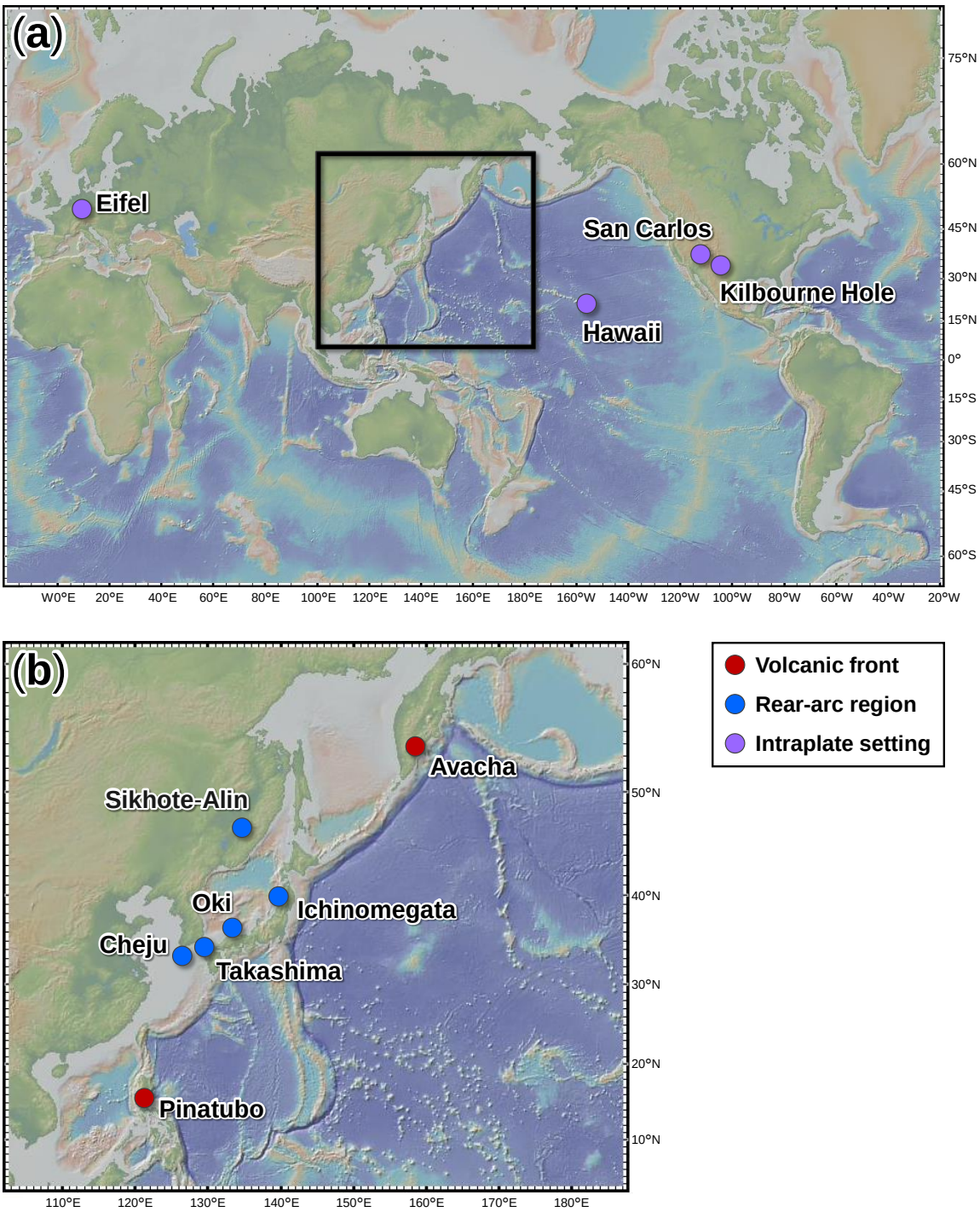

Figure 2.1. Location map of the samples. (a) Map of the samples from intraplate settings. (b) Map of the samples from subduction zones (volcanic fronts and rear-arc regions). The area shown in (b) corresponds to the area in a box in (a). The map was made with the GeoMap App (http://www.geomapapp.org), using the Global Multi-Resolution Topography (GMRT) basemap (Ryan et al., 2009).

2.2. Noble gas analysis

The mantle xenolith samples were coarsely crushed into 0.5–2 mm except for Avx-1 F-part, which is an aggregate of fine grain minerals. From some mantle xenolith samples, olivine separates were obtained by hand-picking under a binocular microscope. All samples were leached with 1N nitric acid. The leached samples with a mass of 0.4–1 g were analyzed using a noble gas mass spectrometric system, MS-IV, at the University of Tokyo (Figure 2.2). Samples were initially baked-out under vacuum at 200 °C overnight. Noble gases were extracted from samples by stepwise crushing method using a Ni-slug moved vertically by an external magnetic field generated by solenoid coils (Figure 2.3). The crushing method enables extraction of noble gases mainly from fluid inclusions (Kurz, 1986). However, during stepwise crushing, the proportion of noble gases released from fluid inclusions relative to those released from other potential sites (e.g., lattice, grain boundaries, or sample surface) may change as the intensity of crushing increases (Hilton et al., 1993; Scarsi, 2000; Sumino et al., 2006; Yokochi et al., 2005). Each sample was heated at 800 °C for 30 min before crushing, in order to reduce adsorbed atmospheric noble gases on the sample surface.

Extracted noble gases were purified by Ti-Zr getters (Ti1 and 2) and getter pumps (GP). Helium and Ne were separated from Ar, Kr, and Xe using a charcoal trap (CH1) cooled in liquid nitrogen. Helium was separated from Ne using a porous sintered stainless steel filter element under cryogenic temperature control (Cryo-trap). Each separated fraction was admitted into a modified VG5400 mass spectrometer, which has a Faraday-cup, Daly multiplier collector, and ion-counting system (Sumino et al., 2001). During He and Ne analyses, a charcoal trap (CH2) or sintered stainless trap was cooled in liquid nitrogen, in order to reduce interferences ($^{12}C^{3+}$, $^{40}Ar^{2+}$, and $^{12}C^{16}O_2^{2+}$ on $^{4}He^{+}$, $^{20}Ne^{+}$, and $^{22}Ne^{+}$, respectively). The interferences of $^{40}Ar^{2+}$ and $^{12}C^{16}O_2^{2+}$ were corrected following the method by Osawa (2004). The sensitivities and correction factors for mass discrimination were calibrated by known amount of air. The correction factor including mass discrimination and sensitivity ratio for He, which was analyzed by a double collector system, was calibrated by an artificial mixture of ^{3}He and ^{4}He, Helium Standard of Japan (Matsuda et al., 2002). Only abundances were measured for Kr and Xe because it was

expected that anomalies in their isotope ratios could not be precisely determined from the 0.4–1 g of samples and that their ratios in the samples from subduction zones would be atmospheric due to subduction influence.

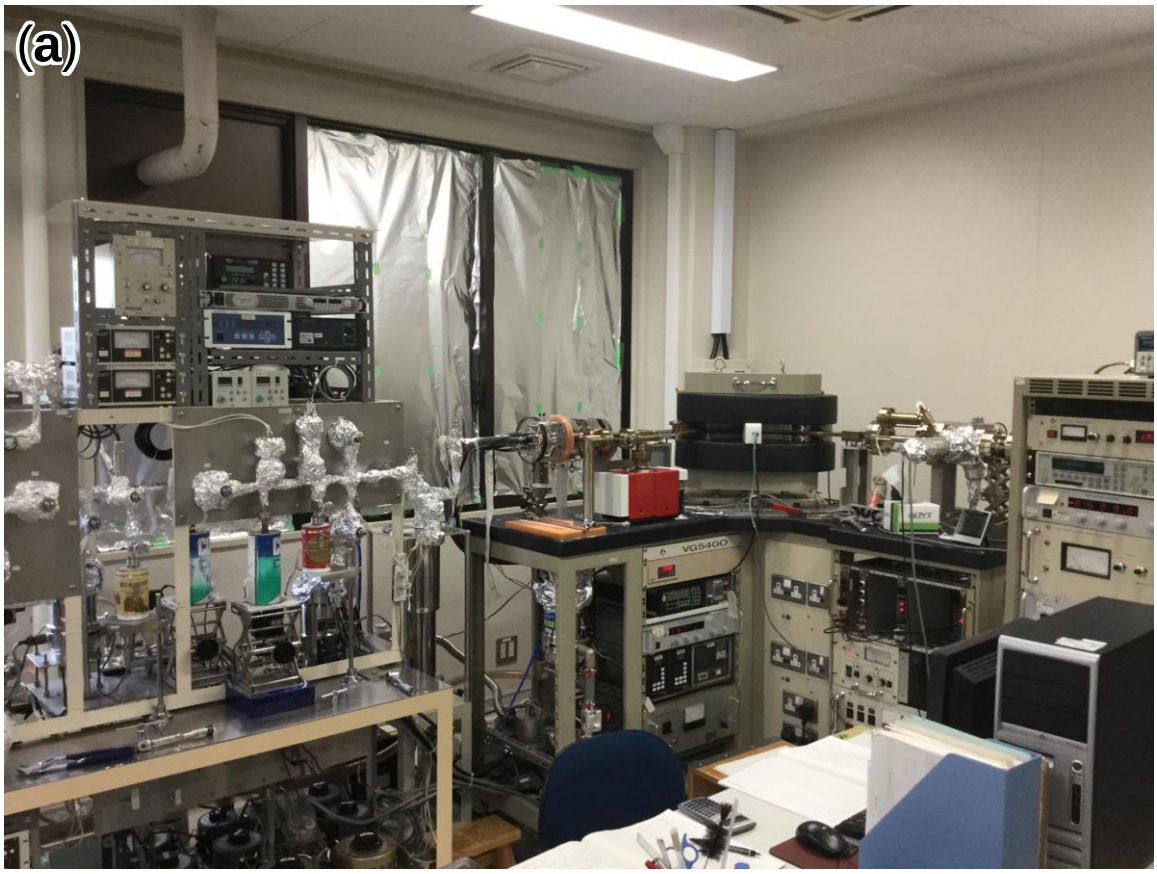

Figure 2.2.

(b)

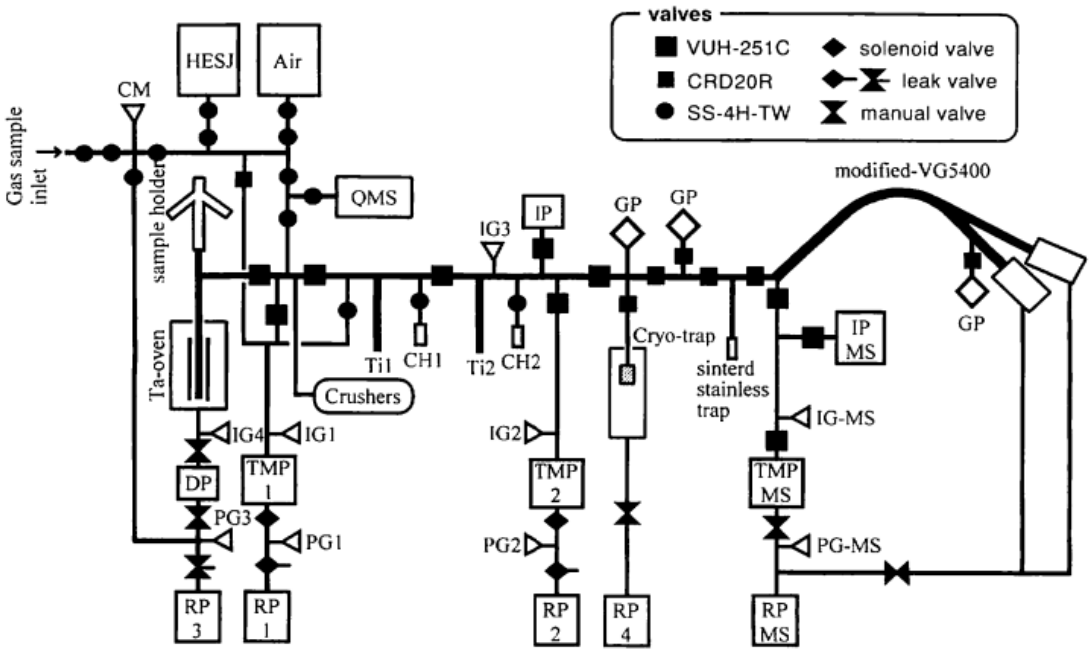

Figure 2.2. The noble gas analysis system, MS-IV. (a) Noble gas extraction and purification line, and mass spectrometer, modified VG5400. (b) Schematic diagram of the analysis system (Sumino et al., 2001).

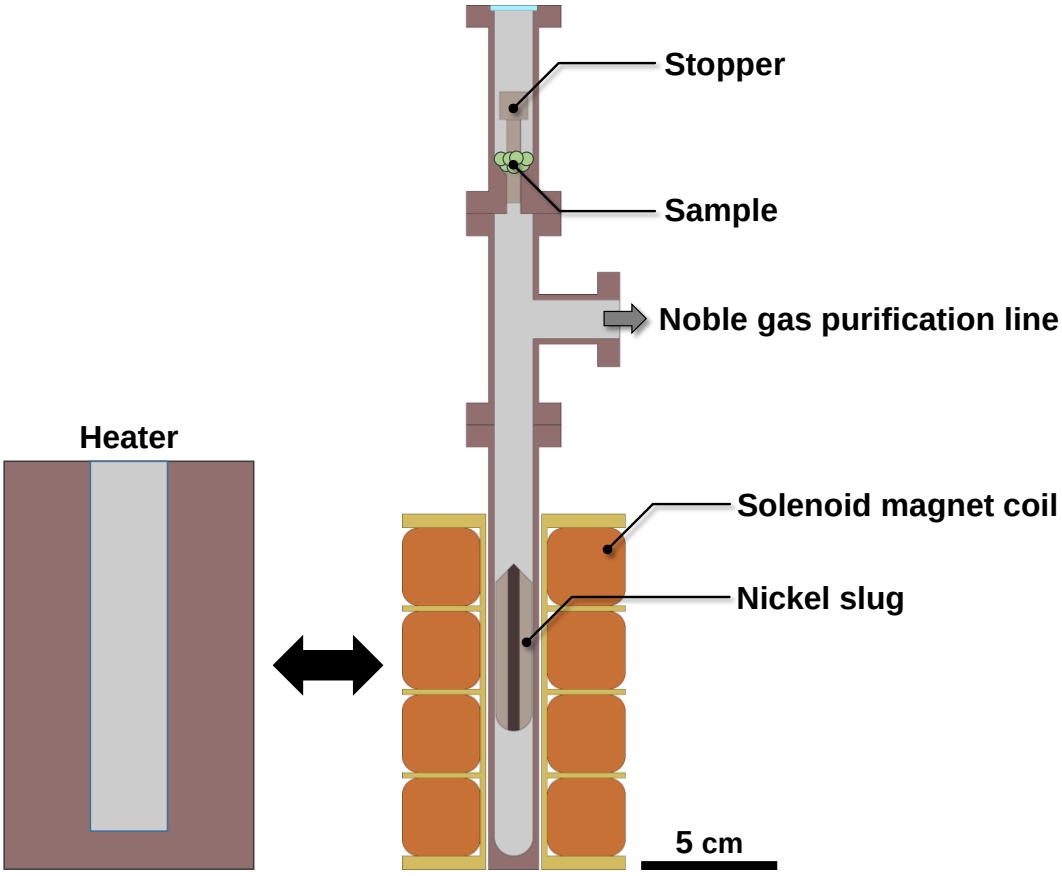

Figure 2.3. The crusher using solenoid coils. Samples were dropped to the bottom by removing the stopper with an external hand magnet. Dropped samples were heated at 800 °C by putting crusher into a heater. Without breaking vacuum after heating, samples were crushed with a Ni-slug moved vertically by an external magnetic field generated by the solenoid coils (Sumino et al., 2001).

2.3. Halogen analysis

Halogens in mantle xenoliths were analyzed using the neutron irradiation noble gas mass spectrometric technique (NI-NGMS), which is an extension of the Ar-Ar and I-Xe dating methods (Böhlke and Irwin, 1992; Johnson et al., 2000; Kendrick, 2012; Ruzié-Hamilton et al., 2016; Turner, 1965). In this method, halogens (Cl, Br, and I) and some elements (K, Ca, Ba, and U) are converted to corresponding isotopes of Ar, Kr, and Xe by neutron irradiation in a nuclear reactor. Since halogens have relatively high cross sections for neutron capture (Table 3.1), and the sensitivity of noble gas mass spectrometry is high, trace amounts of halogens in mantle xenoliths can be determined

(Table 2.2 and Figure 2.4).

The leached mantle xenolith samples, each weighing ~50 mg, were wrapped in Al-foil and placed in aluminum cans. Hb3gr hornblende (Turner et al., 1971), Shallowater meteorite, CaF_2, and K_2SO_4 were placed in the cans together with the samples as monitors of irradiation parameters (section 3.2). Neutron irradiation was carried-out in Japan Research Reactor-3 (JRR-3), Japan Atomic Energy Agency for 24–48 hours, Kyoto University Research Reactor (KUR), Kyoto University for 5 hours, or TRIGA Reactor, Oregon State University for 205.1 hours. Thermal neutron fluxes in JRR-3, KUR, and TRIGA Reactor, which were determined from analyses of irradiation monitor samples (section 3.2), were about 8×10^{17}, 1×10^{17}, and 4×10^{16} m^{-2} s^{-1}, respectively. In JRR-3 irradiation, Shallowater meteorite, from which epithermal neutron fluence is determined (Johnson et al., 2000; Ruzié-Hamilton et al., 2016), was not analyzed, because epithermal neutron fluence was negligible in previous irradiations in JRR-3.

Samples irradiated in JRR-3 and KUR were analyzed using a noble gas analysis system at the University of Tokyo (Figure 2.5), which I modified from the system described by Ebisawa et al. (2004). I evaluated its detection limits from blank measurements (Table 2.2). Trace amounts of halogens in mantle-derived materials can be quantified using this analysis system (Figure 2.4). Using NI-NGMS, Saito (2012, Master thesis, the University of Tokyo) analyzed halogens in geological reference materials distributed by GSJ (Geological Survey of Japan) and USGS (U.S. Geological Survey), and reported systematically lower halogen concentrations than the reference values for samples with low concentrations. He attributed the discrepancy between obtained and reference concentrations to contamination on the sample surface during preparation of these reference materials. I analyzed halogens in scapolite standards (SP, SY, BB1, and BB2), $[(Na,Ca,K)_4Al_3(Al,Si)_3Si_6O_{24}(Cl,CO_3,SO_4)]$, which are halogen reference materials described by Kendrick (2012) and refined by Kendrick et al. (2013ab) and Ruzié-Hamilton et al. (2016). I obtained consistent values with the refined values (Figure 2.6). This indicates that if care is taken to avoid contamination, halogens can be accurately analyzed using this analysis system.

Analytical procedures for noble gases in the neutron-irradiated samples were almost

the same as described above (section 2.2). Crushing experiments were operated using a hydraulic press (Figure 2.7a). In order to determine bulk halogen compositions, noble gases were also extracted by fusing the samples in a W-coil furnace. For the mantle xenoliths from volcanic fronts, separate aliquots of each sample were used for crushing and fusing experiments. Each sample was fused at 1800 °C for 30 min. For other mantle xenoliths, noble gases in the powders after crushing experiments were extracted by stepped heating at 800 or 900 °C and at 1800 °C. After purification, Ar, Kr, and Xe were separated from He and Ne using a charcoal trap (CH1) cooled in liquid nitrogen. The He and Ne were simultaneously admitted into the mass spectrometer with a charcoal trap (CH2) and sintered stainless steel trap (ST) cooled in liquid nitrogen. The Ar, Kr, and Xe were separated into each fraction using a Cryo-trap and admitted into the mass spectrometer (modified VG 3600; Ebisawa et al., 2004), which has a Faraday-cup, Daly multiplier collector, and ion-counting system.

Samples irradiated in TRIGA Reactor were analyzed using MS1, or ARGUS IV at the University of Manchester. Analyses using ARGUS IV were conducted by Prof. Ray Burgess of the University of Manchester. Analytical procedures at the University of Manchester using MS-1 and ARGUS IV are described by Broadley et al. (2016) and Ruzié-Hamilton et al. (2016), respectively. Crushing experiments were operated using a screw-type crusher constructed from Nupro® vacuum valve (Figure 2.7b, Stuart et al., 1994). Noble gases in the powder samples after crushing experiments were extracted by fusing samples. In the analyses using MS-1, noble gases were extracted by stepped heating from 600 to 1800 °C using 3 steps in a Ta resistance furnace. In the analyses using ARGUS IV, samples were heated using a CO_2 laser (CETAC Fusion CO_2) for 3 minutes until fusion. Extracted noble gases were purified on SAES NP-10 Al–Zr getters. After purification, Ar, Kr, and Xe were concentrated on a charcoal trap cooled in liquid nitrogen and then released into the inlet of the mass spectrometer. The Ar, Kr, and Xe were simultaneously admitted into the mass spectrometer. MS-1 has a Faraday-cup and multiplier, and ARGUS IV has a multi-collection system composed of five Faraday cups and a Compact Discrete Dynode multiplier.

In the samples analyzed in the University of Tokyo and those analyzed using ARGUS

IV, Ca-derived ^{37}Ar (half-life of 35 days) had decayed before the samples were analyzed. However, interference from Ca-derived ^{36}Ar, ^{38}Ar, and ^{39}Ar in the samples irradiated in JRR-3 and KUR is considered to be of minor importance because only small amounts of Ca-derived Ar isotopes are estimated to have been produced based on their low production rates determined in previous irradiations in JRR-3 and KUR. On the other hand, because production of Ca-derived Ar isotopes was significant in TRIGA Reactor irradiation, Ca-derived Ar isotopes were corrected from Ca concentrations obtained using XRF (chapter 6). For KLB-Lhz-12, because XRF data has not been obtained, I corrected Ca-derived Ar isotopes assuming CaO concentration is 2 wt.%. Because Al-foil was altered probably due to reaction with water during irradiation, all of irradiation monitors and some of samples could not be recovered from irradiation in KUR. Therefore, its irradiation conditions were estimated based on results from previous irradiations in KUR.

Table 2.2. Detection limits of elements in NI-NGMS (in units of mol).

Cl	Br	I	K	Ca	Ba	U
2.2×10^{-11}	5.3×10^{-14}	3.8×10^{-15}	1.4×10^{-8}	1.0×10^{-7}	7.3×10^{-12}	8.6×10^{-14}

The detection limit is defined as 4.65σ, where σ is standard deviation of blank measurements (Currie, 1968).

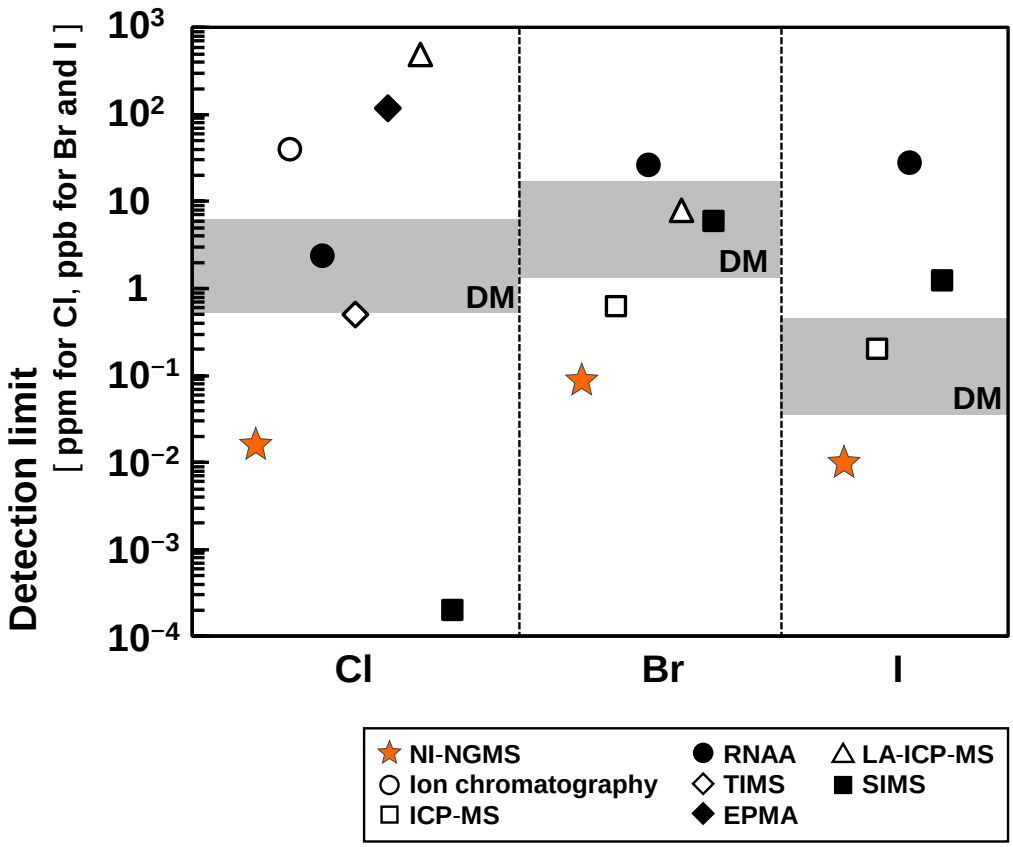

Figure 2.4. Detection limits of halogens in the analysis system which I had developed (NI-NGMS) and various methods used in geochemistry. Shaded area is the range of concentration of the depleted mantle (DM). Sample weight is assumed 50 mg for NI-NGMS. Analytical methods are designated by abbreviated name as follows: NI-NGMS = neutron irradiation noble gas mass spectrometric technique, ICP-MS = inductively coupled plasma-mass spectrometry, RNAA = radiochemical neutron activation analysis, TIMS = thermal ionization mass spectrometry, EPMA = electron probe microanalysis, LA-ICP-MS = laser ablation-ICP-MS, and SIMS = secondary ion mass spectrometry. Data sources: Ion chromatography (Michel and Villemant, 2003), ICP-MS (Chai and Muramatsu, 2007), RNAA (Ozaki and Ebihara, 2007), TIMS (Fujitani and Nakamura, 2006), EPMA and LA-ICP-MS (Hammerli et al., 2013), SIMS (Kusebauch, 2015a), and the depleted mantle (Burgess et al., 2002; Jambon et al., 1995; Kendrick et al., 2012, 2013a; Saal et al., 2002; Salters and Stracke, 2004).

Figure 2.5.

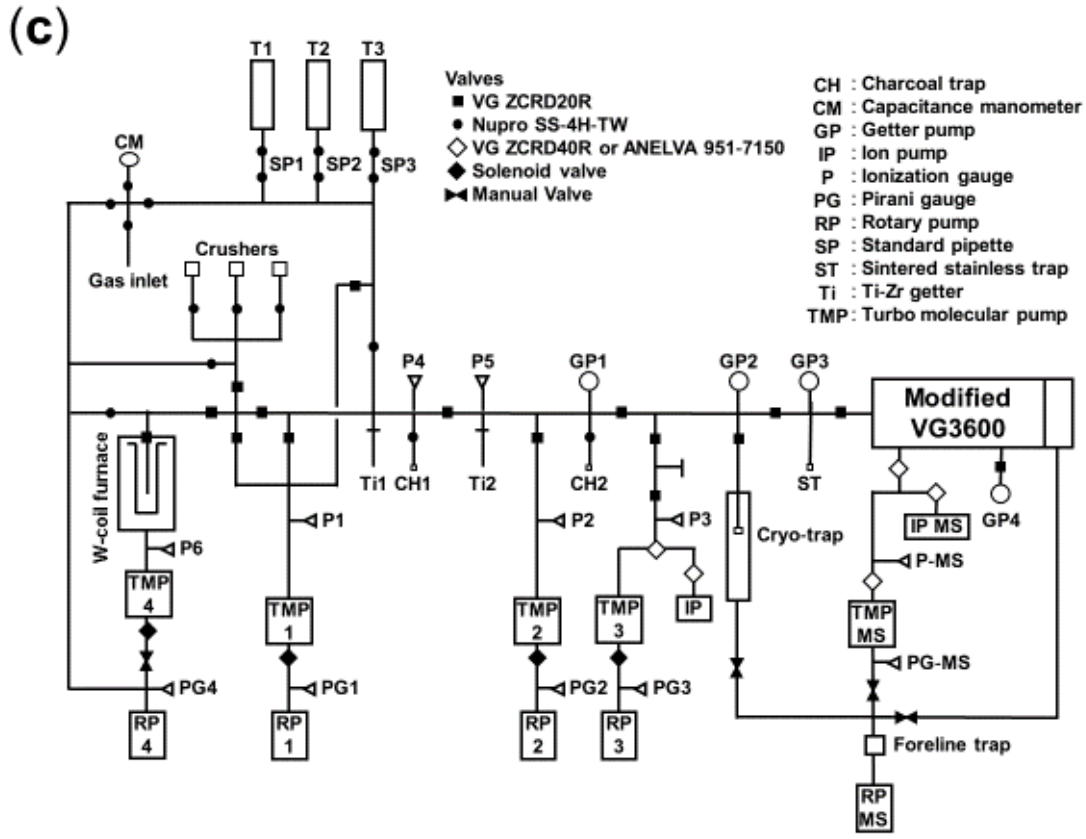

Figure 2.5. (a) Modified VG3600. (b) Noble gas extraction and purification line. (c) Schematic diagram of the analysis system at the University of Tokyo.

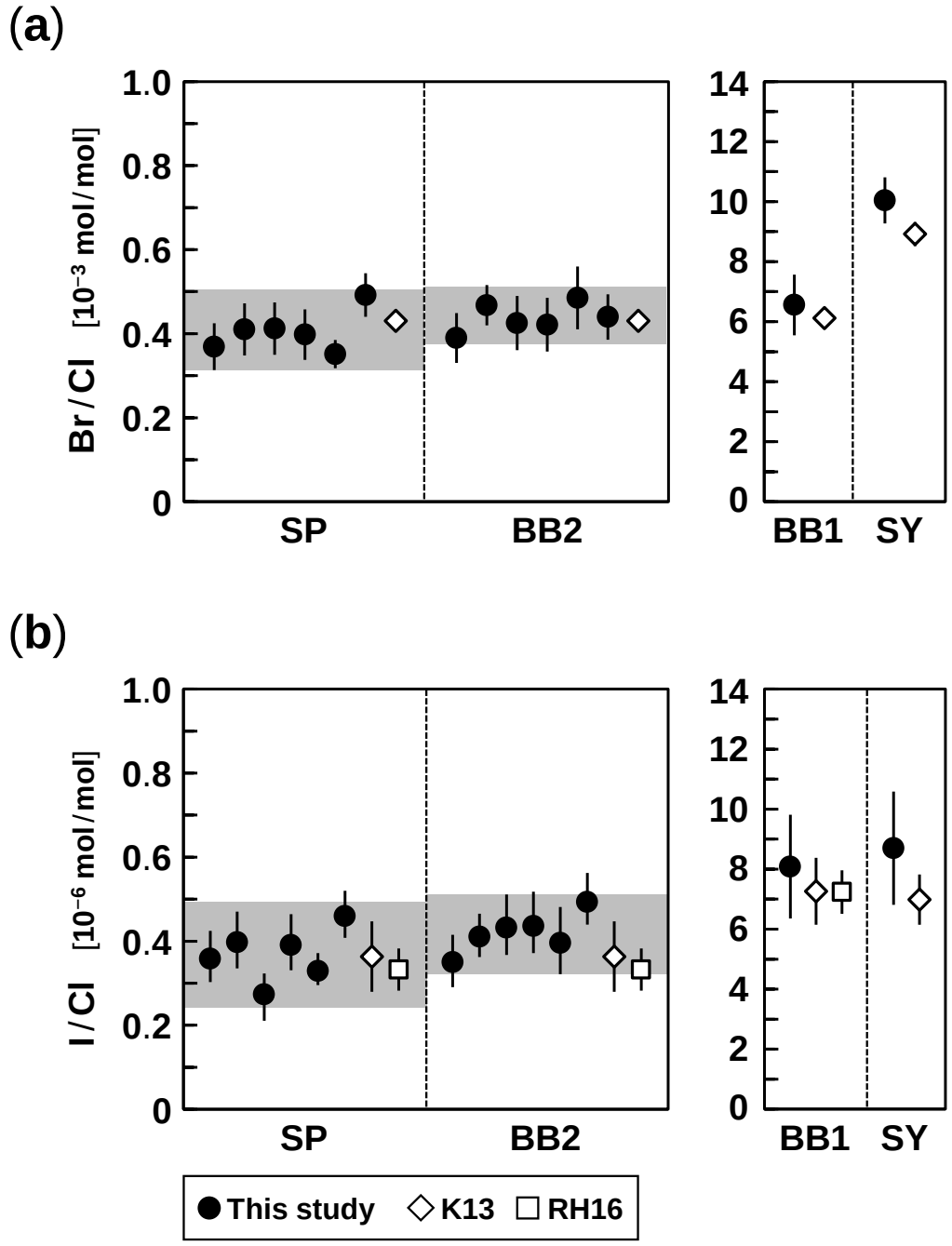

Figure 2.6. (a) Br/Cl ratios and (b) I/Cl ratios of scapolite standards. Errors are 2σ. Shaded areas are the mean values of SP and BB2. Data sources: K13 (Kendrick et al., 2013a) and RH16 (Ruzié-Hamilton et al., 2016).

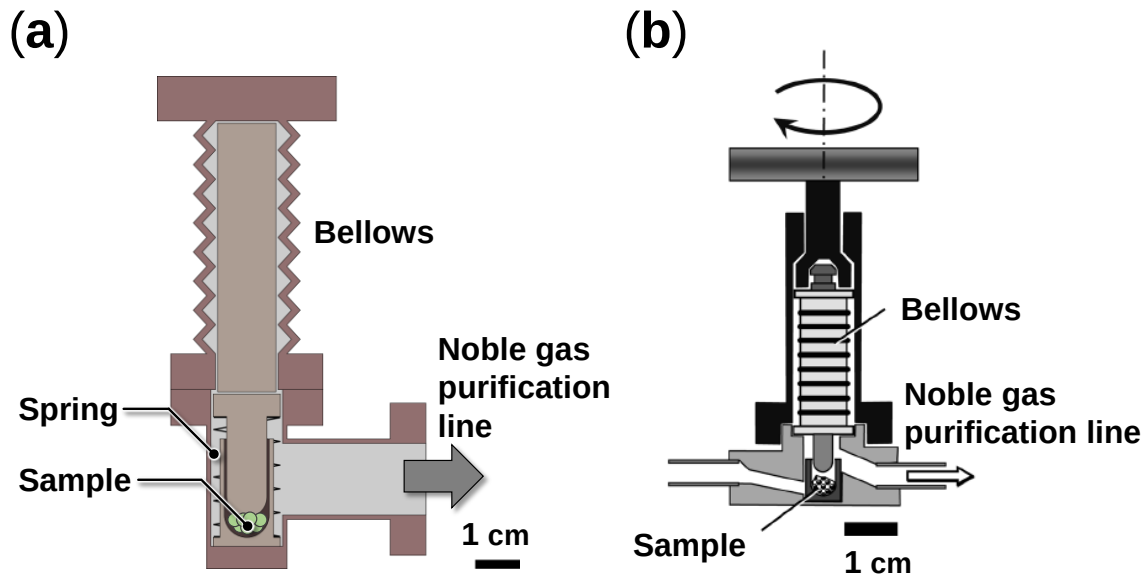

Figure 2.7. (a) The crusher for neutron-irradiated samples at the University of Tokyo. The crusher is hydraulically pressed. (b) The screw-type crusher constructed from Nupro® vacuum valve (modifed after Sumino, 2015).

2.4. Major element analysis

Major element compositions were analyzed for whole rocks of the mantle xenoliths from Ichinomegata except for Ich-30, Eifel, Kilbourne Hole, and San Carlos, and for clinopyroxene (cpx) separates from Ichinomegata mantle xenoliths except for Ich-30. Whole rock samples were washed by methanol in an ultrasonic bath, dried up in an oven overnight, and grinded into powder. Glass beads were prepared from the 0.4 g of the sample powder and 4.0 g of $Li_2B_4O_7$. The cpx separates were obtained by hand-picking under a binocular microscope. The separates were mounted onto Petropoxy 154 (Palouse Petro Products) and polished.

The major element compositions of whole rock samples were determined by X-ray fluorescence (XRF) analysis using Axios (PANalytical) at the University of Tokyo. The major element compositions of cpx samples were determined by electron probe microanalysis (EPMA) using JXA-8900L (JEOL) at the University of Tokyo. Operational settings of EPMA are given in Table 2.3.

Table 2.3. Operational settings of EPMA.

	Spot	Mapping
Beam current [A]	1.2×10^{-8}	1.2×10^{-7}
Accelerating voltage [kV]	15.0	15.0
Beam size [μm]	1	3

2.5. Trace element analysis

Trace element compositions were analyzed for the samples, of which major elements were analyzed. Isotopic ratios of Sr and Nd were also analyzed for the whole rock samples from Ichinomegata. They were analyzed by inductively coupled plasma-mass spectrometry (ICP-MS).

2.5.1. Whole rocks

The grinded powder of about 120 mg were weighted into Teflon beakers. The samples were digestioned in HF-HNO_3-$HClO_4$ (5:3:5) at 120 °C for 1 day. The solutions were evaporated to near dryness at 120 °C and then 4 ml of 4 M HNO_3 was added to the samples. Residues in the HNO_3 solutions were digestioned again after removing the solutions. In some samples, black residues, probably spinel, were observed after the second acid attack. Because spinel has a negligible effect on the budget of trace elements in peridotites (e.g., Bedini and Bodinier, 1999; Stosch and Seck, 1980), spinel was removed from solutions after being washed by 1 ml of 4M HNO_3.

About 5% of the solutions were separated for analyses of trace element concentrations using iCAP Q ICP-MS (Thermo Fisher Scientific) at the University of Tokyo. After doping In and Bi, which were used as internal standards, the solutions were diluted into about 30 ml of 2% HNO_3 solutions. The 3 analyses of the sample solutions were bracketed by analyses of a standard solution, which was made by Prof. Shun'ichi Nakai of the University of Tokyo from XSTC-13 and XSTC-1 distributed by SPEX CertiPrep Inc. and doped Nb, Hf, Ta, Zr, Sr, and Ba. Oxide interferences of LREE and Ba on HREE were corrected by production rates of MO^+/M^+ (M is metal element), which were determined by analyses of Ba-Ce-Pr-Tb and Nd-Sm-Eu-Gd artificial solutions prepared by Prof.

Shun'ichi Nakai. Logarithm of the obtained oxide production rates (MO^+/M^+) and M-O bond energies show a linear relationship (Figure 2.8) as previously reported (Aries et al., 2000; Kent and Ungerer, 2005).

The precision and accuracy of the analyses were evaluated by analyzing JP-1 geological reference material distributed by Geological Survey of Japan. Although some of the values obtained in this study are significantly different from the reference values (Imai et al., 1995), the results in this study are consistent with other studies using ICP-MS (Figure 2.9). Imai et al. (1995) summarized the concentrations of each element obtained by various techniques. However, wide ranges of values were reported for some elements. The reference values may include the overestimating data because of their low concentrations (Shirasaka et al., 2004).

In this study, Sm concentration was obtained by measuring $^{154}Sm^+$, which was interfered by $^{138}BaO^+$. Because of the large isotopic abundance of ^{138}Ba (0.71699; de Laeter et al., 2003), the obtained Sm concentration has large uncertainty or it could not be determined for some samples, which have high Ba/Sm ratio such as JP-1.

Isotope ratios of Sr and Nd were determined from the remainder of the solution. The solution was evaporated to dryness and dissolved into 2 ml of 2 M HCl. Strontium and Nd were separated using cation exchange resin and then separated using Sr and Ln resins distributed by Eichrom Technologies, respectively. Each solution was dried up and added H_2O_2 and HNO_3 in order to decompose organic materials dissolved from the resins. The solution was dried up and added 2% HNO_3. Isotopic ratios of Sr and Nd were analyzed using Neptune Plus ICP-MS (Thermo Fisher Scientific) at the University of Tokyo, which has a multi-collection system composed of Faraday cups. The 2 or 3 analyses of the sample solutions were bracketed by analyses of a standard solution, SRM 987 ($^{87}Sr/^{86}Sr$ = 0.71034) distributed by USGS and JNdi-1 ($^{143}Nd/^{144}Nd$ = 0.512115; Tanaka et al., 2000) for Sr and Nd analyses, respectively.

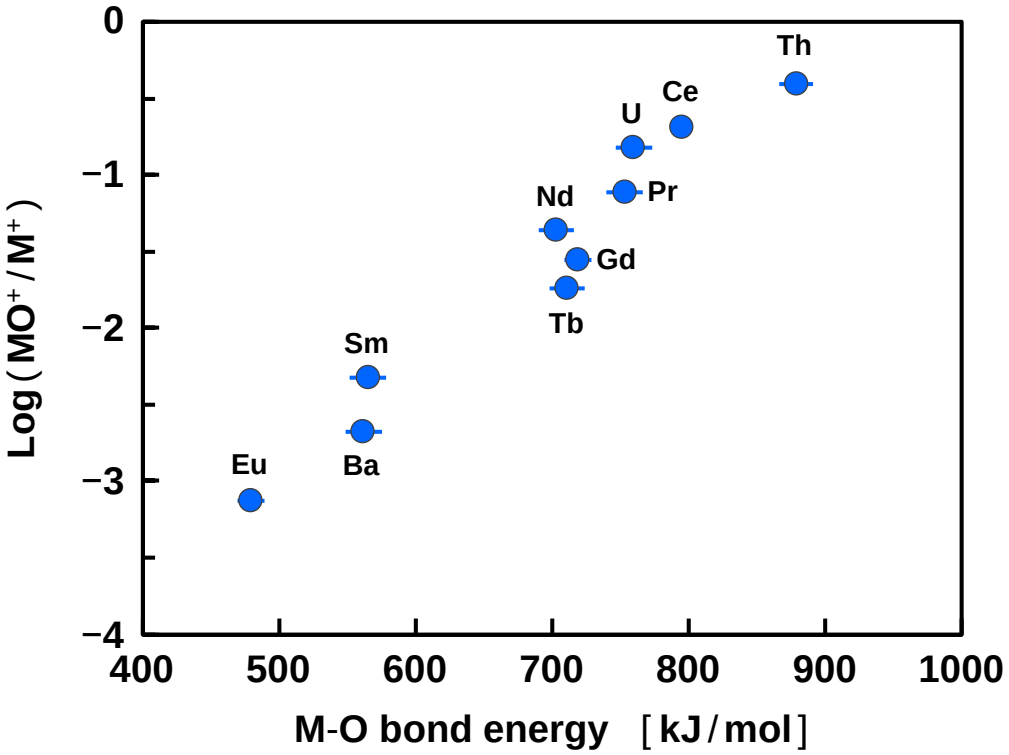

Figure 2.8. Logarithm of oxide production rates MO^+/M^+ versus M-O bond energies. Data source of M-O bond energies: Kerr (1998).

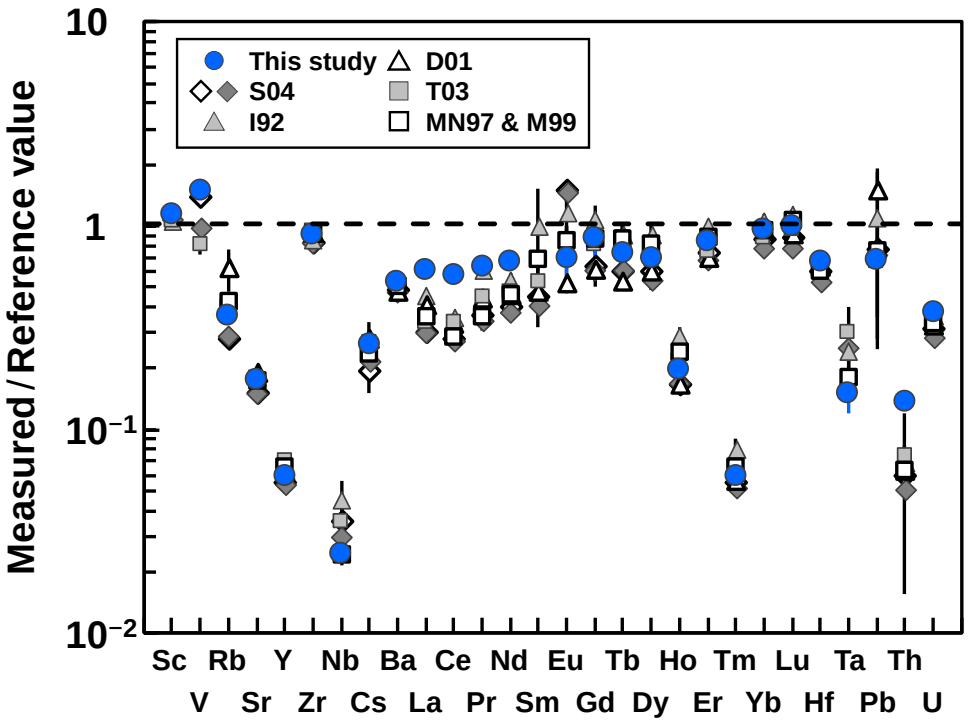

Figure 2.9. Comparison of elemental concentrations obtained from JP-1 with the reference values. Errors are 2σ. The reference values are from Imai et al. (1995). For comparison, data obtained by other studies using ICP-MS are shown. Data sources: S04 (Shirasaka et al., 2004), I92 (Ionov et al., 1992), D01 (Dulski, 2001), T03 (Takazawa et al., 2003), MN97 (Makishima and Nakamura, 1997), and M99 (Makishima et al., 1999).

2.5.2. Cpx separates

After removing carbon coating for EPMA analysis, trace elements in cpx separates were analyzed using a LSX-213 G2+ Nd:YAG laser ablation system (CETAC) coupled with iCAP Q ICP-MS at the University of Tokyo. Analytical procedures were almost same as described in Itano et al. (2016). The data were obtained from 30 μm ablation pits with a laser fluence of 20 J/m^2, repetition rate of 4 Hz. All analyses consist of 20 s baseline measurements and following 40 s measurements with laser ablation sampling, using a time resolved analytical procedure. The 12 to 25 analyses of cpx samples were bracketed by 3 analyses of NIST SRM 613 glass (Pearce et al., 1997). The Ca concentrations determined by EPMA were used as an internal standard. The other element concentrations

were determined using the sensitivity factors relative to Ca obtained from the results of NIST SRM 613 glass analyses. The precision and accuracy of the analyses were evaluated by analyzing BCR-2 geological reference material distributed by USGS and consistent values with the reference values were obtained (Figure 2.10). Oxide interferences of LREE on HREE were not corrected. However, because BCR-2 has LREE/HREE ratios several times higher than the cpx samples (e.g., >4 times higher La/Yb ratios), the oxide interferences on the cpx samples were expected to be negligible.

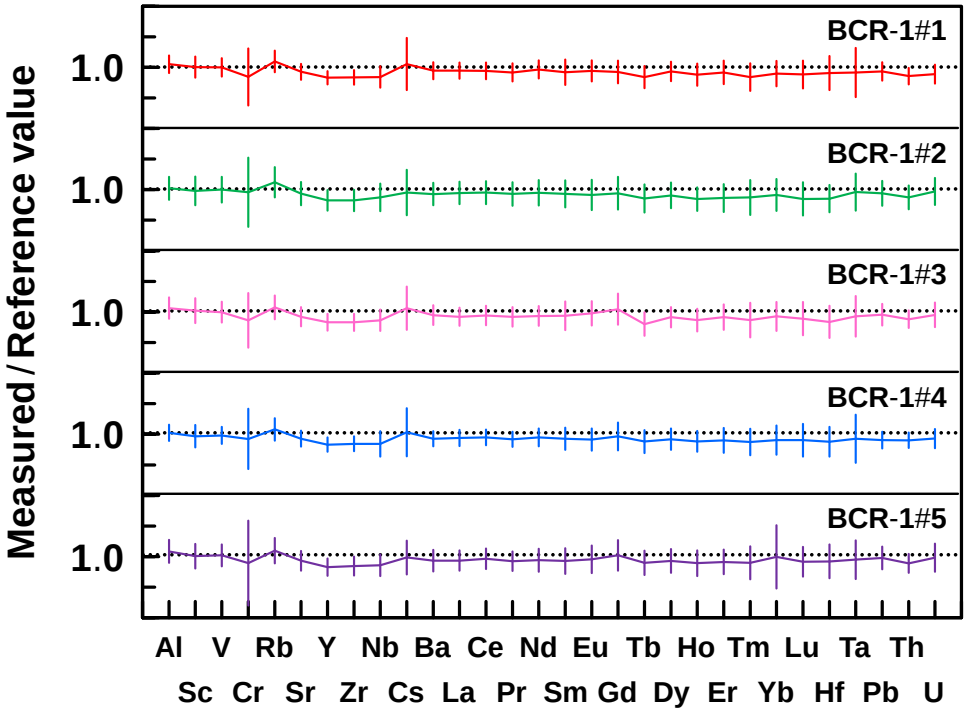

Figure 2.10. Comparison of elemental compositions obtained from BCR-2 with the reference values. Errors are 1σ. Each division of the vertical axis corresponds to 0.5. The reference values are from Govindaraju (1994). The concentrations in BCR-1 (Govindaraju, 1994) are used for Dy, Er, and Ta because their concentrations in BCR-2 have not been reported.

2.6. Fluid inclusion analysis

Compositions and CO_2 densities of fluid inclusions were analyzed for some mantle xenoliths from Ichinomegata, Eifel, Kilbourne Hole, and San Carlos by Raman spectroscopy. The densities of CO_2 in fluid inclusions were determined by a method described by Yamamoto and Kagi (2006). Raman spectra of CO_2 have two main peaks at 1388 (ν_+) and 1285 cm^{-1} (ν_-) (Figure 2.11). The peaks are split by the Fermi resonance and the separation between these two peaks, $\Delta = \nu_+ - \nu_-$, depends on density of CO_2 (Bertrán, 1983). The relationship between densities of CO_2 fluids and Δ values has been obtained by Kawakami et al. (2003), Yamamoto and Kagi (2006), and Yamamoto et al. (2005):

$$\begin{aligned}\text{Density} = \; & -0.00111808(\Delta-100)^8 + 0.04498451(\Delta-100)^7 \\ & - 0.7727143(\Delta-100)^6 + 7.4128146(\Delta-100)^5 \\ & - 43.468301(\Delta-100)^4 + 159.54433(\Delta-100)^3 \\ & - 357.7651(\Delta-100)^2 + 448.2404(\Delta-100) - 240.461\end{aligned} \tag{2.1}$$

Density of CO_2 depends on both temperature and pressure (Figure 2.12). If equilibrium temperature of mantle xenoliths is estimated using a geothermometer, the depth origin of the mantle xenoliths can be estimated (e.g., Yamamoto et al., 2002, 2007).

The samples were mounted onto Petropoxy 154 and doubly polished. Raman spectra of fluid inclusions were obtained using a micro-Raman spectrometer at the University of Tokyo, which is composed of a confocal microscope (BX, 51, Olympus) with a 20× objective, a 514.5-nm Ar ion laser (Ion Laser Technology), a single polychromator (500is Imaging Spectrograph, Bruker Optics) equipped with 1200 and 2400 grooves/mm gratings, and a CCD detector (DU401A-BR-DD, Andor Technology). The laser diameter and power were 2 μm and 20 mW on the sample surface, respectively. Acquisition time was 30 s for H_2O analysis and 20–90 s for CO_2 density analysis depending on the signal intensity. The analyses of each sample were bracketed by 3 analyses of a CO_2 fluid inclusion hosted by olivine in a mantle xenolith from Oki-Kuroshima (Δ = 104.61 cm^{-1}) and the Δ values were calibrated against the Δ value of this fluid inclusion. The accurate

peak positions of CO_2 bands were determined fitting to Lorentzian curve.

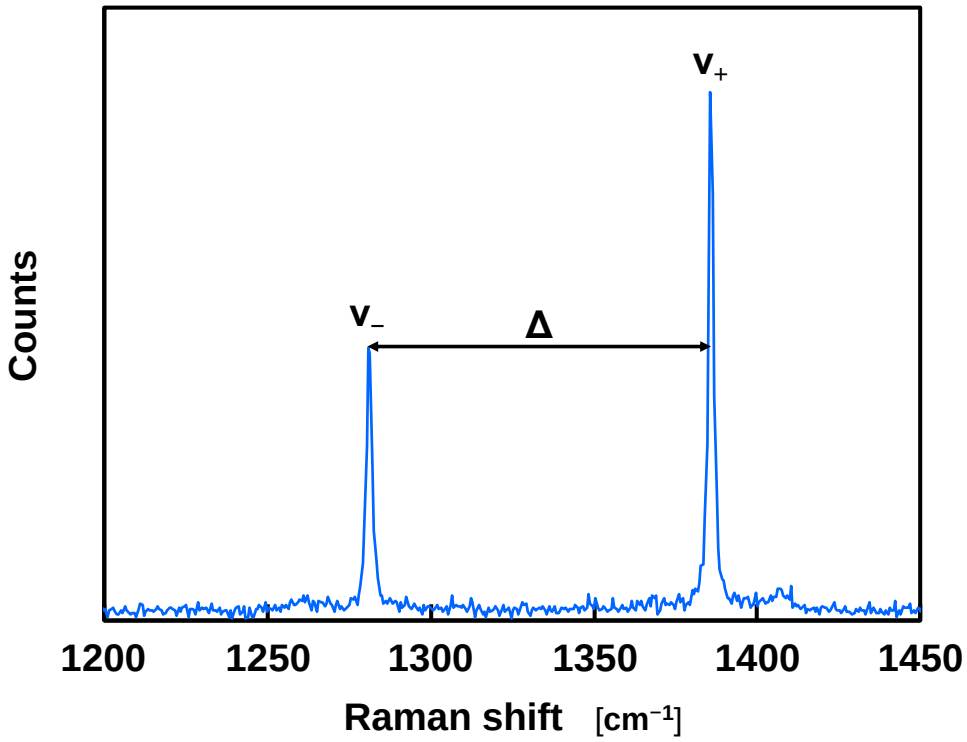

Figure 2.11. Raman spectrum of a CO_2 fluid inclusion hosted by olivine in a mantle xenolith from Oki-Kuroshima.

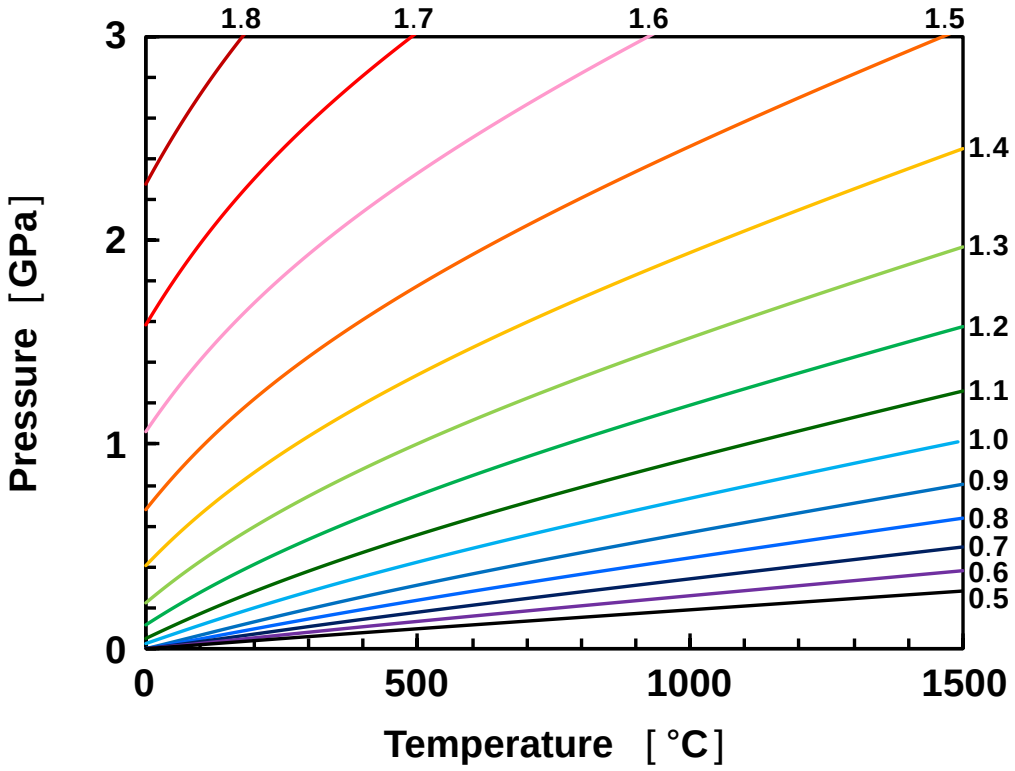

Figure 2.12. P-T phase diagram of CO_2. Contours represent density of CO_2 in the unit of g/cm^3. The equation of state for CO_2 reported by Pitzer and Sterner (1994) is used.

3. Halogen determination using NI-NGMS

本章については、５年以内に雑誌等で刊行予定のため、非公開。

This chapter is not published because it is scheduled to be published in journals or other publications within five years.

4. Halogen and noble gas systematics in mantle xenoliths from volcanic fronts: Subduction mechanism of volatiles from the Earth's surface into the mantle.

4.1. Samples

The volcanic front mantle xenoliths used in this study are from the Avacha volcano (the Kamchatka peninsula, Russia) and the Pinatubo volcano (Luzon island, in the Philippines) (Figure 4.1). The lithologies of the studied mantle xenoliths are spinel-harzburgites with textures and chemical compositions that reflect differing extents of metasomatism (Ishimaru and Arai, 2009; Ishimaru et al., 2007; Kawamoto et al., 2013; Yoshikawa et al., 2016). The samples were provided by Prof. Shoji Arai of Kanazawa University, Prof. Tetsuo Kobayashi of Kagoshima University, Dr. Satoko Ishimaru of Kumamoto University, and Dr. Masako Yoshikawa, Dr. Tatsuhiko Kawamoto, and Mr. Yoshitaka Kumagai of Kyoto University.

The Avacha volcano is located at volcanic front of the Kamchatka arc (Figure 4.1a). The old and cold Pacific plate is subducting beneath the Kamchatka arc (Minster et a., 1974). The activity of the Avacha volcano in Holocene can be divided into two stages, from 7250 to 3700 years before present (bp) and from 3500 years bp to present (Braitseva et al., 1998). The magma is andesitic for the first period and basaltic andesitic for the second. The host rock of the studied Avacha samples is basaltic andesite. There are two subtypes of Avacha peridotite xenoliths characterized by either the presence or absence of fine-grained (<100 μm) olivine domains (Arai et al., 2003). All Avacha samples used in this study were the coarse-grained type, except for Avx-1, which contains domains of fine-grained olivine (Avx-1 F-part). The Avacha samples contain H_2O-rich fluid inclusions (Figure 4.2a) having salinities of 2–8 wt% NaCl-equivalent (Ishimaru, personal comm.).

Hopp and Ionov (2011) reported atmospheric noble gases present in fluid inclusions in Avacha mantle xenoliths, arguing for their incorporation into the mantle wedge via slab-derived fluids. The trace element patterns of mantle xenoliths from Avacha including the samples used in this study show spikes at fluid-mobile elements such as Rb, Ba, U,

Pb, and Sr (Ionov, 2010; Ishimaru et al., 2007). The xenoliths were relatively enriched in light rare earth elements (LREE) compared to heavy rare earth elements (HREE) (Ishimaru et al., 2007). These signatures in trace elements suggest that slab-derived fluids are supplied to the mantle wedge beneath the Avacha volcano.

The Pinatubo volcano is located at volcanic front of the Luzon arc (Figure 4.1b). The young and hot South China Sea plate is subducting beneath the Luzon arc (Briais et al., 1993). The Pinatubo 1991 eruption was the largest eruption of 20^{th} century after 1912 eruption of the Novarupta volcano, Alaska, USA (Schmincke, 2004). The erupted magma of the 1991 eruption was dacitic and the eruption was triggered by an injection of basaltic magma to dacitic magma (Pallister et al., 1992). The host rock of the studied Pinatubo samples is dacite. One Pinatubo sample (P2) contains fine-grained domains, whereas the other sample (P3) is coarse-grained type. The Pinatubo samples contain H_2O-rich fluid inclusions (Figure 4.2b) having salinities of 5.1 ± 1.0 wt% NaCl-equivalent (Kawamoto et al., 2013).

Yoshikawa et al. (2016) studied major and trace element compositions in mantle xenoliths from the Pinatubo volcano including the samples used in this study. The mantle xenoliths showed enrichment in fluid-mobile elements relative to the mantle, indicating the presence of a slab-derived component. Their Nd-Sr isotopic ratios also indicate the presence of slab-derived component. Yoshikawa et al. (2016) argued that the metasomatic agents in the mantle wedge beneath the Pinatubo were aqueous fluids.

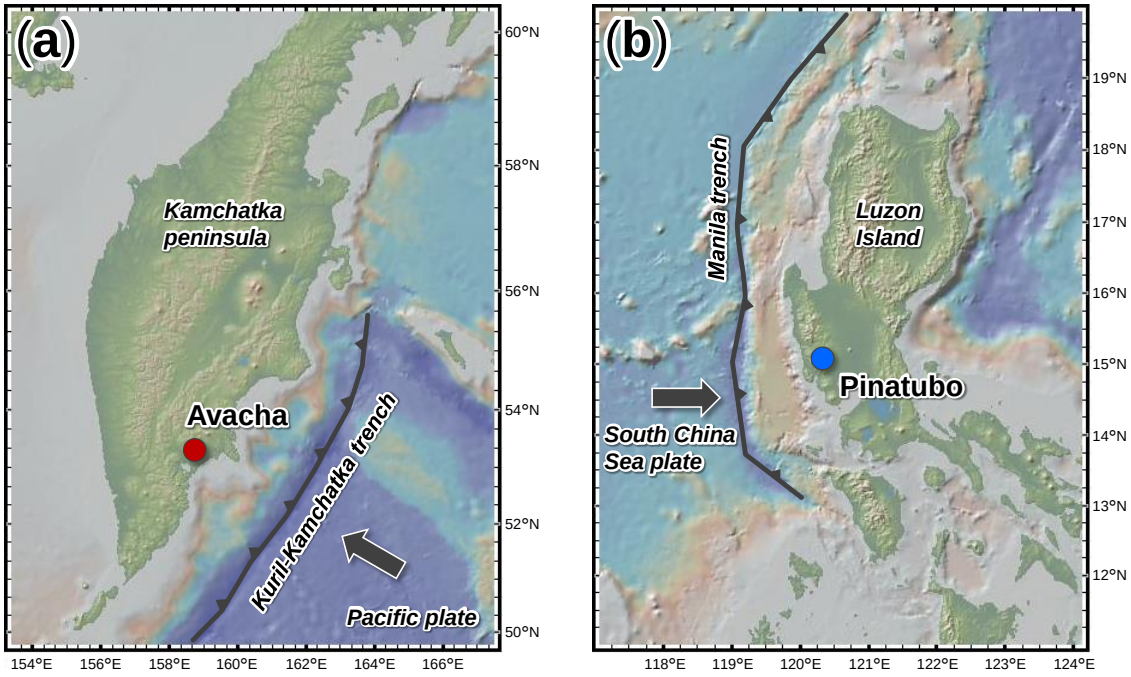

Figure 4.1. Location maps of the samples. (a) The Avacha volcano. (b) The Pinatubo volcano. The maps were made with the GeoMap App (http://www.geomapapp.org), using the Global Multi-Resolution Topography (GMRT) basemap (Ryan et al., 2009).

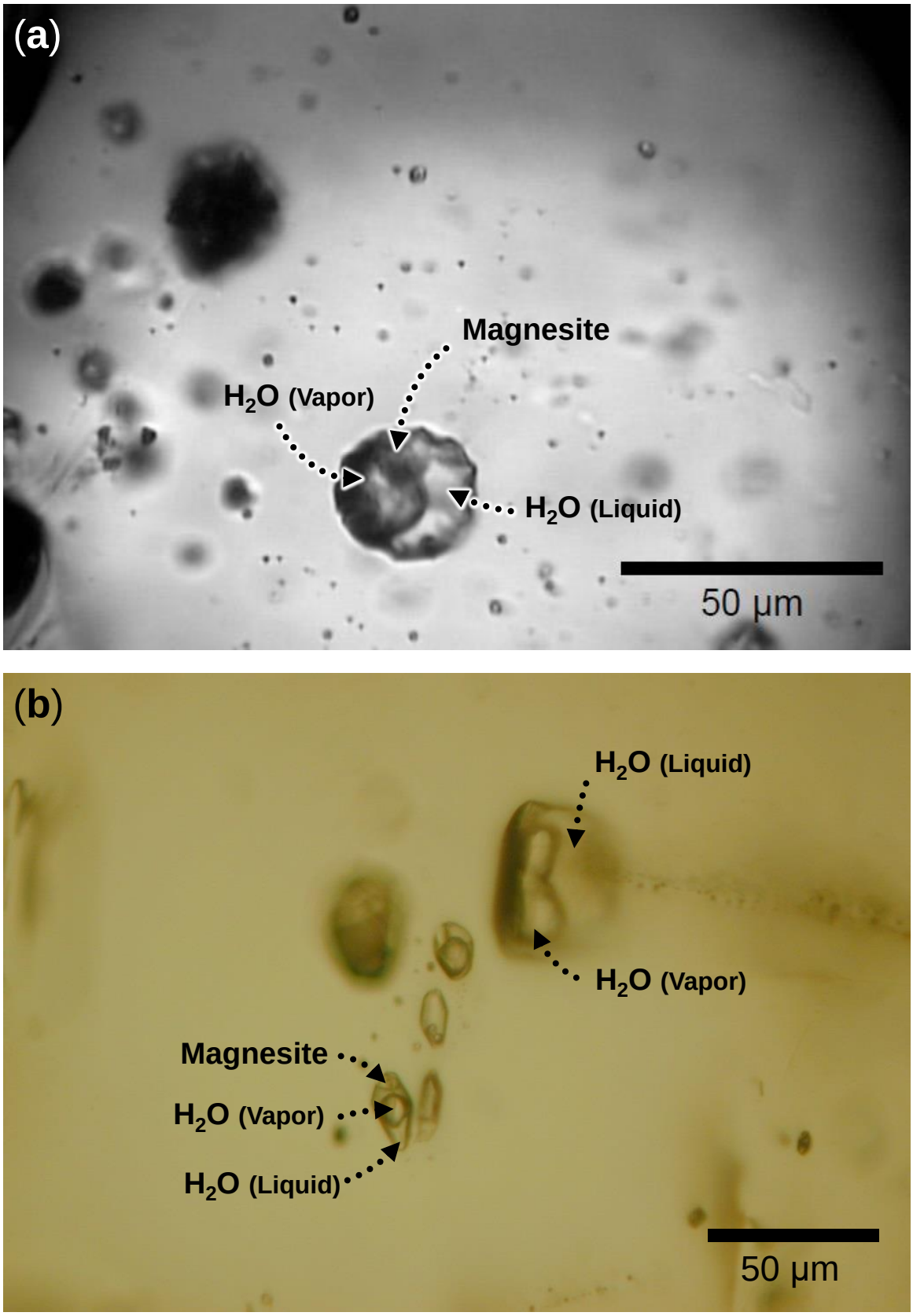
(a)
Magnesite
H2O (Vapor)
H2O (Liquid)
50 µm
(b)
H2O (Liquid)
H2O (Vapor)
Magnesite
H2O (Vapor)
H2O (Liquid)
50 µm

Figure 4.2.

Figure 4.2. Photomicrographs of fluid inclusions in olivine. (a) Sample #629 from the Avacha volcano. (b) Sample P3 from the Pinatubo volcano (Kawamoto et al., 2013). The fluid inclusions are distributed as isolated small clusters or trails. The fluid inclusions are composed mainly of liquid H_2O, magnesite, and a vapor H_2O bubble. Some of the vapor bubbles contain CO_2. Scale bars are 50 μm. Photomicrograph of the Avacha sample is provided by Dr. Satoko Ishimaru.

4.2. Results

4.2.1. Halogen composition

The halogen data are presented in Tables 4.1 and 4.2. Because efficiency of noble gas extraction by crushing was not 100%, i.e., some fluid inclusions still survived after crushing, the amounts of halogens obtained by sample fusion were larger than those obtained by crushing. During stepped crushing, the proportion of noble gases released from fluid inclusions relative to other potential sites (e.g., lattice or grain boundaries) may change as the intensity of crushing increases (Hilton et al., 1993; Scarsi, 2000; Sumino et al., 2006; Yokochi et al., 2005). However, the constant halogen elemental ratios obtained during stepped crushing of each sample indicate that halogen-derived noble gases are released mainly from fluid inclusions. Most of the samples showed slightly lower I/Cl and Br/Cl ratios during heating compared to crushing, suggesting the presence of an additional halogen host phase(s) in the bulk rock.

All samples are strongly enriched in iodine with I/Cl and Br/Cl ratios similar to sedimentary pore fluids and serpentinites as shown in Figure 4.3. Contributions from the mid-ocean ridge basalt (MORB) source mantle and altered oceanic crust (seafloor basalts and meta-gabbros) are of minor importance. Whereas the halogen compositions of fluids in the Pinatubo samples overlap with those of sedimentary pore fluids, the fluids in the Avacha samples deviate from the sedimentary pore fluid trend towards higher I/Cl values. Such iodine enrichment was observed previously in mantle wedge peridotites from Higashi-akaishi (Sumino et al., 2010) and forearc serpentinites from the Mariana arc (Kendrick et al., 2013b).

Table 4.1. Halogen and $^{40}Ar^*$ compositions of mantle xenoliths from the Avacha volcano.

Sample	Extraction	Cl [ppm]	Br [ppb]	I [ppb]	$^{40}Ar^*$ [10^{-8} ccSTP/g]	Br/Cl [10^{-3} mol/mol]	I/Cl [10^{-6} mol/mol]	Cl/$^{40}Ar^*$ [10^{4} mol/mol]
#10	5 MPa	1.97 (16)	7.34 (61)	6.20 (63)	2.60 (19)	1.65 (19)	877 (115)	4.79 (53)
	15 MPa	1.37 (11)	4.94 (41)	4.13 (42)	1.65 (14)	1.60 (19)	845 (110)	5.23 (61)
	25 MPa	0.846 (70)	3.10 (26)	2.39 (24)	0.885 (78)	1.63 (19)	790 (103)	6.04 (73)
	Crush Total	4.19 (21)	15.39 (78)	12.72 (80)	5.14 (25)	1.63 (12)	849 (68)	5.15 (36)
	1800 °C	7.48 (62)	23.1 (19)	17.6 (18)	4.42 (50)	1.37 (16)	658 (86)	10.7 (15)
#122	5 MPa	1.23 (10)	5.48 (46)	5.10 (53)	8.83 (85)	1.98 (23)	1162 (154)	0.88 (11)
	10 MPa	0.485 (40)	2.24 (19)	2.34 (24)	3.99 (34)	2.05 (24)	1348 (179)	0.767 (91)
	20 MPa	0.856 (71)	3.95 (33)	4.20 (43)	7.48 (69)	2.05 (24)	1372 (181)	0.723 (90)
	Crush Total	2.57 (13)	11.67 (59)	11.64 (72)	20.3 (11)	2.02 (15)	1267 (102)	0.799 (61)
	1800 °C	11.92 (98)	46.2 (39)	40.8 (42)	68.6 (60)	1.72 (20)	957 (126)	1.10 (13)
#187	5 MPa	0.749 (62)	2.66 (22)	2.46 (26)	0.68 (25)	1.58 (19)	918 (122)	6.9 (26)
	15 MPa	0.321 (27)	1.165 (98)	1.09 (11)	0.299 (73)	1.61 (19)	952 (126)	6.8 (18)
	25 MPa	0.295 (24)	1.097 (93)	0.823 (85)	0.273 (69)	1.65 (20)	780 (103)	6.8 (18)
	Crush Total	1.364 (72)	4.92 (26)	4.37 (29)	1.26 (27)	1.60 (12)	896 (76)	6.9 (15)
	1800 °C	4.20 (35)	13.0 (1)	10.3 (1)	2.82 (53)	1.38 (16)	685 (90)	9.4 (19)
#203	5 MPa	1.19 (10)	5.24 (44)	3.94 (41)	7.54 (71)	1.96 (23)	925 (123)	1.00 (1)
	15 MPa	0.608 (50)	2.81 (23)	1.83 (19)	4.75 (49)	2.05 (24)	843 (111)	0.81 (11)
	25 MPa	0.353 (29)	1.58 (13)	1.21 (13)	2.82 (27)	1.98 (23)	953 (127)	0.79 (10)
	Crush Total	2.15 (11)	9.62 (51)	6.97 (47)	15.11 (90)	1.99 (15)	906 (77)	0.899 (72)
	1800 °C	12.1 (10)	34.7 (29)	12.2 (12)	33.2 (34)	1.27 (15)	280 (36)	2.31 (30)

Table 4.1. (continued)

Sample	Extraction	Cl [ppm]	Br [ppb]	I [ppb]	$^{40}Ar^*$ [10^{-8} ccSTP/g]	Br/Cl [10^{-3} mol/mol]	I/Cl [10^{-6} mol/mol]	$Cl/^{40}Ar^*$ [10^{4} mol/mol]
#629	5 MPa	0.983 (81)	4.21 (35)	1.96 (20)	6.62 (74)	1.90 (22)	557 (74)	0.94 (13)
	10 MPa	0.334 (28)	1.47 (12)	0.691 (73)	2.26 (24)	1.95 (23)	577 (77)	0.93 (13)
	20 MPa	0.439 (36)	1.97 (16)	0.96 (10)	3.23 (32)	1.99 (23)	611 (81)	0.86 (11)
	Crush Total	1.757 (93)	7.64 (41)	3.61 (24)	12.11 (84)	1.93 (15)	575 (49)	0.916 (80)
	1800 °C	14.7 (12)	39.9 (33)	13.6 (14)	22.5 (24)	1.20 (14)	257 (34)	4.14 (56)
#729	5 MPa	0.589 (49)	2.01 (17)	1.38 (14)	2.61 (21)	1.51 (18)	653 (87)	1.43 (17)
	15 MPa	0.301 (25)	1.167 (97)	0.801 (84)	1.259 (94)	1.72 (20)	745 (99)	1.51 (17)
	25 MPa	0.185 (15)	0.792 (66)	0.511 (54)	0.725 (67)	1.90 (22)	771 (103)	1.62 (20)
	Crush Total	1.075 (57)	3.97 (20)	2.69 (17)	4.59 (24)	1.64 (12)	699 (58)	1.48 (11)
	1800 °C	2.80 (23)	10.89 (91)	6.59 (67)	9.79 (74)	1.73 (20)	658 (86)	1.81 (20)
Avx1 C-part	5 MPa	0.644 (53)	2.50 (21)	2.62 (27)	1.39 (18)	1.72 (20)	1136 (149)	2.93 (46)
	15 MPa	0.227 (19)	0.940 (80)	0.921 (95)	0.495 (61)	1.84 (22)	1136 (150)	2.89 (43)
	25 MPa	0.241 (20)	0.971 (81)	0.99 (10)	0.507 (69)	1.79 (21)	1152 (152)	3.00 (48)
	Crush Total	1.111 (60)	4.41 (24)	4.53 (30)	2.39 (20)	1.76 (13)	1139 (97)	2.94 (30)
	1800 °C	7.78 (64)	17.8 (15)	11.6 (12)	4.71 (42)	1.01 (12)	417 (55)	10.4 (13)
Avx1 F-part	5 MPa	0.248 (21)	1.007 (84)	0.933 (96)	0.88 (19)	1.80 (21)	1051 (139)	1.79 (41)
	15 MPa	0.198 (16)	0.819 (69)	0.787 (82)	0.74 (13)	1.83 (22)	1110 (148)	1.70 (33)
	25 MPa	0.173 (14)	0.738 (62)	0.708 (74)	0.61 (13)	1.89 (22)	1142 (153)	1.78 (41)
	Crush Total	0.620 (30)	2.56 (13)	2.43 (15)	2.23 (26)	1.84 (13)	1095 (85)	1.76 (23)
	1800 °C	3.15 (25)	8.30 (69)	7.53 (76)	5.37 (71)	1.17 (14)	668 (87)	3.71 (58)

Table 4.1. (continued)

Sample	Extraction	Cl [ppm]	Br [ppb]	I [ppb]	$^{40}Ar^*$ [10^{-8} ccSTP/g]	Br/Cl [10^{-3} mol/mol]	I/Cl [10^{-6} mol/mol]	$Cl/^{40}Ar^*$ [10^{4} mol/mol]
Avx33	5 MPa	1.68 (14)	6.31 (52)	6.13 (63)	4.45 (32)	1.67 (20)	1022 (134)	2.38 (26)
	15 MPa	0.616 (5)	2.52 (2)	2.45 (26)	1.60 (12)	1.82 (21)	1110 (148)	2.43 (28)
	25 MPa	0.437 (36)	1.76 (15)	1.93 (20)	1.18 (11)	1.78 (21)	1234 (163)	2.33 (28)
	Crush Total	2.73 (15)	10.59 (58)	10.50 (71)	7.23 (36)	1.72 (13)	1075 (94)	2.38 (18)
	1800 °C	10.00 (83)	30.8 (26)	16.0 (16)	6.30 (54)	1.37 (16)	448 (59)	10.0 (12)
F1	10 MPa	3.42 (28)	11.00 (93)	6.39 (66)	2.20 (29)	1.43 (17)	523 (69)	9.8 (15)
	20 MPa	0.794 (66)	2.65 (22)	1.51 (15)	0.418 (52)	1.48 (17)	530 (70)	12.0 (18)
	30 MPa	1.021 (84)	2.76 (23)	1.76 (18)	0.698 (90)	1.20 (14)	482 (64)	9.2 (14)
	40 MPa	0.486 (40)	1.80 (15)	1.12 (12)	0.350 (62)	1.65 (20)	643 (85)	8.8 (17)
	Crush Total	5.72 (30)	18.21 (99)	10.78 (71)	3.67 (32)	1.41 (11)	527 (45)	9.84 (100)
	1800 °C	6.93 (57)	17.3 (14)	15.3 (15)	4.33 (41)	1.11 (13)	616 (80)	10.1 (13)

Errors are given as least significant figures in brackets at a 1σ level of confidence. $^{40}Ar^*$ is excess ^{40}Ar from atmospheric ratio, defined as $^{40}Ar^* = \{(^{40}Ar/^{36}Ar)_{measured} - (^{40}Ar/^{36}Ar)_{air}\} \times {}^{36}Ar$, where $(^{40}Ar/^{36}Ar)_{air} = 296$ (Ozima and Podosek, 2002).

Table 4.2. Halogen and $^{40}Ar^*$ compositions of mantle xenoliths from the Pinatubo volcano.

Sample	Extraction	Cl [ppm]	Br [ppb]	I [ppb]	$^{40}Ar^*$ [10^{-8} ccSTP/g]	Br/Cl [10^{-3} mol/mol]	I/Cl [10^{-6} mol/mol]	Cl/$^{40}Ar^*$ [10^{4} mol/mol]
P2	5 MPa	1.565 (99)	5.99 (38)	1.51 (13)	1.87 (18)	1.70 (15)	270 (29)	5.29 (62)
	15 MPa	0.743 (47)	2.90 (19)	0.718 (61)	0.816 (99)	1.73 (16)	270 (29)	5.75 (79)
	25 MPa	0.183 (12)	0.842 (54)	0.216 (19)	0.215 (50)	2.04 (18)	330 (36)	5.4 (13)
	Crush Total	2.49 (11)	9.73 (43)	2.45 (15)	2.90 (21)	1.73 (11)	275 (20)	5.43 (47)
	1800 °C	12.77 (80)	36.7 (23)	7.15 (62)	7.5 (20)	1.27 (11)	156 (17)	10.8 (29)
P2 olivine	5 MPa	3.36 (21)	12.49 (79)	3.15 (27)	3.98 (58)	1.65 (15)	262 (28)	5.34 (85)
	15 MPa	1.281 (80)	5.02 (32)	1.34 (12)	1.34 (13)	1.74 (16)	292 (31)	6.03 (68)
	25 MPa	1.082 (68)	4.18 (27)	1.091 (94)	1.16 (10)	1.71 (15)	282 (30)	5.89 (63)
	Crush Total	5.73 (24)	21.69 (89)	5.58 (31)	6.48 (60)	1.68 (10)	272 (19)	5.58 (57)
	1800 °C	12.41 (78)	47.6 (30)	10.28 (89)	9.5 (21)	1.70 (15)	231 (25)	8.3 (19)
P3	5 MPa	1.77 (11)	7.72 (49)	1.49 (13)	3.02 (72)	1.94 (17)	235 (26)	3.70 (91)
	15 MPa	0.926 (58)	3.84 (25)	0.649 (59)	0.91 (17)	1.84 (17)	196 (22)	6.4 (13)
	25 MPa	0.680 (43)	2.69 (17)	0.456 (40)	0.53 (11)	1.75 (16)	187 (20)	8.1 (18)
	Crush Total	3.37 (13)	14.25 (57)	2.59 (15)	4.46 (74)	1.87 (11)	215 (15)	4.78 (82)
	1800 °C	11.54 (72)	44.8 (28)	11.6 (10)	8.1 (24)	1.72 (15)	281 (30)	9.0 (28)
P3 olivine	15 MPa	1.146 (72)	4.58 (29)	1.18 (10)	1.17 (11)	1.77 (16)	287 (31)	6.21 (72)
	25 MPa	0.711 (45)	2.82 (18)	0.813 (70)	0.667 (77)	1.76 (16)	320 (34)	6.74 (89)
	40 MPa	0.668 (42)	2.60 (17)	0.719 (64)	0.604 (70)	1.73 (16)	301 (33)	6.98 (92)
	Crush Total	2.524 (95)	10.00 (38)	2.71 (14)	2.44 (15)	1.758 (94)	300 (19)	6.55 (48)
	1800 °C	16.3 (10)	64.6 (41)	15.1 (13)	11.7 (22)	1.76 (16)	259 (28)	8.8 (17)

Errors are given as least significant figures in brackets at a 1σ level of confidence. $^{40}Ar^*$ is excess ^{40}Ar from atmospheric ratio, defined as $^{40}Ar^* = \{(^{40}Ar/^{36}Ar)_{measured} - (^{40}Ar/^{36}Ar)_{air}\} \times {}^{36}Ar$, where $(^{40}Ar/^{36}Ar)_{air} = 296$ (Ozima and Podosek, 2002).

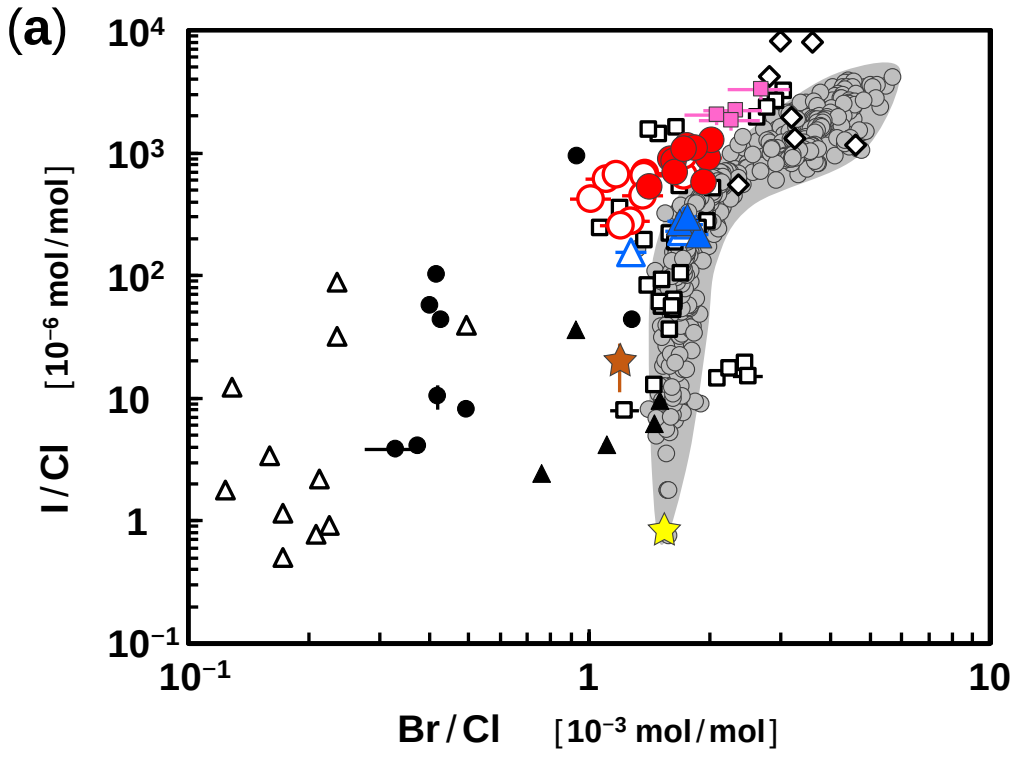

Figure 4.3.

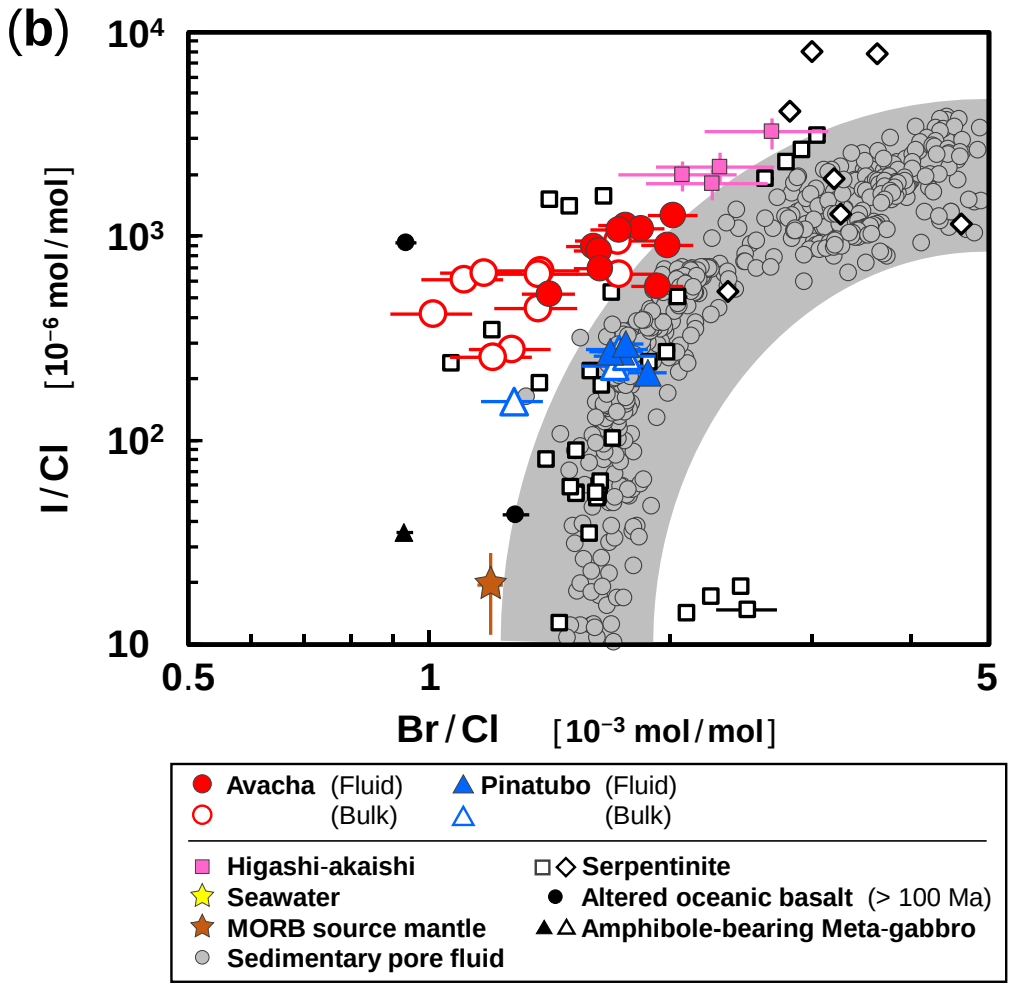

Figure 4.3. I/Cl versus Br/Cl for the studied samples. Fluid and Bulk refer to crushing and heating data, respectively. (b) is a magnification of (a). Errors are 1σ. Data sources: Higashi-akaishi peridotite from Sanbagawa metamorphic belt (Sumino et al., 2010), serpentinites from the oceanic lithosphere (open squares) and forearc (open diamonds) (John et al., 2011; Kendrick et al., 2011, 2013b), sedimentary pore fluids (Fehn et al., 2006; Kastner et al., 1990; Martin et al., 1993; Muramatsu et al., 2007), seawater (Bruland and Lohan, 2014), MORB source mantle (Kendrick et al., 2012a), altered oceanic crust older than 100 Ma (Chavrit et al., 2016), and amphiboles in meta-gabbros (open triangles) and relict minerals and quartz-epidote veins in meta-gabbros (black triangles) (Kendrick et al., 2015a). The halogen ratios reported by Kendrick et al. (2011, 2012a, 2013b) were recalculated using revised values for scapolite monitors (Kendrick et al., 2013a).

4.2.2. Noble gas composition

Noble gas data are presented in Tables 4.3 and 4.4.

Table 4.3. Noble gas compositions of mantle xenoliths from the Avacha volcano.

Sample	$^{3}He/^{4}He$ [Ra]	^{4}He [10^{-8}]	$^{20}Ne/^{22}Ne$	$^{21}Ne/^{22}Ne$	^{20}Ne [10^{-10}]	$^{38}Ar/^{36}Ar$	$^{40}Ar/^{36}Ar$	^{40}Ar [10^{-8}]	^{84}Kr [10^{-12}]	^{132}Xe [10^{-12}]
#10	7.83 (19)	2.36 (12)	9.877 (72)	0.02893 (46)	0.880 (45)	0.18824 (32)	359.71 (39)	15.86 (80)	18.08 (94)	1.22 (10)
	7.88 (30)	0.996 (50)	9.760 (86)	0.02933 (79)	0.219 (11)	n.a.	n.a.	n.a.	n.a.	n.a.
#122	7.70 (16)	7.42 (37)	9.736 (37)	0.02931 (48)	7.26 (36)	0.18774 (60)	346.82 (41)	157.1 (79)	160.4 (89)	8.93 (58)
	7.68 (15)	3.74 (19)	9.811 (42)	0.0284 (14)	3.71 (19)	0.18787 (66)	348.12 (30)	84.4 (42)	88.1 (47)	4.72 (28)
	7.71 (21)	1.852 (93)	9.769 (44)	0.0294 (14)	1.869 (94)	0.18798 (63)	347.77 (35)	44.1 (22)	45.8 (24)	2.43 (21)
#187	7.77 (18)	2.13 (11)	9.792 (37)	0.02907 (92)	3.29 (16)	0.18718 (49)	334.13 (23)	25.5 (13)	25.8 (15)	1.71 (18)
	7.72 (29)	0.715 (36)	9.820 (53)	0.03130 (53)	0.585 (29)	0.18823 (64)	347.48 (44)	6.96 (35)	7.29 (37)	0.488 (56)
	7.54 (40)	0.355 (18)	9.690 (93)	0.0294 (11)	0.242 (12)	0.18777 (70)	352.36 (66)	3.16 (16)	3.42 (18)	0.232 (17)
#203	7.76 (13)	3.90 (20)	9.892 (38)	0.02988 (44)	1.773 (89)	0.18815 (45)	339.24 (53)	35.7 (18)	36.0 (19)	1.96 (23)
	7.72 (14)	2.72 (14)	9.863 (27)	0.0296 (15)	1.365 (68)	0.18851 (41)	338.86 (26)	26.8 (13)	27.6 (14)	1.41 (10)
	7.75 (15)	2.55 (13)	9.834 (37)	0.02923 (69)	1.331 (67)	0.18866 (54)	338.47 (35)	26.6 (13)	27.7 (14)	1.41 (14)
#629	7.60 (12)	4.20 (21)	9.643 (57)	0.0290 (18)	1.674 (84)	0.1877 (11)	335.64 (42)	36.1 (18)	39.1 (21)	2.14 (15)
	7.58 (17)	1.725 (86)	9.843 (40)	0.02916 (75)	0.674 (34)	0.18767 (61)	335.81 (32)	15.72 (79)	17.02 (89)	0.912 (69)
	7.79 (24)	0.870 (44)	9.876 (67)	0.02920 (83)	0.340 (17)	0.18774 (62)	337.07 (30)	8.39 (42)	9.03 (48)	0.517 (42)
#729	7.85 (19)	2.62 (13)	9.720 (80)	0.02923 (75)	0.717 (36)	0.18479 (86)	372.43 (32)	17.65 (89)	20.6 (11)	1.55 (11)
	7.94 (29)	1.118 (56)	9.654 (71)	0.02908 (70)	0.325 (16)	0.18771 (90)	375.47 (18)	7.73 (39)	9.02 (48)	0.678 (56)
	8.12 (31)	0.542 (27)	9.91 (10)	0.0287 (15)	0.1120 (56)	0.18757 (77)	380.65 (34)	3.66 (18)	4.33 (22)	0.318 (22)
Avx1 C-part	7.52 (13)	3.89 (22)	9.788 (24)	0.02909 (90)	1.683 (84)	0.18911 (67)	352.16 (71)	16.54 (83)	15.99 (85)	1.08 (10)
	7.55 (21)	1.306 (65)	9.823 (66)	0.02933 (68)	0.386 (19)	0.18879 (66)	358.75 (71)	5.02 (25)	5.34 (28)	0.421 (28)
Avx1 F-part	7.71 (18)	3.42 (17)	9.705 (70)	0.02890 (65)	2.08 (10)	0.18786 (93)	322.90 (40)	16.45 (83)	15.31 (80)	1.01 (11)
	7.63 (41)	0.866 (44)	9.75 (12)	0.02882 (93)	0.433 (22)	0.18804 (90)	327.76 (24)	3.80 (19)	3.72 (20)	0.264 (19)
	6.8 (10)	0.362 (20)	9.62 (14)	0.0276 (15)	0.1772 (90)	0.1878 (13)	329.39 (50)	1.571 (79)	1.65 (11)	0.151 (11)

Table 4.3. (continued)

Sample	$^{3}He/^{4}He$ [Ra]	^{4}He [10^{-8}]	$^{20}Ne/^{22}Ne$	$^{21}Ne/^{22}Ne$	^{20}Ne [10^{-10}]	$^{38}Ar/^{36}Ar$	$^{40}Ar/^{36}Ar$	^{40}Ar [10^{-8}]	^{84}Kr [10^{-12}]	^{132}Xe [10^{-12}]
Avx33	7.74 (12)	4.30 (22)	9.837 (58)	0.02904 (50)	0.533 (27)	0.18874 (71)	352.64 (33)	8.87 (45)	8.78 (53)	0.520 (31)
	7.72 (16)	3.33 (17)	9.887 (54)	0.02920 (53)	0.561 (28)	0.18847 (50)	347.00 (35)	7.18 (36)	6.82 (38)	0.411 (37)
	7.70 (22)	1.805 (90)	9.730 (84)	0.02904 (55)	0.216 (11)	0.18871 (86)	353.12 (38)	3.32 (17)	3.19 (17)	0.197 (24)
F1	7.92 (17)	2.49 (12)	9.669 (43)	0.02910 (44)	0.644 (32)	0.18833 (76)	370.75 (21)	13.88 (70)	16.45 (85)	1.097 (69)
	8.16 (35)	0.508 (25)	9.64 (13)	0.0301 (12)	0.1012 (51)	0.1877 (10)	380.52 (45)	2.68 (13)	3.22 (17)	0.219 (24)
	8.20 (48)	0.321 (16)	9.46 (13)	0.0284 (11)	0.679 (34)	0.18831 (46)	373.60 (39)	1.866 (94)	2.09 (11)	0.1336 (86)

Errors are given as least significant figures in brackets at a 1σ level of confidence. Units of noble gas concentrations are ccSTP/g. n.a.: not analyzed.

Table 4.4. Noble gas compositions of mantle xenoliths from the Pinatubo volcano.

Sample	$^{3}He/^{4}He$ [Ra]	^{4}He [10^{-8}]	$^{20}Ne/^{22}Ne$	$^{21}Ne/^{22}Ne$	^{20}Ne [10^{-10}]	$^{38}Ar/^{36}Ar$	$^{40}Ar/^{36}Ar$	^{40}Ar [10^{-8}]	^{84}Kr [10^{-12}]	^{132}Xe [10^{-12}]
P2	7.52 (13)	3.74 (19)	9.762 (74)	0.02923 (38)	1.241 (62)	0.18850 (58)	324.68 (18)	13.44 (68)	12.56 (63)	0.810 (59)
	7.51 (18)	1.989 (99)	9.826 (74)	0.02938 (38)	0.751 (38)	0.18748 (46)	327.41 (19)	6.91 (35)	6.00 (34)	0.393 (37)
	7.52 (15)	1.455 (73)	9.947 (81)	0.02909 (58)	0.428 (21)	0.18785 (62)	335.07 (57)	3.99 (20)	3.48 (18)	0.238 (17)
P2 olivine	7.45 (11)	12.08 (60)	9.768 (85)	0.02989 (87)	0.602 (30)	0.1879 (10)	429.33 (85)	11.36 (57)	9.57 (51)	0.839 (64)
	7.54 (18)	3.60 (18)	9.82 (13)	0.03030 (75)	0.1501 (75)	0.18806 (49)	443.11 (52)	3.33 (17)	2.87 (17)	0.277 (16)
	7.44 (27)	1.537 (77)	9.70 (14)	0.0309 (21)	0.0732 (38)	0.18761 (63)	429.26 (60)	1.501 (75)	1.395 (73)	0.174 (19)
P3	7.46 (12)	4.28 (21)	9.723 (33)	0.0286 (11)	2.24 (11)	0.18786 (50)	347.79 (27)	21.1 (11)	17.37 (89)	0.984 (73)
	7.51 (15)	1.462 (73)	9.824 (82)	0.02953 (33)	0.525 (26)	0.18783 (82)	361.91 (58)	6.22 (31)	5.42 (30)	0.348 (38)
	7.76 (32)	0.624 (31)	9.733 (83)	0.02925 (62)	0.1801 (90)	0.18611 (52)	369.03 (29)	2.61 (13)	2.51 (14)	0.168 (13)
P3 olivine	7.39 (11)	5.25 (26)	9.720 (35)	0.0296 (12)	1.643 (82)	0.18733 (79)	377.40 (47)	21.7 (11)	18.64 (98)	1.24 (13)
	7.47 (24)	1.454 (73)	9.841 (96)	0.02987 (80)	0.291 (15)	0.18809 (60)	390.02 (27)	6.08 (31)	5.70 (80)	0.403 (31)
	7.56 (37)	0.729 (37)	9.70 (13)	0.02975 (66)	0.1288 (65)	0.18772 (83)	391.9 (11)	3.07 (15)	2.90 (16)	0.207 (18)

Errors are given as least significant figures in brackets at a 1σ level of confidence. Units of noble gas concentrations are ccSTP/g.

4.2.2.1. Isotopic composition of He, Ne, and Ar

The constant $^{3}He/^{4}He$ ratios obtained for crushing steps from each sample (Tables 4.3 and 4.4) indicate that He is mainly released from fluid inclusions and that the fluid inclusions are homogeneous about He. The weighted mean $^{3}He/^{4}He$ values are 7.724 ± 0.019 and 7.478 ± 0.023 Ra (1 Ra = atmospheric ratio of 1.399×10^{-6}; Ozima and Podosek, 2002) for the Avacha and Pinatubo samples, respectively. These ratios are consistent with the $^{3}He/^{4}He$ value of MORB (8 ±1 Ra; Moreira and Kurz, 2013). Hopp and Ionov (2011) obtained a slightly wider range of between 5.2 and 8.1 Ra from Avacha mantle xenoliths.

Isotopic ratios of Ne and Ar are dominated by atmospheric compositions (Figures 4.4 and 4.5). Hereafter I refer to 'atmospheric noble gases' as those that show isotopic ratios similar to the air (elemental ratios may be different from those of the air). Although some samples showed small variation in $^{40}Ar/^{36}Ar$ ratio during stepwise crushing, all of data are lower than 450, mostly lower than 400 (Figure 4.4), which are significantly lower than that of the MORB source mantle (~40000; Holland and Ballentine, 2006).

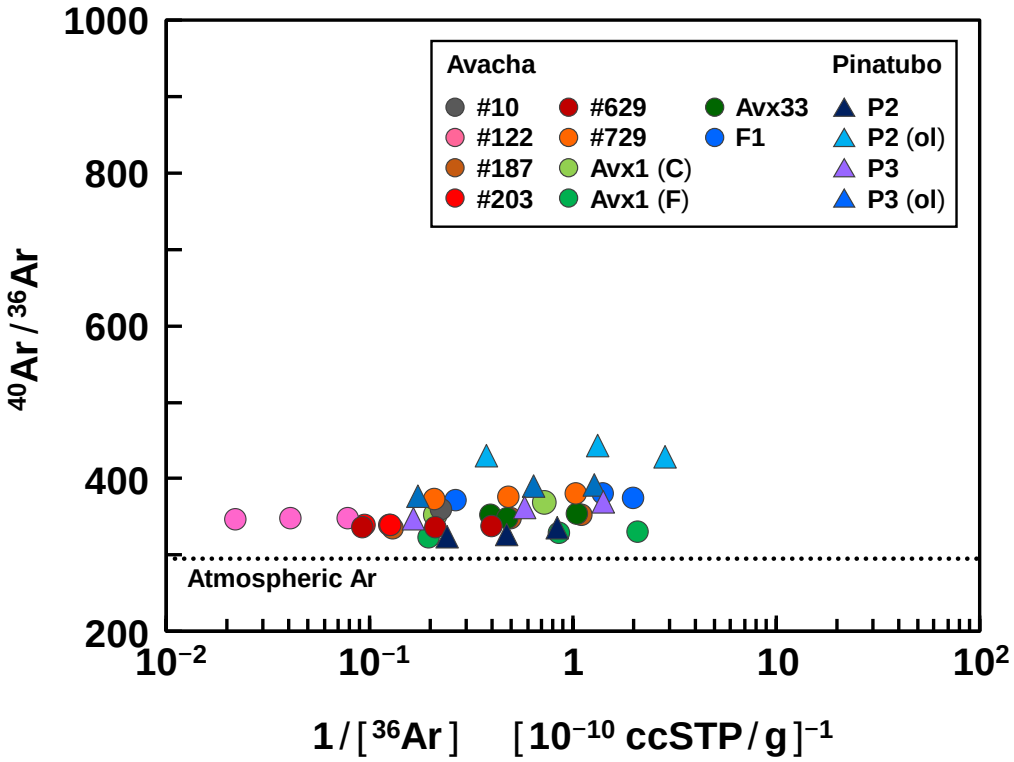

Figure 4.4. $^{40}Ar/^{36}Ar$ versus ^{36}Ar concentration for the studied samples. A dashed line represents the atmospheric $^{40}Ar/^{36}Ar$ ratio (296; Ozima and Podosek, 2002). Errors are 1σ.

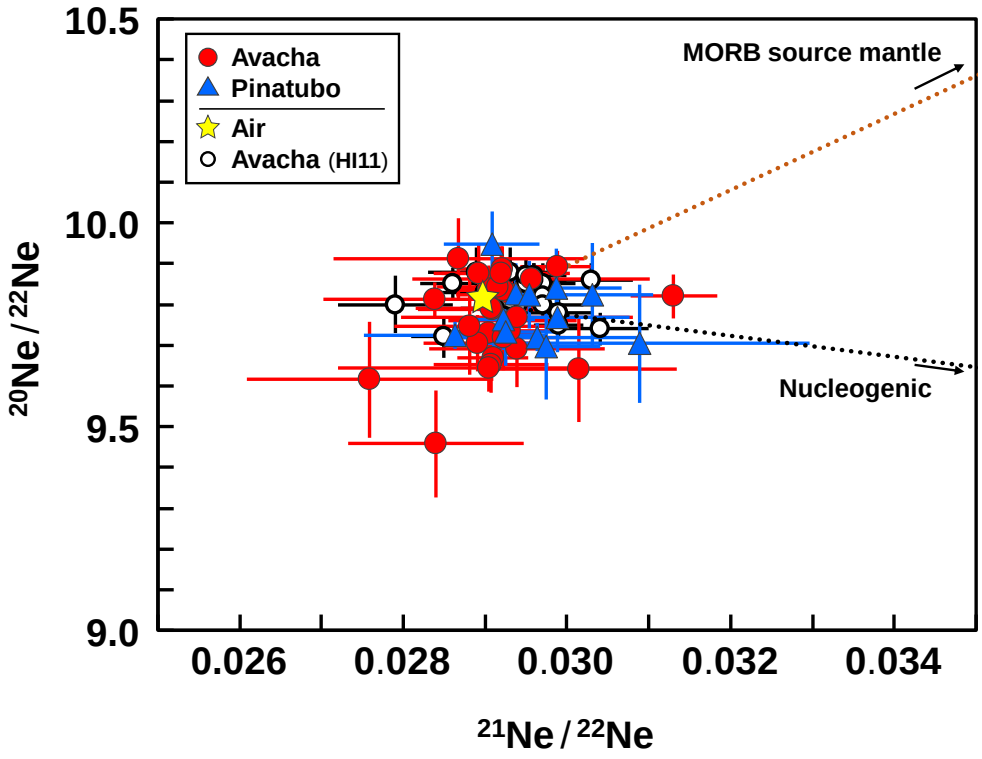

Figure 4.5. $^{20}Ne/^{22}Ne$ versus $^{21}Ne/^{22}Ne$ for the studied samples. Brown and black dashed lines are mixing lines between air, and the MORB source mantle ($^{20}Ne/^{22}Ne$ = 12.49 ± 0.04 and $^{21}Ne/^{22}Ne$ = 0.0578 ± 0.0003) and nucleogenic Ne ($^{20}Ne/^{22}Ne$ = 0 and $^{21}Ne/^{22}Ne$ = 0.469 ± 0.006), respectively. Errors are 1σ. Data sources: air and nucleogenic Ne (Ozima and Podosek, 2002), the MORB source mantle (Holland and Ballentine, 2006), and Avacha mantle xenoliths HI11 (Hopp and Ionov, 2011).

4.2.2.2. Elemental composition of noble gases

Elemental ratios of noble gases are presented in Tables 4.5 and 4.6. In 3D plots of $^{22}Ne/^{36}Ar$, $^{84}Kr/^{36}Ar$, and $^{132}Xe/^{36}Ar$ ratios (Figure 4.6), data of the studied samples plot between seawater and air. Previously, Hopp and Ionov (2011) obtained similar noble gas elemental ratios for Avacha mantle xenoliths and their data are shown for comparison in Figure 4.6.

The $^{4}He/^{40}Ar^{*}$ ratios (Figure 4.7; $^{40}Ar^{*} = \{(^{40}Ar/^{36}Ar)_{measured} - (^{40}Ar/^{36}Ar)_{air}\} \times {}^{36}Ar$) are 0.3–3.4 for Avacha, and 1.0–3.4 for Pinatubo. The range of these values overlap with $^{4}He/^{40}Ar^{*}$ ratio of MORB (1.5; Moreira et al., 1998) and the $^{4}He/^{40}Ar^{*}$ production ratio

in the MORB source mantle (1.6–4.2; Graham, 2002), which was estimated from K/U ratio (13000) and accumulation time (from 4.5 Gyr to $\gg 1/\lambda_{235U} \approx 1$ Gyr). Although some samples showed lower $^{4}He/^{40}Ar^{*}$ ratios, similarly low ratios were reported for Avacha mantle xenoliths (0.16–0.90; Hopp and Ionov, 2011) and those from various localities (Graham, 2002 and references therein).

Table 4.5. Elemental ratios of noble gases of mantle xenoliths from the Avacha volcano.

Sample	$^{22}Ne/^{36}Ar$	$^{84}Kr/^{36}Ar$	$^{132}Xe/^{36}Ar$	$^{4}He/^{40}Ar^{*}$
#10	0.0202 (15)	0.0410 (30)	0.00277 (27)	0.841 (60)
#122	0.0165 (12)	0.0354 (26)	0.00197 (16)	0.322 (23)
	0.0156 (11)	0.0364 (27)	0.00195 (15)	0.296 (21)
	0.0151 (11)	0.0361 (26)	0.00191 (19)	0.282 (20)
#187	0.0441 (31)	0.0339 (26)	0.00224 (26)	0.732 (52)
	0.0297 (21)	0.0364 (26)	0.00244 (31)	0.694 (49)
	0.0278 (20)	0.0382 (28)	0.00258 (23)	0.703 (50)
#203	0.0170 (12)	0.0342 (25)	0.00187 (24)	0.858 (62)
	0.0175 (12)	0.0349 (25)	0.00179 (16)	0.804 (57)
	0.0172 (12)	0.0353 (26)	0.00180 (20)	0.764 (54)
#629	0.0161 (11)	0.0363 (27)	0.00199 (17)	0.985 (70)
	0.0146 (10)	0.0364 (26)	0.00195 (18)	0.925 (66)
	0.01383 (99)	0.0363 (26)	0.00207 (20)	0.851 (61)
#729	0.0156 (11)	0.0435 (32)	0.00327 (29)	0.724 (51)
	0.0164 (12)	0.0438 (32)	0.00329 (32)	0.683 (49)
	0.01175 (84)	0.0450 (32)	0.00330 (28)	0.666 (47)
Avx1 C-part	0.0366 (26)	0.0340 (25)	0.00229 (25)	1.48 (11)
	0.0288 (20)	0.0392 (28)	0.00309 (26)	1.318 (94)
Avx1 F-part	0.0421 (30)	0.0301 (22)	0.00198 (24)	2.50 (18)
	0.0382 (28)	0.0321 (24)	0.00228 (20)	2.35 (17)
	0.0386 (28)	0.0347 (29)	0.00317 (29)	2.27 (17)
Avx33	0.0215 (15)	0.0349 (27)	0.00207 (16)	3.02 (21)
	0.0274 (19)	0.0330 (25)	0.00199 (20)	3.15 (22)
	0.0235 (17)	0.0339 (25)	0.00210 (28)	3.36 (24)

Table 4.5. (continued)

Sample	$^{22}Ne/^{36}Ar$	$^{84}Kr/^{36}Ar$	$^{132}Xe/^{36}Ar$	$^{4}He/^{40}Ar^*$
F1	0.0178 (13)	0.0440 (32)	0.00293 (24)	0.888 (63)
	0.0149 (11)	0.0459 (33)	0.00312 (37)	0.855 (61)
	0.0144 (10)	0.0417 (30)	0.00268 (22)	0.828 (59)

Errors are given as least significant figures in brackets at a 1σ level of confidence. $^{40}Ar^*$ is excess ^{40}Ar from atmospheric ratio, defined as $^{40}Ar^* = \{(^{40}Ar/^{36}Ar)_{measured} - (^{40}Ar/^{36}Ar)_{air}\} \times {}^{36}Ar$, where $(^{40}Ar/^{36}Ar)_{air} = 296$ (Ozima and Podosek, 2002).

Table 4.6. Elemental ratios of noble gases of mantle xenoliths from the Pinatubo volcano.

Sample	$^{22}Ne/^{36}Ar$	$^{84}Kr/^{36}Ar$	$^{132}Xe/^{36}Ar$	$^{4}He/^{40}Ar^*$
P2	0.0307 (22)	0.0303 (22)	0.00196 (17)	3.15 (22)
	0.0362 (26)	0.0284 (21)	0.00186 (20)	3.00 (21)
	0.0362 (26)	0.0292 (21)	0.00200 (17)	3.13 (23)
P2 olivine	0.0233 (17)	0.0362 (27)	0.00317 (29)	3.43 (24)
	0.0203 (15)	0.0381 (29)	0.00368 (28)	3.25 (23)
	0.0216 (16)	0.0399 (29)	0.00498 (60)	3.30 (23)
P3	0.0381 (27)	0.0287 (21)	0.00162 (15)	1.365 (97)
	0.0311 (22)	0.0315 (24)	0.00202 (24)	1.291 (92)
	0.0261 (19)	0.0355 (27)	0.00237 (22)	1.206 (86)
P3 olivine	0.0294 (21)	0.0324 (24)	0.00216 (24)	1.123 (80)
	0.0190 (14)	0.0366 (55)	0.00259 (24)	0.992 (70)
	0.0170 (12)	0.0371 (28)	0.00264 (26)	0.970 (69)

Errors are given as least significant figures in brackets at a 1σ level of confidence. $^{40}Ar^*$ is excess ^{40}Ar from atmospheric ratio, defined as $^{40}Ar^* = \{(^{40}Ar/^{36}Ar)_{measured} - (^{40}Ar/^{36}Ar)_{air}\} \times {}^{36}Ar$, where $(^{40}Ar/^{36}Ar)_{air} = 296$ (Ozima and Podosek, 2002).

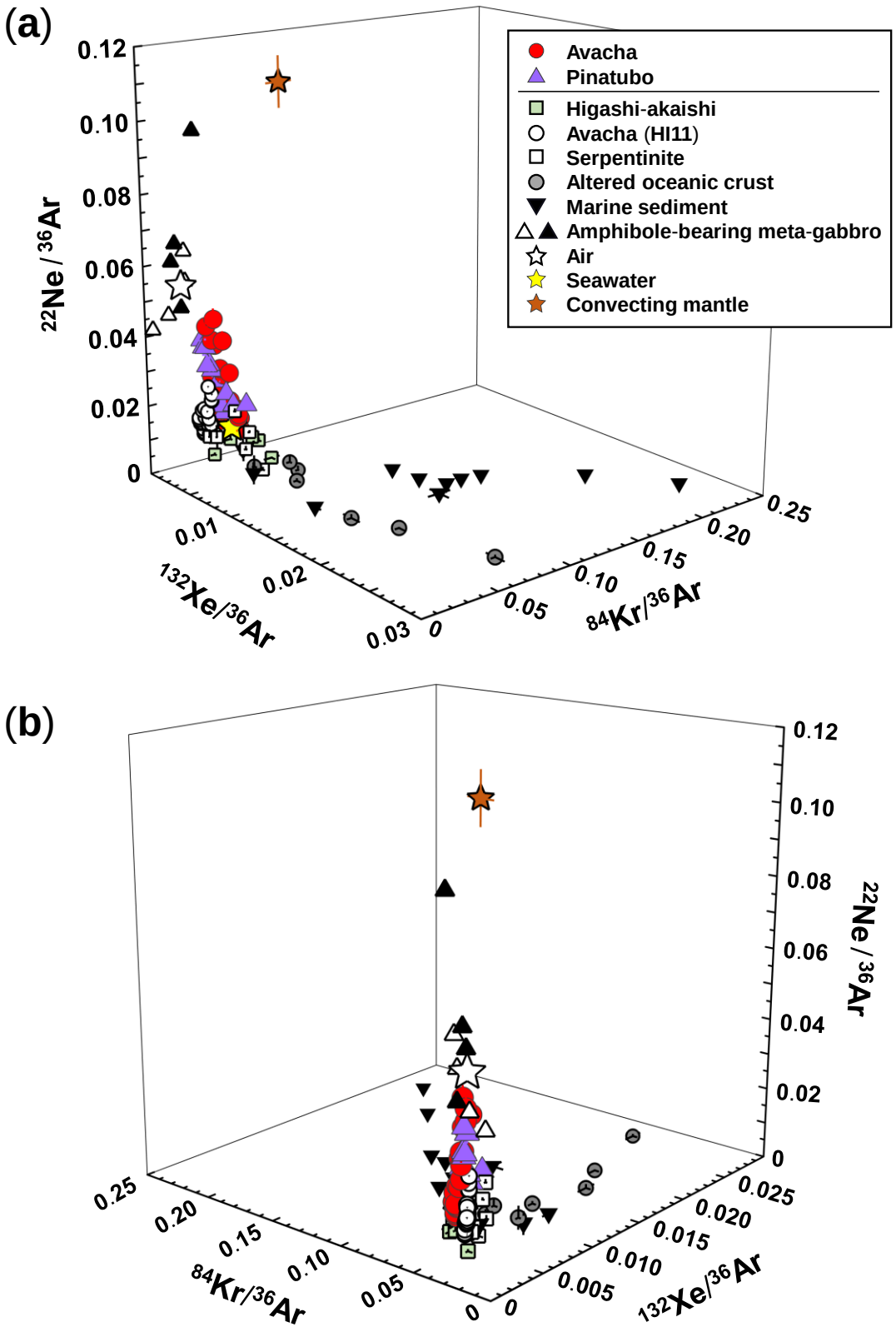
(a)
Avacha
Pinatubo
Higashi-akaishi
Avacha (HI11)
Serpentinite
Altered oceanic crust
Marine sediment
Amphibole-bearing meta-gabbro
Air
Seawater
Convecting mantle
22Ne/36Ar
0.12
0.10
0.08
0.06
0.04
0.02
0
132Xe/36Ar
0.01
0.02
0.03
0
84Kr/36Ar
0.05
0.10
0.15
0.20
0.25
(b)
22Ne/36Ar
0.12
0.10
0.08
0.06
0.04
0.02
0
84Kr/36Ar
0.25
0.20
0.15
0.10
0.05
0
132Xe/36Ar
0
0.005
0.010
0.015
0.020
0.025

Figure 4.6.

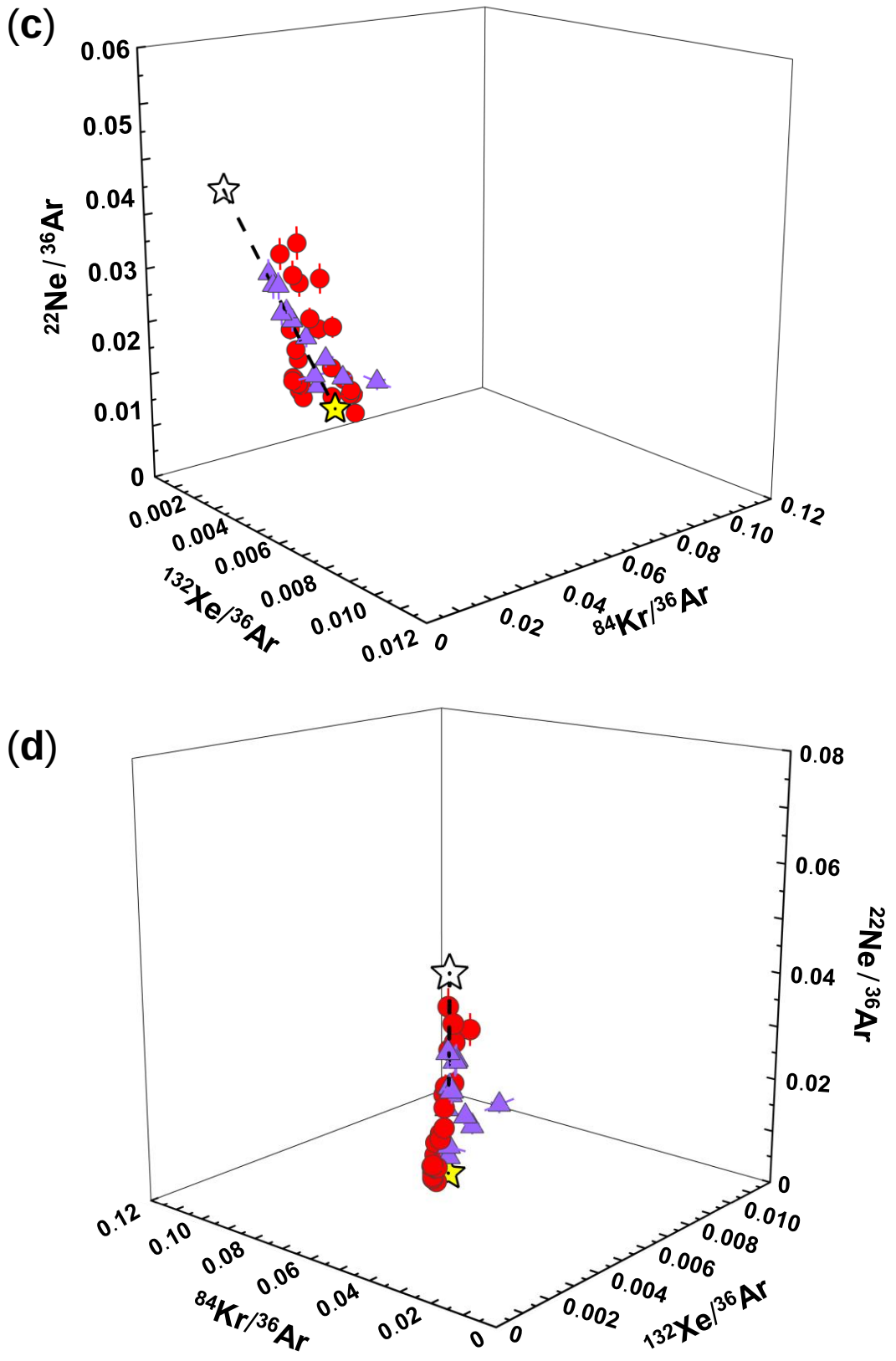

Figure 4.6. (continued)

Figure 4.6. $^{22}Ne/^{36}Ar$ versus $^{84}Kr/^{36}Ar$ versus $^{132}Xe/^{36}Ar$ for the samples from volcanic fronts. (b) is a rotation of (a). (c) and (d) are magnifications of (a) and (b), respectively, including only data of the volcanic front samples which lie close to a mixing line between air and seawater (dashed line). Errors are 1σ. Data sources: air and seawater at 0 °C (Ozima and Podosek, 2002), the convecting mantle (Holland and Ballentine, 2006), Higashi-akaishi peridotites from Sanbagawa metamorphic belt (Sumino et al., 2010), Avacha sample HI11 (Hopp and Ionov, 2011), marine sediments (Matsuda and Nagao, 1986; Staudacher and Allègre, 1988), serpentinites (Kendrick et al., 2011, 2013b), altered oceanic crust (Chavrit et al., 2016; Staudacher and Allègre, 1988), and amphiboles in meta-gabbros (open triangles) and relict minerals and quartz-epidote veins in meta-gabbros (black triangles) (Kendrick et al., 2015a).

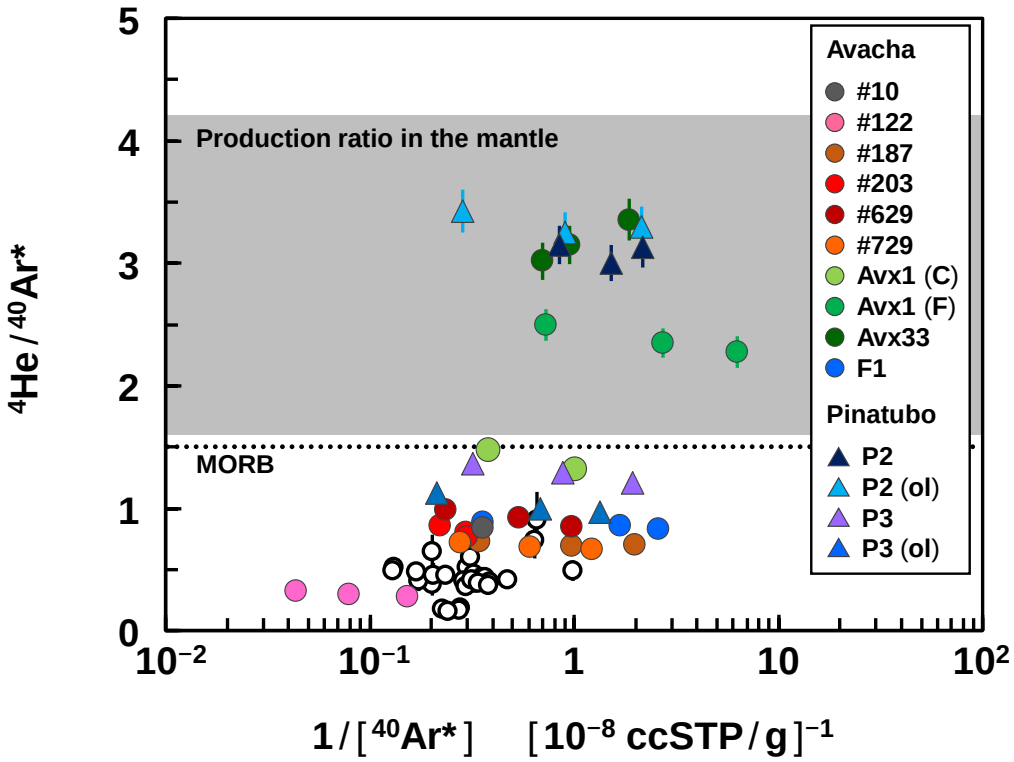

Figure 4.7. $^{4}He/^{40}Ar^{*}$ versus $^{40}Ar^{*}$ concentration for the studied samples. Data obtained during stepwise crushing of each sample are shown in same symbol. Shaded area is the range of the production ratio in the MORB source mantle (Graham, 2002). A dashed line is a $^{4}He/^{40}Ar^{*}$ ratio of MORB (Moreira et al., 1998). Errors are 1σ. Data source: Avacha sample HI11 (Hopp and Ionov, 2011).

4.2.3. Cl/H_2O and $^{36}Ar/H_2O$ ratios of fluid inclusions

Cl/H_2O and $^{36}Ar/H_2O$ ratios of fluid inclusions are presented in Table 4.7. The salinity (Cl/H_2O ratio) of the H_2O-rich fluid inclusions has been determined in olivine from the mantle xenolith samples using microthermometry (Ishimaru, personal comm.; Kawamoto et al., 2013). The $^{36}Ar/H_2O$ values are derived using the following relationship:

$$\frac{^{36}\mathrm{Ar}}{\mathrm{H_2O}} = \left(\frac{\mathrm{Cl}}{\mathrm{H_2O}}\right) \times \left(\frac{^{40}\mathrm{Ar}}{\mathrm{Cl}}\right)_{\mathrm{irradiated,crushed}} \Big/ \left(\frac{^{40}\mathrm{Ar}*}{^{36}\mathrm{Ar}}\right)_{\mathrm{unirradiated}} \quad (4.1)$$

$$\left(\frac{^{40}\mathrm{Ar}*}{^{36}\mathrm{Ar}}\right)_{\text{unirradiated}} = \left(\frac{^{40}\mathrm{Ar}}{^{36}\mathrm{Ar}}\right)_{\text{measured}} - \left(\frac{^{40}\mathrm{Ar}}{^{36}\mathrm{Ar}}\right)_{\text{air}} \quad (4.2)$$

In the above equation, (^{40}Ar*/^{36}Ar) of unirradiated samples is preferred because they are considered to be least air-contaminated, i.e. they were heated at 800 °C prior to crushing without being exposed to air between heating and crushing. Nevertheless, as discussed in section 4.3.1, some air contamination is present. The correlation of ^{22}Ne/^{36}Ar, ^{84}Kr/^{36}Ar, and ^{132}Xe/^{36}Ar between air and seawater (Figure 4.6) enables the correction of air contamination to ^{36}Ar by fitting the ^{22}Ne/^{36}Ar ratios to the seawater value. The air contamination-corrected ^{36}Ar/H_2O ratios are listed in Table 4.7.

The Cl/H_2O and ^{36}Ar/H_2O ratios of the studied fluid inclusions are compared with those of sedimentary pore fluid, serpentine from forearc and the oceanic lithosphere, fluids released from serpentine during first stage of stepwise dehydration, and fluid inclusions in quartz veins in metapelites from Besshi, Sanbagawa metamorphic belt (Figure 4.8). The fluid inclusions in quartz veins in metapelites from the Besshi, Sanbagawa metamorphic belt, are regarded as representing fluids captured during the prograde path, or near the peak metamorphic stage of subduction (Yoshida and Hirajima, 2012). Halogen and noble gas signatures of these fluid inclusions are also sedimentary pore fluid-like and almost identical to those of the Higashi-akaishi peridotites (Sumino et al., 2010, 2011).

The Cl/H_2O ratios of marine sedimentary pore fluids are almost identical to that of seawater, because only Br and iodine are released from organic materials in marine sediment (e.g., Fehn et al., 2006), and I assume ^{36}Ar/H_2O ratios of marine sedimentary pore fluids are equivalent to that of seawater. I calculated the Cl/H_2O and ^{36}Ar/H_2O ratios of serpentine from the Cl and ^{36}Ar concentrations of serpentinites, the degree of serpentinization in each serpentinite (Kendrick et al., 2011, 2013b), and the chemical formula of serpentine (13 wt.% of H_2O). The Cl/H_2O and ^{36}Ar/H_2O ratios of the fluid inclusions in metapelites were calculated using the same method as for the studied fluid inclusions.

The Cl/H_2O and $^{36}Ar/H_2O$ ratios of the studied fluid inclusions are similar to or higher than those of sedimentary pore fluid and significantly higher than those of serpentine in the oceanic lithosphere (Figure 4.8). The Cl/H_2O and $^{36}Ar/H_2O$ ratios of the fluids released during the first stage of serpentine dehydration increase by an order of magnitude from those of serpentine (Kendrick et al., 2011). The range of $^{36}Ar/H_2O$ ratios of the studied fluid inclusions is overlapping with that of the fluid inclusions in the Sanbagawa metapelites.

Table 4.7. Ratios of chlorine, ^{36}Ar and H_2O (in units of mol/mol).

Sample	Cl/H_2O (10^{-2})	$^{36}Ar/H_2O$ (10^{-9})	$Cl/^{36}Ar$ (10^6)
Avacha			
#203 (n = 11)	0.60 (29)	15.3 (75)	0.389 (31)
air contamination-corrected		*13.7 (67)*	*0.434 (35)*
#629 (n = 28)	0.72 (32)	19.9 (88)	0.365 (32)
air contamination-corrected		*19.0 (84)*	*0.382 (34)*
#729 (n = 22)	2.04 (69)	16.2 (56)	1.253 (94)
air contamination-corrected		*16.2 (56)*	*1.253 (97)*
F1 (n = 42)	2.6 (15)	3.2 (19)	8.32 (84)
air contamination-corrected		*3.0 (18)*	*8.78 (89)*
Pinatubo			
P3 (n = 33)	1.65 (32)	4.7 (12)	3.49 (60)
air contamination-corrected		*3.18 (83)*	*5.20 (89)*
P3 olivine (n = 33)	1.65 (32)	2.64 (55)	6.28 (46)
air contamination-corrected		*2.23 (47)*	*7.41 (55)*
Seawater (0°C)	0.98	1.03	9.57

Errors are given as least significant figures in brackets at a 1σ level of confidence. Italics used for air contamination-corrected data. n: number of analyzed fluid inclusions for salinity determinations (Ishimaru, personal comm.; Kawamoto et al., 2013). Data sources: Cl/H_2O ratios in fluid inclusions (Ishimaru, personal comm.; Kawamoto et al., 2013) and seawater at 0 °C (Bruland and Lohan, 2014; Ozima and Podosek, 2002).

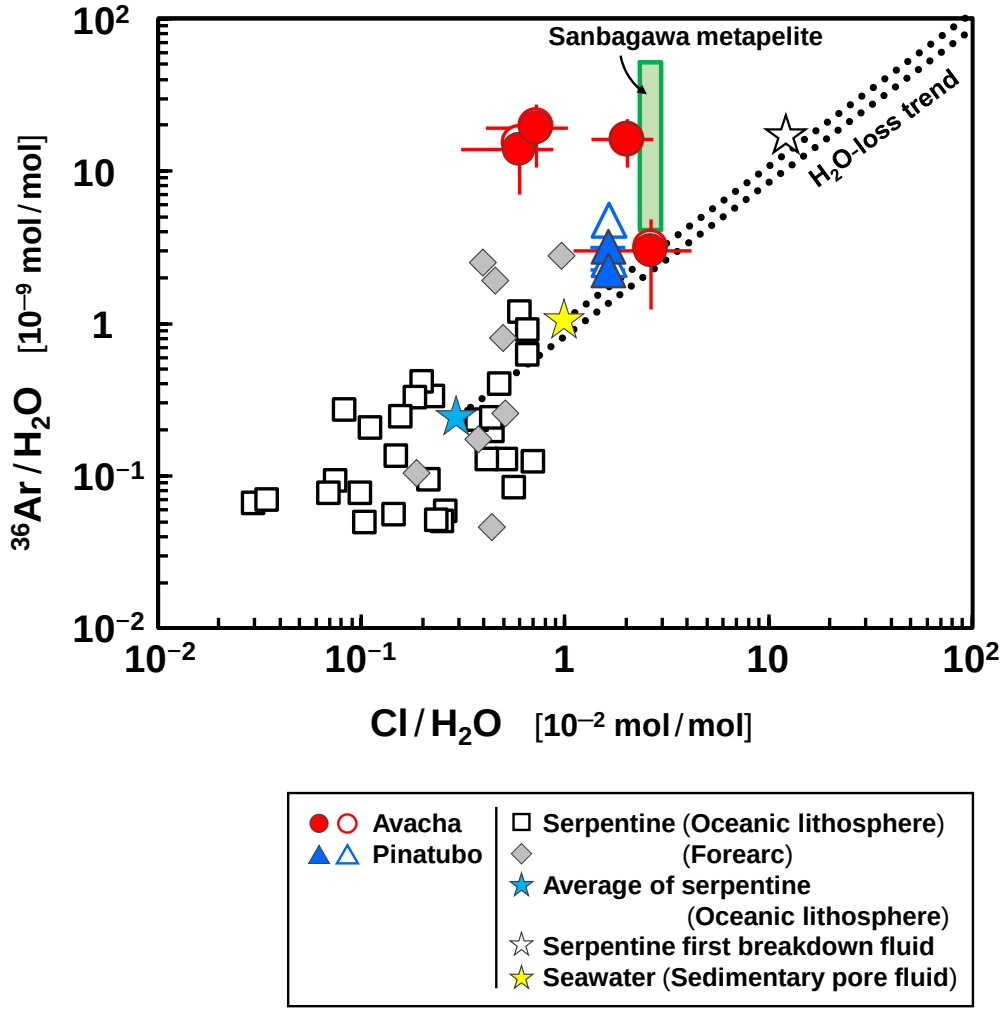

Figure 4.8. $^{36}Ar/H_2O$ versus Cl/H_2O. Solid symbols for Avacha and Pinatubo represent data corrected for ^{36}Ar contamination from air, based on the $^{22}Ne/^{36}Ar$ ratios, open symbols are uncorrected values. Dashed lines are fractionation lines corresponding to simple H_2O loss from starting compositions of seawater and serpentine. Errors are 1σ (errors for uncorrected data are not shown for clarity). Data sources: fluid inclusions in quartz veins in metapelites (shown in green box) from Besshi, Sanbagawa metamorphic belt (Sumino et al., 2011; Yoshida and Hirajima, 2012), serpentine (Kendrick et al., 2011, 2013b), fluids released from serpentine during first stage of stepwise dehydration (Serpentine first breakdown fluids) (Kendrick et al., 2011), and seawater at 0 °C (Bruland and Lohan, 2014; Ozima and Podosek, 2002).

4.3. Discussion

4.3.1. Noble gases in the mantle xenoliths from volcanic fronts

The studied samples showed atmospheric $^{40}Ar/^{36}Ar$ and MORB-like $^{3}He/^{4}He$ ratios (Tables 4.3 and 4.4, Figure 4.4). Because He, especially ^{3}He, is depleted in air and relatively enriched in the mantle (Porcelli et al., 2002; Ozima and Podosek, 2002), ^{3}He can be regarded as a pure mantle component. The amounts of ^{3}He obtained for crushing steps from each sample show a clear positive correlation with those of ^{36}Ar (Figure 4.9). This indicates that ^{36}Ar and ^{3}He have not been decoupled in the studied fluid inclusions, i.e., the atmospheric Ar is a subducted component present in the mantle wedge (Matsumoto et al., 2001).

The 3D diagram of $^{22}Ne/^{36}Ar$-$^{84}Kr/^{36}Ar$-$^{132}Xe/^{36}Ar$ (Figure 4.6) indicates overwhelming contributions from air- and seawater-derived components to the studied samples, although the data show a slight deviation from the mixing line between air and seawater towards high Kr/Ar and Xe/Ar and/or high Ne/Ar values. This 3D diagram also indicates a negligible contribution of the altered oceanic crust or marine sediment-related noble gases. Deviation from the air–seawater mixing cannot be explained by mantle-derived noble gases because the atmospheric Ne isotopic ratios of the samples (Figure 4.5) indicates limited contribution from mantle-derived noble gases except for He and $^{40}Ar^{*}$, which are scarce in air and seawater. Mass-dependent fractionation can account for increasing Kr/Ar and Xe/Ar values. However, this process is ruled-out because it should lead to Ne/Ar ratios lower than the air value, and this is the opposite to that observed in Figure 4.6.

During stepwise crushing, most of the samples showed constant $^{40}Ar/^{36}Ar$ and $^{132}Xe/^{36}Ar$ ratios, or a linear correlation between these ratios extending from the unfractionated air value (Figure 4.10a). Such relationships were also observed between $^{40}Ar/^{36}Ar$, and $^{84}Kr/^{36}Ar$ and $^{22}Ne/^{36}Ar$ ratios (Figures 4.10bc). These relationships support that the $^{22}Ne/^{36}Ar$-$^{84}Kr/^{36}Ar$-$^{132}Xe/^{36}Ar$ data are explained by simple mixing between unfractionated air and seawater.

The origin of the unfractionated air-like component is unclear at present; however, it is possible that some over-pressured fluid inclusions ruptured during ascent in the crust

or during eruption, and were subsequently refilled with air-derived noble gases that penetrated along microfractures before resealing of the inclusions (Ballentine and Barfod, 2000). If the air-like component was incorporated into the samples close to and/or at the Earth's surface, then the original noble gas elemental ratios of the samples were seawater-like. This interpretation seems to conflict with the correlation between ^{3}He and ^{36}Ar. The influence of air contamination in the studied samples may be too small to observe in the scale of Figure 4.9.

As mentioned above, He is depleted in air and also in seawater (Porcelli et al., 2002; Ozima and Podosek, 2002). The MORB-like He in the studied samples (Tables 4.3 and 4.4) can be regarded as acquired from the ambient mantle by slab-derived-fluid, of which noble gas compositions were seawater-like. Although their range overlaps with the data obtained in this study, Hopp and Ionov (2011) reported lower $^{3}He/^{4}He$ ratios for Avacha mantle xenoliths. They suggested that the lower $^{3}He/^{4}He$ values of Avacha xenoliths were a feature of the continental lithospheric mantle beneath the Avacha volcano reflecting a higher $(U+Th)/^{3}He$ ratio than the MORB source mantle due to ancient metasomatism. The fluid inclusions in each Avacha sample studied here showed identical $^{3}He/^{4}He$ ratios during stepped crushing (weighted RSD = 0.5–1%), whereas the $^{3}He/^{4}He$ ratios reported by Hopp and Ionov (2011) showed a greater range (weighted RSD = 4–14%) (Figure 4.11). The larger variation in the He isotope data obtained by Hopp and Ionov (2011) may indicate that two or more He components are present in the mantle beneath the Avacha volcano, although only one component is observed in this study.

Because there is no $^{40}Ar^{*}$ in seawater and air due to its definition (Eq. 4.2), $^{40}Ar^{*}$ can be considered to be derived from the ambient mantle like as He. Contributions of $^{40}Ar^{*}$ from oceanic crust and/or sediment can potentially explain the low $^{4}He/^{40}Ar^{*}$ ratios because these materials also contain $^{40}Ar^{*}$. However, this is rejected on the basis that it is inconsistent with the other noble gas data (Figure 4.6). $^{4}He/^{40}Ar^{*}$ ratios can be fractionated by different processes in the mantle. Kinetic fractionation of noble gases during melting may account for lower $^{4}He/^{40}Ar^{*}$ ratios (Burnard, 2004, Yamamoto et al., 2009a). Since lighter noble gases diffuse faster, preferential diffusion of He into the melt during melt extraction results in a lower $^{4}He/^{40}Ar^{*}$ ratio in the residual mantle (Burnard,

2004; Yamamoto et al., 2009a). Alternatively, solubility-controlled fractionation can also explain the low $^{4}He/^{40}Ar^{*}$ ratio of the mantle because different solubilities of He and Ar into melt (Heber et al., 2007) result in more depletion of He in the residual mantle than Ar. Hopp and Ionov (2011) suggested that fluids exsolved from melt would have lower $^{4}He/^{40}Ar^{*}$ ratio than the melt because He is more soluble in silicate melt than Ar (Herber et al., 2007). Hopp and Ionov (2011) also argued that noble gas elemental ratios (e.g., $^{132}Xe/^{36}Ar$) in Avacha mantle xenoliths were also fractionated during the fluid exsolution process. However, as discussed earlier, I argue that small variations in noble gas elemental ratios of the Avacha (and Pinatubo) samples resulted from incorporation of unfractionated air into fluid inclusions during and/or after eruption. Because the fluid inclusions in the studied samples are expected to preserve seawater-like elemental ratios of Ne, Ar, Kr, and Xe without significant fractionation, fractionation between He and Ar after fluid entrapment is excluded. The mantle beneath arcs has experienced several melt extraction events and as a response the mantle wedge would develop low $^{4}He/^{40}Ar^{*}$ ratios. Therefore, the mantle wedge may have had low $^{4}He/^{40}Ar^{*}$ ratio before the studied slab-derived fluids migrated in the mantle wedge.

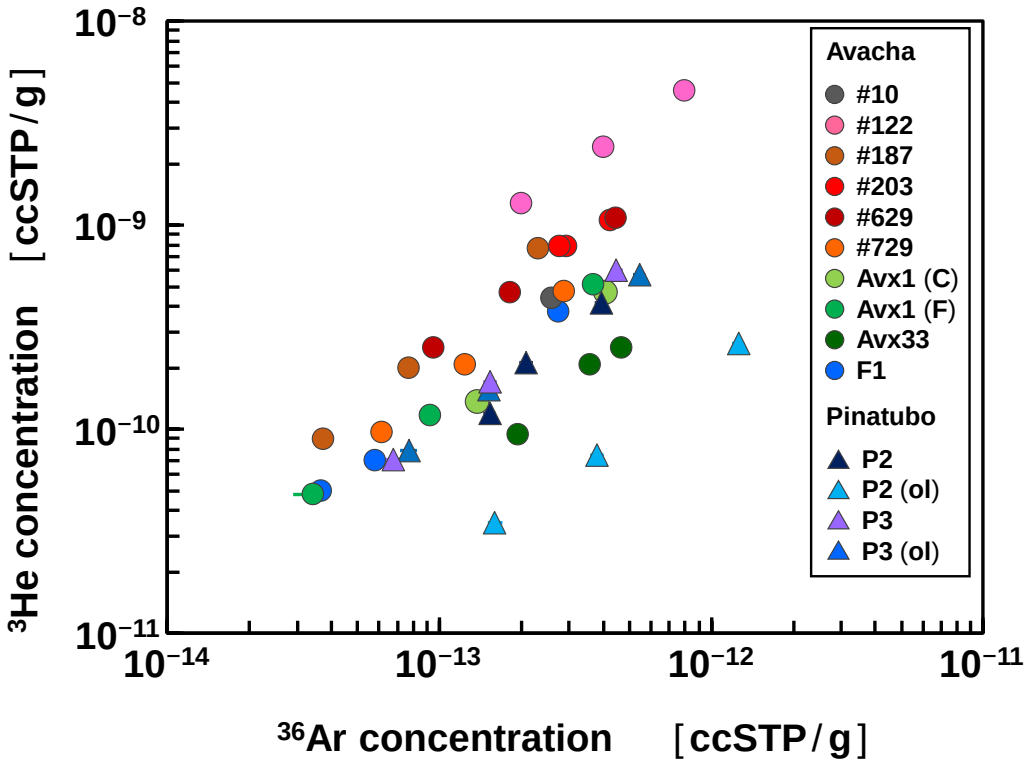

Figure 4.9. ^{3}He concentration versus ^{36}Ar concentration for the studied samples. Data obtained for crushing steps from each sample are shown in same symbol. Errors are 1σ.

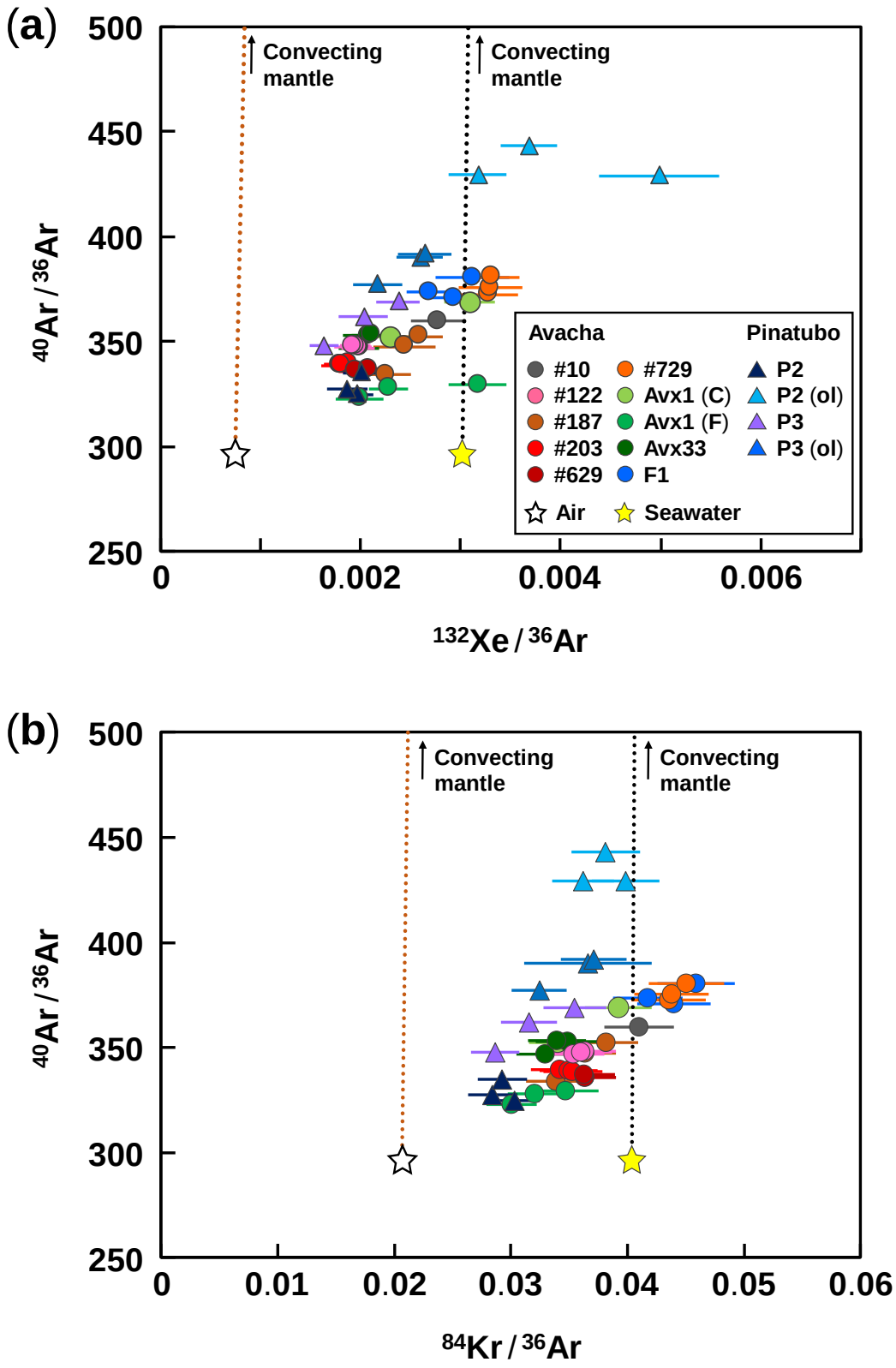
(a)
Convecting mantle
Convecting mantle
Avacha
Pinatubo
#10
#122
#187
#203
#629
#729
Avx1 (C)
Avx1 (F)
Avx33
F1
P2
P2 (ol)
P3
P3 (ol)
Air
Seawater
500
450
400
350
300
250
0
0.002
0.004
0.006
40Ar / 36Ar
132Xe / 36Ar
(b)
Convecting mantle
Convecting mantle
500
450
400
350
300
250
0
0.01
0.02
0.03
0.04
0.05
0.06
40Ar / 36Ar
84Kr / 36Ar

Figure 4.10.

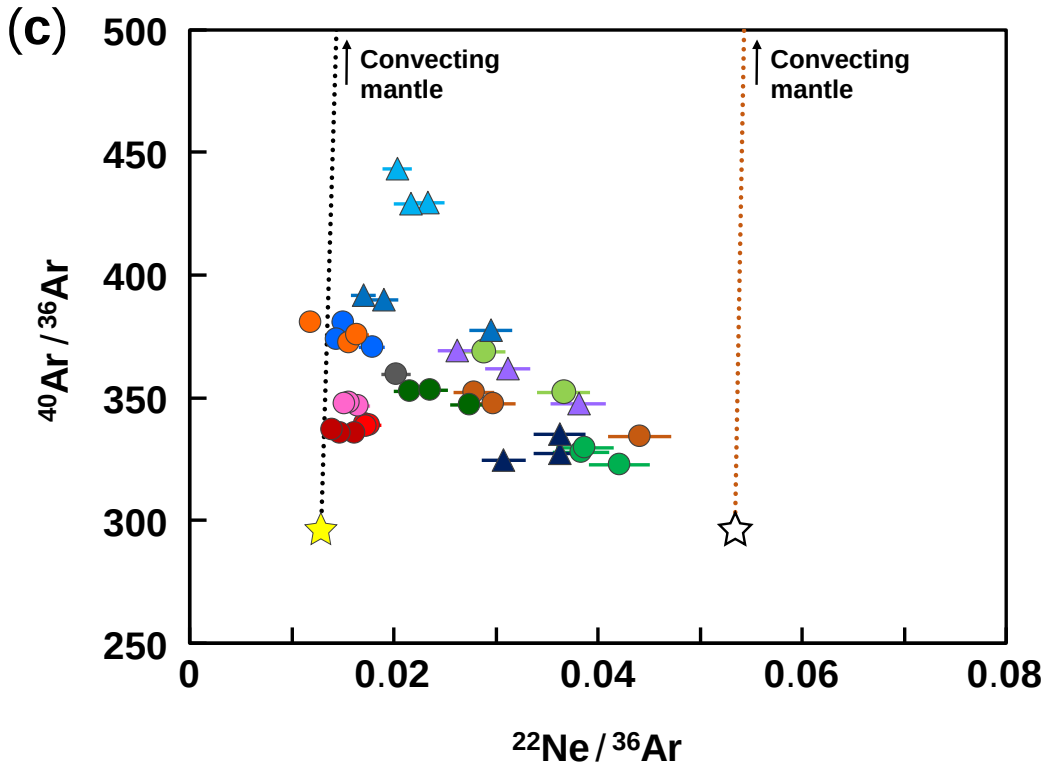

Figure 4.10. $^{40}Ar/^{36}Ar$ versus (a) $^{132}Xe/^{36}Ar$, (b) $^{84}Kr/^{36}Ar$, and (c) $^{22}Ne/^{36}Ar$. Brown and black dashed lines are mixing lines between the convecting mantle, and unfractionated air and seawater at 0 °C, respectively. Errors are 1σ. Data sources: air and seawater at 0 °C (Ozima and Podosek, 2002), and the convecting mantle (Holland and Ballentine, 2006).

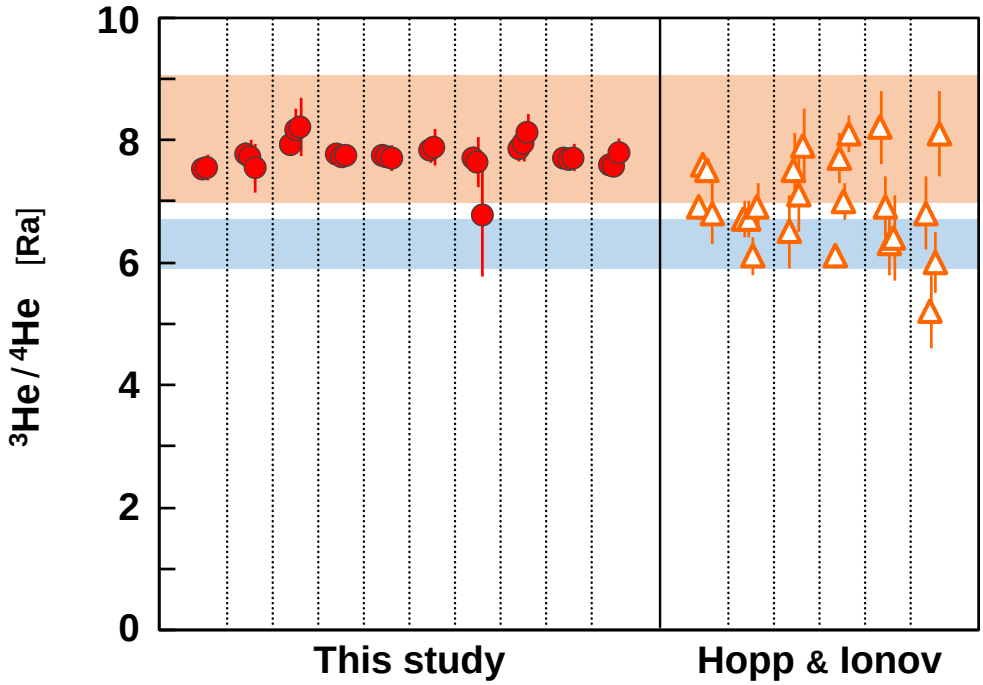

Figure 4.11. $^3He/^4He$ obtained in this study and Hopp and Ionov (2011). The data obtained during stepwise crushing of each sample are plotted in same columns. The ranges shown by red and blue are those of $^3He/^4He$ ratios of the MORB source mantle (Moreira and Kurz, 2013) and European subcontinetal lithospheric mantle (Gautheron et al., 2005), respectively. Errors are 1σ.

4.3.2. Halogens in the mantle xenoliths from volcanic fronts

Small deviation from the sedimentary pore fluid trend toward higher I/Cl ratios was observed in the Avacha samples (Figure 4.3). Similar deviations in Higashi-akaishi peridotites and serpentinites from the Mariana forearc were attributed the iodine enrichment to breakdown of organic matter in sediments (Kendrick et al., 2013b; Sumino et al., 2010). However, because a contribution form marine sediment-derived noble gases is limited in the Avacha samples (Figure 4.6), I argue that the iodine enrichment in the Avacha samples resulted from small fractionation of halogens during subduction processes rather than break down of sedimentary materials as discussed in section 4.3.3.2. The small fractionation of halogens is also supported by a relatively large (factor of two) variation in the I/Cl ratios of the Avacha samples.

However, even after small fractionation of halogens, their elemental ratios are similar to sedimentary pore fluids and serpentinites. The interpretation for a sedimentary pore fluid origin for halogens is entirely consistent with the noble gas data as discussed in the previous section because sedimentary pore fluid is expected to be equivalent to seawater about noble gases. Moreover, their high I/Cl and relatively seawater-like Br/Cl ratios are difficult to explain by an alternative simple fractionation process, although it is noted in this respect that there is a limited available halogen partitioning data under mantle conditions (Bureau et al., 2000, 2016). Therefore, I argue that the consistency between halogen and noble gas signatures is strong evidence that the halogen and noble gas signatures derived from sedimentary pore fluid have been preserved during the subduction processes without significant fractionation.

Most of samples showed lower I/Cl and Br/Cl ratios during heating compared to crushing (Table 4.1 and 4.2, Figure 4.3), suggesting the presence of an additional halogen host phase(s) in the bulk rock. Amphibole is reported to be present in the studied mantle xenoliths (Ishimaru et al., 2007; Kawamoto et al., 2013). Amphibole may potentially contain relatively high Cl concentrations associated with low Br/Cl and I/Cl ratios. Although it was not collected from a mantle xenolith, Cl concentration of Hb3gr hornblende, one of irradiation monitors, is high (2379 ppm; Roddick, 1983). I analyzed halogens of Hb3gr using NI-NGMS and obtained low Br/Cl and I/Cl ratios, 0.00497–0.00606 × 10^{-3} mol/mol and 1.66–3.25 × 10^{-6} mol/mol, respectively. Kendrick (2012) also reported low Br/Cl and I/Cl ratios for Hb3gr, 0.015–0.167 × 10^{-3} mol/mol and 1.42–12.10 × 10^{-6} mol/mol, respectively (the values were recalculated using revised values for scapolite monitors in Kendrick et al., 2013a). However, the Cl concentrations of amphibole in the Avacha and Pinatubo samples determined by EPMA, which were analyzed by Dr. Satoko Ishimaru of Kumamoto University, are low (≤400 ppm) or below detection limit (130 ppm). The low Cl concentrations in amphibole and low modal amounts of this mineral in the mantle xenolith samples (<2.5%, mostly <1.0% in the Avacha samples; Ishimaru et al., 2007) require the presence of an additional Cl-bearing phase(s). Silicate glass present in some Avacha xenoliths (Ishimaru et al., 2007; Ishimaru and Arai, 2009) contains 1000–2000 ppm of Cl and is likely to have low Br/Cl and I/Cl

ratios. Olivine separates of the Pinatubo samples yield comparable I/Cl and Br/Cl ratios during heating and crushing (Table 5.2), indicating that fluids are the only source of halogens contained in this mineral phase. However, irrespective of halogen variation between fluid and bulk compositions, the halogen compositions of the samples remain overwhelmingly dominated by a marine sedimentary pore fluid signature carried by the fluid.

4.3.3. Subduction mechanism of marine sedimentary pore fluid-derived volatiles

Sedimentary pore fluid-like signatures of halogens and noble gases are considered to be preserved during subduction processes. These signatures are present in two different subduction zones, which show a strong contrast in the thermal structures of their subducting slabs (van Keken et al., 2011). This suggests that subduction of sedimentary pore fluid-derived noble gases and halogens is a ubiquitous phenomenon in modern subduction zones and that its influence is not necessarily restricted to the interface between the mantle wedge and subducting slab (Sumino et al., 2010) and the influence significantly extends into the mantle wedge beneath volcanic fronts.

Despite having distinctly different solubilities in H_2O-rich fluids and silicate minerals, noble gases and halogens retain their primary sedimentary pore fluid signature. This indicates that they are not decoupled during volatile cycling in the mantle wedge. In other words, sedimentary pore fluid-derived water may be subducted and supplied to the mantle wedge directly as a free fluid phase, trapped either as fluid inclusions and/or as fluids in the pore spaces of a slab, or that they are being transported by a hydrous mineral capable of retaining the sedimentary pore fluid-like signatures. Subduction of a free fluid phase is considered unlikely because the pore spaces of sediments collapse at shallow subduction levels due to compaction, resulting in an insignificant flux of water into the mantle by this process (e.g., Jarrard, 2003). Hyndman and Peacock (2003) also suggested that the flux of water carried by pore spaces of sediments and basalts is insignificant beneath volcanic fronts even in a cold subduction zone. Serpentinites are known to show sedimentary pore fluid-like signatures (John et al., 2011; Kendrick et al., 2011, 2013b).

However, the Cl/H_2O and $^{36}Ar/H_2O$ ratios of the fluid inclusions are distinctly different from those of serpentine (Figure 4.8).

It is possible that the composition of the slab-derived fluids was modified following release from the slab and prior to being trapped as fluid inclusions in the peridotite studied here. Because of the high diffusivity of H under the mantle condition (e.g., Ingrin and Blanchard, 2006), any loss of this element from fluid inclusions would increase Cl/H_2O and $^{36}Ar/H_2O$ ratios after the fluids were trapped. However, the Cl/H_2O and $^{36}Ar/H_2O$ ratios of the studied fluid inclusions do not follow H_2O-loss lines from seawater and serpentine values (Figure 4.8). This indicates that simple H-loss cannot account for the Cl/H_2O and $^{36}Ar/H_2O$ ratios of these fluid inclusions. Because of the distinct geochemical behaviors of Cl, ^{36}Ar, and H_2O, Cl/H_2O and $^{36}Ar/H_2O$ ratios can be relatively easy to fractionate compared to elemental ratios of halogens and noble gases. The fluid inclusions of the Sanbagawa quartz vein also showed high $^{36}Ar/H_2O$ ratios with a range overlapping with those of mantle xenoliths. This may indicate most of the fractionation took place within the slab during fluid migration, although the fluid inclusions were trapped by mantle minerals at several tens of km above the subducting slabs.

It is unlikely that halogens and noble gases preserve their primary signatures even after large fractionation processes. As shown in Figure 4.8, the Cl/H_2O and $^{36}Ar/H_2O$ ratios of the fluids released during the first stage of serpentine dehydration increase by an order of magnitude. However, this stepwise dehydration involves halogen fractionation (John et al., 2011; Kendrick et al., 2011). This is inconsistent with the halogen signatures of the studied fluid inclusions (Figure 4.3). Although some relative enrichment in Cl and ^{36}Ar are still required, it is apparent that the extent of fractionation from seawater is much less than from serpentine.

4.3.3.1. Mechanism of volatile incorporation into oceanic plates

In conventional subduction concepts, volatile species are incorporated into hydrous minerals formed in an open system with an essentially infinite water-rock (W/R) ratio (Figure 4.12a). The chemical compositions in those hydrous minerals are controlled by partitioning behavior of each element between the minerals and the water source. Under

high W/R ratio, the chemical composition of dissolved components in the water is at steady state and concentrations of incompatible elements in hydrous minerals, especially noble gases, will be kept low and constant during hydrous mineral formation. In contrast, hydration in a closed system with a very low W/R ratio results in minimal change, not only in noble gas and halogen compositions, but also in the ratios of incompatible elements to water, because all of the water and dissolved species are eventually incorporated into the hydrous mineral unless they reach mineral saturation levels. Although the chemical composition of the hydrous minerals formed in a closed system may also be controlled by partitioning behavior of each elements at least in small scale, the compositions of the original water will be preserved within the whole of the closed system.

Closed system hydration may occur at the slab outer rise, where oceanic plates bend prior to entering subduction zones and the bending forms faults (Figure 4.12b). Seawater and/or sedimentary pore fluid are thought to be incorporated into the mantle layer via faults (Peacock, 2001; Ranero et al., 2003). Based on numerical experiments, Faccenda et al. (2009) suggested that subhydrostatic conditions or pressure gradient pumping of water into the mantle occurs along the faults formed at the slab outer rise. The injected fluids react with the oceanic crust and mantle surrounding the faults to form hydrous minerals (Faccenda et al., 2009). In this environment, if hydration is faster than exchanging of water with its external source due to a low W/R ratio, then the water injected along the faults will be chemically isolated from the external source (Figure 4.12b). This hydration mechanism would effectively be in a closed system and the original Cl/H_2O and $^{36}Ar/H_2O$ ratios of the injected sedimentary pore water will be preserved in the newly formed hydrous minerals.

Hydrous minerals such as serpentine have a ring structure formed by their SiO_4 network, where significant amounts of noble gases can be incorporated (Jackson et al., 2013, 2015). Although most of seafloor and forearc serpentine showed low Cl/H_2O and $^{36}Ar/H_2O$ ratios (Figure 4.8), serpentine with higher ratios than those of sedimentary pore fluids has also been found (Kendrick et al., 2013b; Sharp and Barnes, 2004). This evidence in natural samples indicates that serpentine has enough capacity to incorporate

halogens and noble gases in order to preserve the original compositions of sedimentary pore fluid in a closed system.

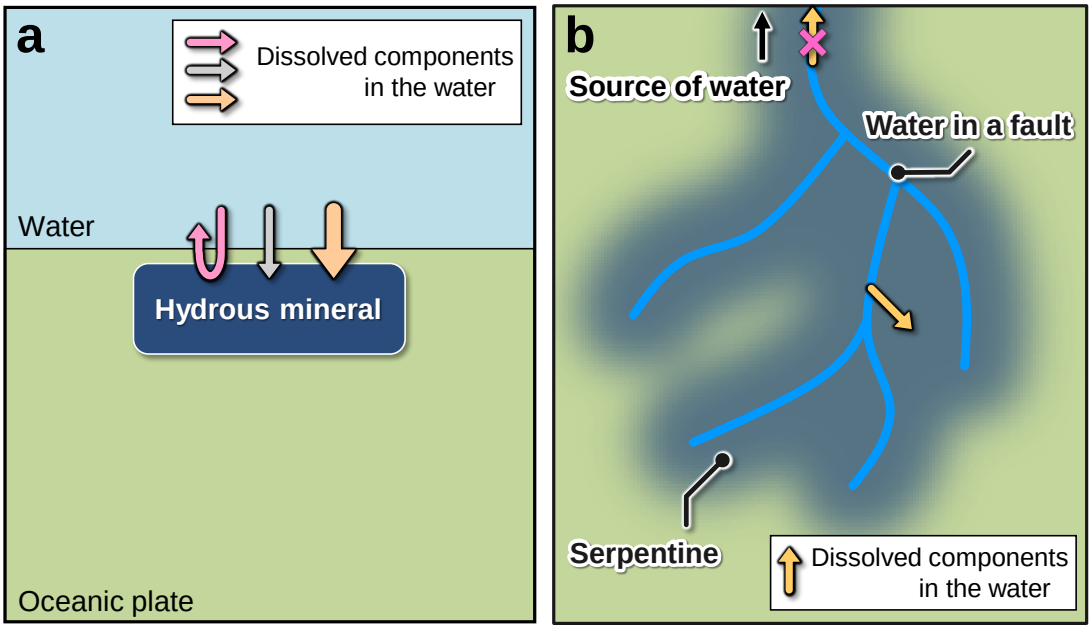

Figure 4.12. (a) Conventional concept of volatile subduction. Volatile species are incorporated into hydrous minerals formed in an open system with an essentially infinite water-rock ratio. The chemical compositions in those hydrous minerals are controlled by partitioning behavior of each element between the minerals and the water source, resulting in fractionation from original compositions of the water. (b) Mechanism of volatile incorporation into serpentine proposed in this study. Serpentinization occurs in low water/rock ratio along faults formed at the outer rise. The serpentinization is enough fast to isolate the water in the faults from its external source, resulting in preservation of the original compositions of the water. Figures are not to scale.

4.3.3.2. Volatile transportation into the mantle wedge

As discussed earlier, serpentine dehydration is a stepwise process and halogen elemental ratios fractionate during the stepwise dehydration (John et al., 2011; Kendrick et al., 2011). However, because the first dehydration step occurs at relatively shallow

depths, the anhydrous oceanic lithospheric mantle has significant water capacity (e.g., van Keken et al., 2011). At this shallow depth, Wada et al. (2011) argued that the released fluids from serpentine hydrate the ambient anhydrous region of the oceanic lithospheric mantle where initial serpentinization have locally occurred. As discussed in the previous section, I assume that serpentinization locally occurs, i.e., along faults formed by bending of oceanic plates. Although some of the fluids released from the shallower sections may escape from the slab, this dehydration-hydration process can be regarded as a closed system being maintained within the whole of the oceanic lithospheric mantle.

After fluids are released from hydrous minerals, they will interact with surrounding rocks during migrating in the slab (e.g., Herms et al., 2012). The fluids will contain relatively abundant halogens and noble gases compared to the rocks and these elements are incompatible into mineral phases. However, the fluid compositions may change during fluid-rock interaction processes as the W/R ratio decreases. On the other hand, the extent of the interaction will be relatively small if the fluid flow is highly channelized (e.g., John et al., 2012). Noble gas elemental compositions in the fluid will be preserved in such environment because of their high incompatibilities in mineral phases, high fluid-mobility, and the large contrast in concentrations between fluids and rocks. In contrast, the behavior of halogens, especially that of Cl, may be more complicated because some minerals incorporate halogens with elemental fractionation (e.g., Kusebauch et al., 2015b). Although the halogen elemental ratios of the Avacha samples are similar to those of sedimentary pore fluids, they showed relatively large variation (factor of two) compared to the Pinatubo samples (Figure 4.3). This may reflect the small halogen fractionation during fluid-rock interaction.

It is possible that Cl, ^{36}Ar, and H_2O fractionate when a portion of the released fluids from serpentine hydrates the surrounding rocks during migration in the slab. Some hydrous phases such as lawsonite and phengite are stable in the subducting slab at sub-arc depth (e.g., van Keken et al., 2011). Because of high incompatibilities of noble gases, the hydration process will consume water but little of the noble gases. This can explain the high $^{36}Ar/H_2O$ ratios in the studied fluid inclusions (Figure 4.8). Some fluid inclusions did not follow simple H_2O-loss trend and showed higher $^{36}Ar/H_2O$ ratios at given Cl/H_2O

ratios than the H_2O-loss trend. The $Cl/^{36}Ar$ ratios of the studied fluid inclusions are lower than that of seawater (Table 4.7). These indicate that not only H_2O but also halogens were also removed from the fluids during this hydration process. The extent of deviation from the H_2O-loss trend may depend on hydrous minerals formed during this process. The small deviation of the halogen elemental ratios of the Avacha samples from the sedimentary pore fluid trend (Figure 4.6) can also be explained by fractionation during this process because of higher incompatibility of iodine in mineral phases than Cl.

4.4. Conclusions

The halogen and noble gas signatures of the H_2O-rich fluid inclusions in the mantle xenoliths sampled along the volcanic fronts from two subduction zones showing contrasting thermal regimes are similar to those of marine sedimentary pore fluids and serpentinites. I argue that the consistency between halogen and noble gas signatures is strong evidence that the halogen and noble gas signatures derived from sedimentary pore fluid have been preserved during the subduction processes without significant fractionation. On the other hand, the Cl/H_2O and $^{36}Ar/H_2O$ ratios in the studied fluid inclusions are higher than those in sedimentary pore fluids and serpentine in the oceanic lithosphere. Based on the halogen-noble gas-H_2O systematics, I propose subduction mechanism of sedimentary pore fluid-derived volatiles: (i) water derived from sedimentary pore fluid is incorporated into serpentine in a closed system formed along fracture zones developed at the outer rise, where oceanic plates bend prior to entering subduction zones, (ii) dehydration-hydration process within the oceanic lithospheric mantle maintains the closed system until the final stage of serpentine dehydration, (iii) a portion of the fluids released at the final stage of serpentine dehydration hydrates the overlying slab. The first and second processes enable preservation of sedimentary pore fluid signatures during subduction processes. The last process results in elevated $^{36}Ar/H_2O$ and Cl/H_2O ratios in the remainder of the aqueous fluids due to their high incompatibilities in minerals. However, the sedimentary pore fluid-like halogen and noble gas signatures are preserved in the remainder fluids due to highly channelized fluid flow.

5. Halogen and trace element systematics in mantle xenoliths from rear-arc regions: Variation in the extent of subduction influence

本章については、５年以内に雑誌等で刊行予定のため、非公開。

This chapter is not published because it is scheduled to be published in journals or other publications within five years.

6. Halogen and trace element systematics in mantle xenoliths from intraplate settings: Subduction of halogens and halogen compositions in the mantle

本章については、５年以内に雑誌等で刊行予定のため、非公開。

This chapter is not published because it is scheduled to be published in journals or other publications within five years.

7. Conclusions

本章については、５年以内に雑誌等で刊行予定のため、非公開。

This chapter is not published because it is scheduled to be published in journals or other publications within five years.

Acknowledgements

I gratefully thank Professor Hiroyuki Kagi (the University of Tokyo), Professor Keisuke Nagao (Korea Polar Research Institute, South Korea), who was my former supervisor, and Dr. Hirochika Sumino (the University of Tokyo) for their supports, guidance, and encouragements during the course of this work. I also gratefully thank Professor Ray Burgess (the University of Manchester) and Professor Chris Ballentine (University of Oxford) for valuable discussions and their insightful comments. Professor Ray Burgess is also acknowledged for his support during my stay in the University of Manchester and for his analyses of some of my samples.

I would like to thank Professor Shoji Arai (Kanazawa University), Professor Tetsuo Kobayashi (Kagoshima University), Professor Michihiko Nakamura (Tohoku University), Professor Eiichi Takahashi (Tokyo Institute of Technology), Dr. Satoko Ishimaru (Kumamoto University), Dr. Masako Yoshikawa, Dr. Tatsuhiko Kawamoto (Kyoto University), Dr. Junji Yamamoto (Hokkaido University), and Mr. Yoshitaka Kumagai (Kyoto University) for providing me with precious mantle xenolith samples. I would like to thank Professor Shun'ichi Nakai and Dr. Tsuyoshi Iizuka (the University of Tokyo) for providing me a chance and giving me great help for analyses of trace elements using ICP-MS. They are also acknowledged for many insightful advises.

I would like to thank Dr. Michael Broadley for many discussions. I thank Dr. Tim John and Dr. Jens Hopp for their constructive comments on the paper that I published. I also thank Professor Toshitaka Gamo, Professor Motoyuki Matsuo, and Dr. Jun Okabayashi (the University of Tokyo) for their constructive comments.

I thank Mr. Hideto Yoshida, Mr. Akihiro Kobayashi, Mr. Jun Nagao, and Ms. Mao Watanabe (the University of Tokyo) for their technical supports during analyses of EPMA, XRF, ICP-MS, and Raman spectroscopy. I also thank Dr. Patricia Clay for providing me the data of irradiation monitors of the MN2014b irradiation. I would like to thank members of the Radioisotope Center, Isotope Chemistry Laboratory, and RI Experiment Facility (the University of Tokyo) for providing experimental facilities, and the staffs of IMR (Institute for Materials Research, Tohoku University), KURRI (Kyoto University

Research Reactor Institute), and Radiation Center (Oregon State University) for the neutron irradiation.

I am very grateful to all staffs and members in the Geochemical Research Center, the University of Tokyo, for their many help and encouragement.

This work was financially supported by Grant-in-Aid for JSPS fellows for Young Scientists (DC1).

References

Aiuppa, A., Baker, D., Webster, J., 2009. Halogens in volcanic systems. Chemical Geology 263, 1-18.

Arai, S., Ishimaru, S., Okrugin, V.M., 2003. Metasomatized harzburgite xenoliths from Avacha volcano as fragments of mantle wedge of the Kamchatka arc: implication for the metasomatic agent. Island Arc 12, 233-246.

Aries, S., Valladon, M., Polvé, M., Dupré, B., 2000. A routine method for oxide and hydroxide interference corrections in ICP-MS chemical analysis of environmental and geological samples. Geostandards Newsletter 24, 19-31.

Böhlke, J.K., Irwin, J.J., 1992. Laser microprobe analyses of noble gas isotopes and halogens in fluid inclusions: Analyses of microstandards and synthetic inclusions in quartz. Geochimica et Cosmochimica Acta 56, 187-201.

Baldridge, W.S., Perry, F.V., Vaniman, D.T., Nealey, L.D., Leavy, B.D., Laughlin, A.W., Kyle, P., Bartov, Y., Steinitz, G., Gladney, E.S., 1991. Middle to late Cenozoic magmatism of the southeastern Colorado Plateau and central Rio Grande rift (New Mexico and Arizona, USA): A model for continental rifting. Tectonophysics 197, 327-354.

Ballentine, C.J., Barfod, D.N., 2000. The origin of air-like noble gases in MORB and OIB. Earth and Planetary Science Letters 180, 39-48.

Ballentine, C.J., Holland, G., 2008. What CO_2 well gases tell us about the origin of noble gases in the mantle and their relationship to the atmosphere. Philosophical Transactions of the Royal Society of London A: Mathematical, Physical and Engineering Sciences 366, 4183-4203.

Barnes, J.D., Sharp, Z.D., Fischer, T.P., 2008. Chlorine isotope variations across the Izu-Bonin-Mariana arc. Geology 36, 883-886.

Barnes, J.D., Sharp, Z.D., Fischer, T.P., Hilton, D.R., Carr, M.J., 2009. Chlorine isotope variations along the Central American volcanic front and back arc. Geochemistry, Geophysics, Geosystems 10, Q11S17.

Bedini, R.M., Bodinier, J.-L., 1999. Distribution of incompatible trace elements between the constituents of spinel peridotite xenoliths: ICP-MS data from the East African Rift. Geochimica et Cosmochimica Acta 63, 3883-3900.

Benjamin, E.R., Plank, T., Wade, J.A., Kelley, K.A., Hauri, E.H., Alvarado, G.E., 2007. High water contents in basaltic magmas from Irazu Volcano, Costa Rica. Journal of Volcanology and Geothermal Research 168, 68-92.

Bernatowicz, T.J., 1981. Noble gases in ultramafic xenoliths from San Carlos, Arizona. Contributions to Mineralogy and Petrology 76, 84-91.

Bernini, D., Wiedenbeck, M., Dolejš, D., Keppler, H., 2013. Partitioning of halogens between mantle minerals and aqueous fluids: implications for the fluid flow regime in subduction zones. Contributions to Mineralogy and Petrology 165, 117-128.

Bertrán, J.F., 1983. Study of the Fermi doublet ν_1-$2\nu_2$ in the Raman spectra of CO_2 in different phases. Spectrochimica Acta Part A: Molecular Spectroscopy 39, 119-121.

Bianchi, D., Sarmiento, J.L., Gnanadesikan, A., Key, R.M., Schlosser, P., Newton, R., 2010. Low helium flux from the mantle inferred from simulations of oceanic helium isotope data. Earth and Planetary Science Letters 297, 379-386.

Bolfan-Casanova, N., 2005. Water in the Earth's mantle. Mineralogical Magazine 69, 229-257.

Bradshaw, T.K., Hawkesworth, C.J., Gallagher, K., 1993. Basaltic volcanism in the Southern Basin and Range: no role for a mantle plume. Earth and Planetary Science Letters 116, 45-62.

Braitseva, O.A., Bazanova, L.I., Melekestsev, I.V., Sulerzhitskiy, L.D., 1998. Large

Holocene eruptions of Avacha volcano, Kamchatka (7250–3700 ^{14}C years BP). Volcanol Seismol 20, 1-27.

Brazzle, R.H., Pravdivtseva, O.V., Meshik, A.P., Hohenberg, C.M., 1999. Verification and interpretation of the I-Xe chronometer. Geochimica et Cosmochimica Acta 63, 739-760.

Briais, A., Patriat, P., Tapponnier, P., 1993. Updated interpretation of magnetic anomalies and seafloor spreading stages in the South China Sea: Implications for the Tertiary tectonics of Southeast Asia. Journal of Geophysical Research: Solid Earth (1978–2012) 98, 6299-6328.

Broadley, M.W., Ballentine, C.J., Chavrit, D., Dallai, L., Burgess, R., 2016. Sedimentary halogens and noble gases within Western Antarctic xenoliths: Implications of extensive volatile recycling to the sub continental lithospheric mantle. Geochimica et Cosmochimica Acta 176, 139-156.

Bruland, K.W., Lohan, M.C., 2014. Controls of trace metals in seawater, in: Mottl, M.J., Elderfield, H. (Eds.), The Oceans and Marine Geochemistry, 2 ed. Elsevier, pp. 19-51.

Buikin, A., Trieloff, M., Hopp, J., Althaus, T., Korochantseva, E., Schwarz, W.H., Altherr, R., 2005. Noble gas isotopes suggest deep mantle plume source of late Cenozoic mafic alkaline volcanism in Europe. Earth and Planetary Science Letters 230, 143-162.

Bureau, H., Auzende, A.-L., Marocchi, M., Raepsaet, C., Munsch, P., Testemale, D., Mézouar, M., Kubsky, S., Carrière, M., Ricolleau, A., 2016. Modern and past volcanic degassing of iodine. Geochimica et Cosmochimica Acta 173, 114-125.

Bureau, H., Keppler, H., Métrich, N., 2000. Volcanic degassing of bromine and iodine: experimental fluid/melt partitioning data and applications to stratospheric chemistry. Earth and Planetary Science Letters 183, 51-60.

Burgess, R., Cartigny, P., Harrison, D., Hobson, E., Harris, J., 2009. Volatile composition of microinclusions in diamonds from the Panda kimberlite, Canada: Implications for

chemical and isotopic heterogeneity in the mantle. Geochimica et Cosmochimica Acta 73, 1779-1794.

Burgess, R., Layzelle, E., Turner, G., Harris, J.W., 2002. Constraints on the age and halogen composition of mantle fluids in Siberian coated diamonds. Earth and Planetary Science Letters 197, 193-203.

Burnard, P., 2004. Diffusive fractionation of noble gases and helium isotopes during mantle melting. Earth and Planetary Science Letters 220, 287-295.

Cameron, J.A., Singh, B., 2008. Nuclear data sheets for A= 38. Nuclear Data Sheets 109, 1-170.

Caracausi, A., Avice, G., Burnard, P.G., Füri, E., Marty, B., 2016. Chondritic xenon in the Earth's mantle. Nature 533, 82-85.

Carpenter, R., 1969. Factors controlling the marine geochemistry of fluorine. Geochimica et Cosmochimica Acta 33, 1153-1167.

Chai, J.Y., Muramatsu, Y., 2007. Determination of bromine and iodine in twenty‐three geochemical reference materials by ICP‐MS. Geostandards and Geoanalytical Research 31, 143-150.

Chavrit, D., Burgess, R., Sumino, H., Teagle, D.A.H., Droop, G., Shimizu, A., Ballentine, C.J., 2016. The contribution of hydrothermally altered ocean crust to the mantle halogen and noble gas cycles. Geochimica et Cosmochimica Acta 183, 106-124.

Chough, S.K., Kwon, S.-T., Ree, J.-H., Choi, D.K., 2000. Tectonic and sedimentary evolution of the Korean peninsula: a review and new view. Earth-Science Reviews 52, 175-235.

Coltice, N., Marty, B., Yokochi, R., 2009. Xenon isotope constraints on the thermal evolution of the early Earth. Chemical Geology 266, 4-9.

Crisp, J.A., 1984. Rates of magma emplacement and volcanic output. Journal of Volcanology and Geothermal Research 20, 177-211.

Currie, L.A., 1968. Limits for qualitative detection and quantitative determination. Application to radiochemistry. Analytical chemistry 40, 586-593.

Dalou, C., Koga, K.T., Shimizu, N., Boulon, J., Devidal, J.-L., 2012. Experimental determination of F and Cl partitioning between lherzolite and basaltic melt. Contributions to Mineralogy and Petrology 163, 591-609.

Day, J.M.D., Barry, P.H., Hilton, D.R., Burgess, R., Pearson, D.G., Taylor, L.A., 2015. The helium flux from the continents and ubiquity of low-$^{3}He/^{4}He$ recycled crust and lithosphere. Geochimica et Cosmochimica Acta 153, 116-133.

de Laeter, J.R., Böhlke, J.K., De Bièvre, P., Hidaka, H., Peiser, H.S., Rosman, K.J.R., Taylor, P.D.P., 2003. Atomic weights of the elements. Review 2000 (IUPAC Technical Report). Pure and Applied Chemistry 75, 683-800.

Dreibus, G., Spettel, B., Wänke, H., 1979. Halogens in meteorites and their primordial abundances. Physics and Chemistry of the Earth 11, 33-38.

Dulski, P., 2001. Reference materials for geochemical studies: New analytical data by ICP-MS and critical discussion of reference values. Geostandards Newsletter 25, 87-125.

Dunai, T.J., Baur, H., 1995. Helium, neon, and argon systematics of the European subcontinental mantle: Implications for its geochemical evolution. Geochimica et Cosmochimica Acta 59, 2767-2783.

Dziewonski, A.M., Anderson, D.L., 1981. Preliminary reference Earth model. Physics of the earth and planetary interiors 25, 297-356.

Ebihara, M., Ozaki, H., Kato, F., Nakahara, H., 1997. Determination of chlorine, bromine and iodine in rock samples by radiochemical neutron activation analysis. Journal of radioanalytical and nuclear chemistry 216, 107-112.

Ebisawa, N., Sumino, H., Okazaki, R., Takigami, Y., Hirano, N., Nagao, K., Kaneoka, I., 2004. Construction of I-Xe and ^{40}Ar-^{39}Ar dating system using a modified VG3600 mass spectrometer and the first I-Xe data obtained in Japan. Journal of the Mass Spectrometry Society of Japan 52, 219-229.

Elderfield, H., Truesdale, V.W., 1980. On the biophilic nature of iodine in seawater. Earth and Planetary Science Letters 50, 105-114.

Elderfield, H., 1986. Strontium isotope stratigraphy. Palaeogeography, Palaeoclimatology, Palaeoecology 57, 71-90.

Fabbrizio, A., Stalder, R., Hametner, K., Günther, D., 2013. Experimental chlorine partitioning between forsterite, enstatite and aqueous fluid at upper mantle conditions. Geochimica et Cosmochimica Acta 121, 684-700.

Faccenda, M., 2014. Water in the slab: A trilogy. Tectonophysics 614, 1-30.

Faccenda, M., Gerya, T.V., Burlini, L., 2009. Deep slab hydration induced by bending-related variations in tectonic pressure. Nature Geoscience 2, 790-793.

Fehn, U., Lu, Z., Tomaru, H., 2006. Data report: ^{129}I/I ratios and halogen concentrations in pore water of hydrate ridge and their relevance for the origin of gas hydrates: A progress report, in: Tréhu, A.M., Bohrmann, G., Torres, M.E., Colwell, F.S. (Eds.), Proceedings of the Ocean Drilling Program, Scientific Results, pp. 1-25.

Fischer, T.P., 2008. Fluxes of volatiles (H_2O, CO_2, N_2, Cl, F) from arc volcanoes. Geochemical Journal 42, 21-38.

Flanagan, F.J., 1976. Description and analyses of eight new USGS rock standards. U.S. Geological Survey Professional Paper 840.

Fujibayashi, N., Nagao, T., Kagami, H., Iwata, M., Tazaki, K., 1989. Spatial variation in the Sr and Nd isotope compositions of Cenozoic alkali basalts from the Chugoku district, SW Japan. Journal of Mineralogy, Petrology and Economic 84, 429-443.

Fujitani, T., Nakamura, N., 2006. Determination of chlorine in nine rock reference materials by isotope dilution mass spectrometry. Geostandards and Geoanalytical Research 30, 113-120.

Fukao, Y., Obayashi, M., Nakakuki, T., 2009. Stagnant slab: a review. Annual Review of Earth and Planetary Sciences 37, 19-46.

Gautheron, C., Moreira, M., 2002. Helium signature of the subcontinental lithospheric mantle. Earth and Planetary Science Letters 199, 39-47.

Gautheron, C., Moreira, M., Allègre, C., 2005. He, Ne and Ar composition of the European lithospheric mantle. Chemical Geology 217, 97-112.

Govindaraju, K., 1994. 1994 compilation of working values and sample description for 383 geostandards. Geostandards newsletter 18, 1-158.

Graham, D.W., 2002. Noble gas isotope geochemistry of mid-ocean ridge and ocean island basalts: Characterization of mantle source reservoirs, in: Porcelli, D., Ballentine, C.J., Wieler, R. (Eds.), Noble Gases in Geochemistry and Cosmochemistry. Reviews in Mineralogy and Geochemistry, pp. 247-317.

Hacker, B.R., 2008. H_2O subduction beyond arcs. Geochemistry, Geophysics, Geosystems 9, Q03001.

Halldórsson, S.A., Barnes, J.D., Stefánsson, A., Hilton, D.R., Hauri, E.H., Marshall, E.W., 2016. Subducted lithosphere controls halogen enrichments in the Iceland mantle plume source. Geology 44, 679-682.

Hammerli, J., Rusk, B., Spandler, C., Emsbo, P., Oliver, N.H.S., 2013. In situ quantification of Br and Cl in minerals and fluid inclusions by LA-ICP-MS: A powerful tool to identify fluid sources. Chemical Geology 337-338, 75-87.

Hanyu, T., Tatsumi, Y., Nakai, S.i., Chang, Q., Miyazaki, T., Sato, K., Tani, K., Shibata, T., Yoshida, T., 2006. Contribution of slab melting and slab dehydration to magmatism in

the NE Japan arc for the last 25 Myr: Constraints from geochemistry. Geochemistry, Geophysics, Geosystems 7.

Hauff, F., Hoernle, K., Schmidt, A., 2003. Sr-Nd-Pb composition of Mesozoic Pacific oceanic crust (Site 1149 and 801, ODP Leg 185): Implications for alteration of ocean crust and the input into the Izu‐Bonin‐Mariana subduction system. Geochemistry, Geophysics, Geosystems 4.

Heber, V.S., Brooker, R.A., Kelley, S.P., Wood, B.J., 2007. Crystal–melt partitioning of noble gases (helium, neon, argon, krypton, and xenon) for olivine and clinopyroxene. Geochimica et Cosmochimica Acta 71, 1041-1061.

Herms, P., John, T., Bakker, R.J., Schenk, V., 2012. Evidence for channelized external fluid flow and element transfer in subducting slabs (Raspas Complex, Ecuador). Chemical Geology 310, 79-96.

Hilton, D.R., Fischer, T.P., Marty, B., 2002. Noble gases and volatile recycling at subduction zones, in: Porcelli, D., Ballentine, C.J., Wieler, R. (Eds.), Noble Gases in Geochemistry and Cosmochemistry. Reviews in Mineralogy and Geochemistry, pp. 319-370.

Hilton, D.R., Hammerschmidt, K., Teufel, S., Friedrichsen, H., 1993. Helium isotope characteristics of Andean geothermal fluids and lavas. Earth and Planetary Science Letters 120, 265-282.

Hirose, F., Nakajima, J., Hasegawa, A., 2008. Three‐dimensional seismic velocity structure and configuration of the Philippine Sea slab in southwestern Japan estimated by double-difference tomography. Journal of Geophysical Research: Solid Earth (1978–2012) 113.

Holland, G., Ballentine, C.J., 2006. Seawater subduction controls the heavy noble gas composition of the mantle. Nature 441, 186-191.

Honda, M., McDougall, I., Patterson, D.B., Doulgeris, A., Clague, D.A., 1991. Possible solar noble-gas component in Hawaiian basalts. Nature 349, 149-151.

Hopp, J., Ionov, D.A., 2011. Tracing partial melting and subduction-related metasomatism in the Kamchatkan mantle wedge using noble gas compositions. Earth and Planetary Science Letters 302, 121-131.

Hyndman, R.D., Peacock, S.M., 2003. Serpentinization of the forearc mantle. Earth and Planetary Science Letters 212, 417-432.

Imai, N., Terashima, S., Itoh, S., Ando, A., 1995. 1994 compilation of analytical data for minor and trace elements in seventeen GSJ geochemical reference samples,"igneous rock series". Geostandards Newsletter 19, 135-213.

Ingrin, J., Blanchard, M., 2006. Diffusion of hydrogen in minerals. Reviews in Mineralogy and Geochemistry 62, 291-320.

Inoue, T., Yurimoto, H., Kudoh, Y., 1995. Hydrous modified spinel, $Mg_{1.75}SiH_{0.5}O_4$: A new water reservoir in the mantle transition region. Geophysical Research Letters 22, 117-120.

Ionov, D.A., 2010. Petrology of mantle wedge lithosphere: new data on supra-subduction zone peridotite xenoliths from the andesitic Avacha volcano, Kamchatka. Journal of Petrology 51, 327-361.

Ionov, D.A., Savoyant, L., Dupuy, C., 1992. Application of the ICP-MS technique to trace element analysis of peridotites and their minerals. Geostandards Newsletter 16, 311-315.

Ishimaru, S., Arai, S., 2009. Highly silicic glasses in peridotite xenoliths from Avacha volcano, Kamchatka arc; implications for melting and metasomatism within the sub-arc mantle. Lithos 107, 93-106.

Ishimaru, S., Arai, S., Ishida, Y., Shirasaka, M., Okrugin, V.M., 2007. Melting and multi-stage metasomatism in the mantle wedge beneath a frontal arc inferred from highly

depleted peridotite xenoliths from the Avacha volcano, southern Kamchatka. Journal of Petrology 48, 395-433.

Itano, K., Iizuka, T., Chang, Q., Kimura, J.-I., Maruyama, S., 2016. U–Pb chronology and geochemistry of detrital monazites from major African rivers: Constraints on the timing and nature of the Pan-African Orogeny. Precambrian Research 282, 139-156.

Ito, E., Harris, D.M., Anderson, A.T., 1983. Alteration of oceanic crust and geologic cycling of chlorine and water. Geochimica et Cosmochimica Acta 47, 1613-1624.

Iwamori, H., Albaréde, F., Nakamura, H., 2010. Global structure of mantle isotopic heterogeneity and its implications for mantle differentiation and convection. Earth and Planetary Science Letters 299, 339-351.

Jackson, C.R.M., Parman, S.W., Kelley, S.P., Cooper, R.F., 2013. Noble gas transport into the mantle facilitated by high solubility in amphibole. Nature Geoscience 6, 562-565.

Jackson, C.R.M., Parman, S.W., Kelley, S.P., Cooper, R.F., 2015. Light noble gas dissolution into ring structure-bearing materials and lattice influences on noble gas recycling. Geochimica et Cosmochimica Acta 159, 1-15.

Jambon, A., Déruelle, B., Dreibus, G., Pineau, F., 1995. Chlorine and bromine abundance in MORB: the contrasting behaviour of the Mid-Atlantic Ridge and East Pacific Rise and implications for chlorine geodynamic cycle. Chemical Geology 126, 101-117.

Jarrard, R.D., 2003. Subduction fluxes of water, carbon dioxide, chlorine, and potassium. Geochemistry, Geophysics, Geosystems 4, 8905.

John, T., Gussone, N., Podladchikov, Y.Y., Bebout, G.E., Dohmen, R., Halama, R., Klemd, R., Magna, T., Seitz, H.-M., 2012. Volcanic arcs fed by rapid pulsed fluid flow through subducting slabs. Nature Geoscience 5, 489-492.

John, T., Layne, G.D., Haase, K.M., Barnes, J.D., 2010. Chlorine isotope evidence for crustal recycling into the Earth's mantle. Earth and Planetary Science Letters 298, 175-

182.

John, T., Scambelluri, M., Frische, M., Barnes, J.D., Bach, W., 2011. Dehydration of subducting serpentinite: implications for halogen mobility in subduction zones and the deep halogen cycle. Earth and Planetary Science Letters 308, 65-76.

Johnson, L.H., Burgess, R., Turner, G., Milledge, H.J., Harris, J.W., 2000. Noble gas and halogen geochemistry of mantle fluids: comparison of African and Canadian diamonds. Geochimica et Cosmochimica Acta 64, 717-732.

Jolivet, L., Tamaki, K., 1992. Neogene kinematics in the Japan Sea region and volcanic activity of the northeast Japan arc.

Kanbe, M., Kitao, K., 2001. Nuclear data sheets for A= 128. Nuclear Data Sheets 94, 227-395.

Kaneoka, I., Takaoka, N., 1978. Excess ^{129}Xe and high $^{3}He/^{4}He$ ratios in olivine phenocrysts of Kapuho lava and xenolithic dunites from Hawaii. Earth and Planetary Science Letters 39, 382-386.

Kastner, M., Elderfield, H., Martin, J.B., Suess, E., Kvenvolden, K.A., Garrison, R.E., 1990. Diagenesis and interstitial-water chemistry at the Peruvian continental margin—major constituents and strontium isotopes, in: Suess, E., von Huene, R. (Eds.), Proceedings of the Ocean Drilling Program, Scientific Results, pp. 413-440.

Katsui, Y., Yamamoto, M., Nemoto, S., Niida, K., 1979. Genesis of calc-alkalic andesites from Oshima-Ōshima and Ichinomegata volcanoes, North Japan. Journal of the Faculty of Science, Hokkaido University 19, 157-168.

Kawakami, Y., Yamamoto, J., Kagi, H., 2003. Micro-Raman densimeter for CO_2 inclusions in mantle-derived minerals. Applied spectroscopy 57, 1333-1339.

Kawamoto, T., Mibe, K., Bureau, H., Reguer, S., Mocuta, C., Kubsky, S., Thiaudière, D., Ono, S., Kogiso, T., 2014. Large-ion lithophile elements delivered by saline fluids to the

sub-arc mantle. Earth, Planets and Space 66, 1-11.

Kawamoto, T., Nakajima, J., Reynard, B., Toh, H., 2015. Special issue 'Geofluid processes in subduction zones and mantle dynamics'. Earth, Planets and Space 67, 1-4.

Kawamoto, T., Yoshikawa, M., Kumagai, Y., Mirabueno, M.H.T., Okuno, M., Kobayashi, T., 2013. Mantle wedge infiltrated with saline fluids from dehydration and decarbonation of subducting slab. Proceedings of the National Academy of Sciences 110, 9663-9668.

Kendrick, M.A., 2012. High precision Cl, Br and I determinations in mineral standards using the noble gas method. Chemical Geology 292-293, 116-126.

Kendrick, M.A., Arculus, R., Burnard, P., Honda, M., 2013a. Quantifying brine assimilation by submarine magmas: Examples from the Galápagos Spreading Centre and Lau Basin. Geochimica et Cosmochimica Acta 123, 150-165.

Kendrick, M.A., Honda, M., Pettke, T., Scambelluri, M., Phillips, D., Giuliani, A., 2013b. Subduction zone fluxes of halogens and noble gases in seafloor and forearc serpentinites. Earth and Planetary Science Letters 365, 86-96.

Kendrick, M.A., Honda, M., Vanko, D.A., 2015a. Halogens and noble gases in Mathematician Ridge meta-gabbros, NE Pacific: implications for oceanic hydrothermal root zones and global volatile cycles. Contributions to Mineralogy and Petrology 170, 1-20.

Kendrick, M.A., Jackson, M.G., Hauri, E.H., Phillips, D., 2015b. The halogen (F, Cl, Br, I) and H_2O systematics of Samoan lavas: Assimilated-seawater, EM2 and high-$^3He/^4He$ components. Earth and Planetary Science Letters 410, 197-209.

Kendrick, M.A., Kamenetsky, V.S., Phillips, D., Honda, M., 2012a. Halogen systematics (Cl, Br, I) in mid-ocean ridge basalts: a Macquarie Island case study. Geochimica et Cosmochimica Acta 81, 82-93.

Kendrick, M.A., Scambelluri, M., Honda, M., Phillips, D., 2011. High abundances of

noble gas and chlorine delivered to the mantle by serpentinite subduction. Nature Geoscience 4, 807-812.

Kendrick, M.A., Woodhead, J.D., Kamenetsky, V.S., 2012b. Tracking halogens through the subduction cycle. Geology 40, 1075-1078.

Kennedy, H.A., Elderfield, H., 1987a. Iodine diagenesis in non-pelagic deep-sea sediments. Geochimica et Cosmochimica Acta 51, 2505-2514.

Kennedy, H.A., Elderfield, H., 1987b. Iodine diagenesis in pelagic deep-sea sediments. Geochimica et Cosmochimica Acta 51, 2489-2504.

Kennett, B.L.N., Engdahl, E.R., 1991. Traveltimes for global earthquake location and phase identification. Geophysical Journal International 105, 429-465.

Kent, A.J.R., Ungerer, C.A., 2005. Production of barium and light rare earth element oxides during LA-ICP-MS microanalysis. Journal of Analytical Atomic Spectrometry 20, 1256-1262.

Keppler, H., 1996. Constraints from partitioning experiments on the composition of subduction-zone fluids. Nature 380, 237-240.

Kerr, J.A., 1998. Strengths of chemical bonds, CRC Handbook of Chemistry and Physics, 78 ed. CRC Press, pp. 51-73.

Kerrick, D., 2002. Serpentinite seduction. Science 298, 1344-1345.

Khazov, Y., Mitropolsky, I., Rodionov, A., 2006. Nuclear data sheets for A= 131. Nuclear Data Sheets 107, 2715-2930.

Kim, K.H., Nagao, K., Tanaka, T., Sumino, H., Nakamura, T., Okuno, M., Lock, J.B., Youn, J.S., Song, J., 2005. He-Ar and Nd-Sr isotopic compositions of ultramafic xenoliths and host alkali basalts from the Korean peninsula. Geochemical Journal 39, 341-356.

Kimura, J.I., Kunikiyo, T., Osaka, I., Nagao, T., Yamauchi, S., Kakubuchi, S., Okada, S.,

Fujibayashi, N., Okada, R., Murakami, H., Kusano, T., Umeda, K., Hayashi, S., Ishimaru, T., Ninomiya, A., Tanase, A., 2003. Late Cenozoic volcanic activity in the Chugoku area, southwest Japan arc during back-arc basin opening and reinitiation of subduction. Island Arc 12, 22-45.

Kirby, S.H., Green II, H.W., 1980. Dunite xenoliths from Hualalai volcano: evidence for mantle diapiric flow beneath the island of Hawaii. American Journal of Science 280, 550-575.

Kobayashi, Y., Arai, S., 1981. Ultramafic nodules in alkali basalt from Taka-shima, Saga Prefecture, Japan. Geoscience Report of Shizuoka University 6, 11-24. (in Japanese with English abstract)

Kohlstedt, D.L., Keppler, H., Rubie, D.C., 1996. Solubility of water in the α, β and γ phases of $(Mg, Fe)_2SiO_4$. Contributions to Mineralogy and Petrology 123, 345-357.

Kumagai, Y., Kawamoto, T., Yamamoto, J., 2014. Evolution of carbon dioxide-bearing saline fluids in the mantle wedge beneath the Northeast Japan arc. Contributions to Mineralogy and Petrology 168, 1056.

Kunz, J., 1999. Is there solar argon in the Earth's mantle? Nature 399, 649-650.

Kurz, M.D., 1986. Cosmogenic helium in a terrestrial igneous rock. Nature 320, 435-439.

Kusebauch, C., John, T., Barnes, J.D., Klügel, A., Austrheim, H.O., 2015b. Halogen element and stable chlorine isotope fractionation caused by fluid–rock interaction (Bamble Sector, SE Norway). Journal of Petrology 56, 299-324.

Kusebauch, C., John, T., Whitehouse, M.J., Klemme, S., Putnis, A., 2015a. Distribution of halogens between fluid and apatite during fluid-mediated replacement processes. Geochimica et Cosmochimica Acta 170, 225-246.

Lacan, F., Tachikawa, K., Jeandel, C., 2012. Neodymium isotopic composition of the oceans: A compilation of seawater data. Chemical Geology 300, 177-184.

Le Voyer, M., Rose-Koga, E.F., Shimizu, N., Grove, T.L., Schiano, P., 2010. Two contrasting H_2O-rich components in primary melt inclusions from Mount Shasta. Journal of Petrology 51, 1571-1595.

Lodders, K., Fegley, B., 1998. The planetary scientist's companion. Oxford University Press, New York.

Ludwig, K.R., 2012. Isoplot 3.75-4.15, a geochronological toolkit for Microsoft Excel. Berkeley Geochronology Center Special Publication No. 5.

Makishima, A., Nakamura, E., 1997. Suppression of matrix effects in ICP‐MS by high power operation of ICP: Application to precise determination of Rb, Sr, Y, Cs, Ba, REE, Pb, Th and U at ng g‐1 Levels in milligram silicate samples. Geostandards Newsletter 21, 307-319.

Makishima, A., Nakamura, E., Nakano, T., 1999. Determination of Zirconium, Niobium, Hafnium and Tantalum at ng g^{-1} levels in geological materials by direct nebulisation of sample HF solution into FI-ICP-MS. Geostandards Newsletter 23, 7-20.

Martin, J.B., Gieskes, J.M., Torres, M., Kastner, M., 1993. Bromine and iodine in Peru margin sediments and pore fluids: implications for fluid origins. Geochimica et Cosmochimica Acta 57, 4377-4389.

Marty, B., 2012. The origins and concentrations of water, carbon, nitrogen and noble gases on Earth. Earth and Planetary Science Letters 313-314, 56-66.

Marty, B., Avice, G., Sano, Y., Altwegg, K., Balsiger, H., Hässig, M., Morbidelli, A., Mousis, O., Rubin, M., 2016. Origins of volatile elements (H, C, N, noble gases) on Earth and Mars in light of recent results from the ROSETTA cometary mission. Earth and Planetary Science Letters 441, 91-102.

Marty, B., Tolstikhin, I.N., 1998. CO_2 fluxes from mid-ocean ridges, arcs and plumes. Chemical Geology 145, 233-248.

Martynov, Y.A., Khanchuk, A., 2013. Cenozoic volcanism of the eastern Sikhote Alin: Petrological studies and outlooks. Petrology 21, 85-99.

Matsuda, J., Matsubara, K., Yajima, H., Yamamoto, K., 1989. Anomalous Ne enrichment in obsidians and Darwin glass: diffusion of noble gases in silica-rich glasses. Geochimica et Cosmochimica Acta 53, 3025-3033.

Matsuda, J., Nagao, K., 1986. Noble gas abundances in a deep-sea sediment core from eastern equatorial Pacific. Geochemical Journal 20, 71-80.

Matsuda, J., Matsumoto, T., Sumino, H., Nagao, K., Yamamoto, J., Miura, Y., Kaneoka, I., Takahata, N., Sano, Y., 2002. The $^{3}He/^{4}He$ ratio of the new internal He Standard of Japan (HESJ). Geochemical Journal 36, 191-195.

Matsumoto, T., Chen, Y., Matsuda, J., 2001. Concomitant occurrence of primordial and recycled noble gases in the Earth's mantle. Earth and Planetary Science Letters 185, 35-47.

McDonough, W.F., Sun, S.-S., 1995. The composition of the Earth. Chemical geology 120, 223-253.

McDougall, I., Harrison, T.M., 1999. Geochronology and Thermochronology by the $^{40}Ar/^{39}Ar$ Method. Oxford University Press.

Meisel, T., Walker, R.J., Irving, A.J., Lorand, J.-P., 2001. Osmium isotopic compositions of mantle xenoliths: a global perspective. Geochimica et Cosmochimica Acta 65, 1311-1323.

Michel, A., Villemant, B., 2003. Determination of halogens (F, Cl, Br, I), sulfur and water in seventeen geological reference materials. Geostandards Newsletter 27, 163-171.

Minster, J.B., Jordan, T.H., Molnar, P., Haines, E., 1974. Numerical modelling of instantaneous plate tectonics. Geophysical Journal International 36, 541-576.

Mitsui, Y., Hirahara, K., 2009. Coseismic thermal pressurization can notably prolong earthquake recurrence intervals on weak rate and state friction faults: Numerical experiments using different constitutive equations. Journal of Geophysical Research: Solid Earth (1978–2012) 114.

Miura, Y., Nagao, K., 1991. Noble gases in six GSJ igneous rock samples. Geochemical Journal 25, 163-171.

Miyake, Y., 1994. Geochemistry of igneous rocks of Shimane Peninsula, formed within a Miocene back-arc rifting zone at the Japan Sea margin. Geochemical Journal 28, 451-472.

Mizukami, T., Wallis, S.R., Yamamoto, J., 2004. Natural examples of olivine lattice preferred orientation patterns with a flow-normal a-axis maximum. Nature 427, 432-436.

Moreira, M., Kunz, J., Allègre, C., 1998. Rare gas systematics in popping rock: isotopic and elemental compositions in the upper mantle. Science 279, 1178-1181.

Moreira, M.A., Kurz, M.D., 2013. Noble gases as tracers of mantle processes and magmatic degassing, in: Burnard, P. (Ed.), The Noble Gases as Geochemical Tracers. Springer, pp. 371-391.

Morgan, W.J., 1971. Convection plumes in the lower mantle. Nature 230, 42-43.

Mukhopadhyay, S., 2012. Early differentiation and volatile accretion recorded in deep-mantle neon and xenon. Nature 486, 101-104.

Muramatsu, Y., Doi, T., Tomaru, H., Fehn, U., Takeuchi, R., Matsumoto, R., 2007. Halogen concentrations in pore waters and sediments of the Nankai Trough, Japan: Implications for the origin of gas hydrates. Applied Geochemistry 22, 534-556.

Muramatsu, Y., Wedepohl, K.H., 1998. The distribution of iodine in the earth's crust. Chemical Geology 147, 201-216.

Nagao, K., Takahashi, E., 1993. Noble gases in the mantle wedge and lower crust: an inference from the isotopic analyses of xenoliths from Oki-Dogo and Ichinomegata, Japan. Geochemical Journal 27, 229-240.

Nakamura, E., Campbell, I.H., Sun, S.-S., 1985. The influence of subduction processes on the geochemistry of Japanese alkaline basalts. Nature 316, 55-58.

Nakamura, E., McDougall, I., Campbell, I.H., 1986. K-Ar ages of basalts from the Higashi-Matsuura district, northwestern Kyushu, Japan and regional geochronology of the Cenozoic alkaline volcanic rocks in eastern Asia. Geochemical Journal 20, 91-99.

Nica, N., Cameron, J., Singh, B., 2012. Nuclear Data Sheets for A= 36. Nuclear Data Sheets 113, 1-155.

Nishio, Y., Nakai, S.i., Yamamoto, J., Sumino, H., Matsumoto, T., Prikhod'ko, V.S., Arai, S., 2004. Lithium isotopic systematics of the mantle-derived ultramafic xenoliths: implications for EM1 origin. Earth and Planetary Science Letters 217, 245-261.

Niu, Y., Langmuir, C.H., Kinzler, R.J., 1997. The origin of abyssal peridotites: a new perspective. Earth and Planetary Science Letters 152, 251-265.

Ohtani, E., 2005. Water in the mantle. Elements 1, 25-30.

Ohtani, E., 2015. Hydrous minerals and the storage of water in the deep mantle. Chemical Geology 418, 6-15.

Okamura, S., Martynov, Y.A., Furuyama, K., Nagao, K., 1998. K−Ar ages of the basaltic rocks from Far East Russia: Constraints on the tectono-magmatism associated with the Japan Sea opening. Island Arc 7, 271-282.

Osawa, T., 2004. A new correction technique for mass interferences by $^{40}Ar^{++}$ and CO_2^{++} during isotope analysis of a small amount of Ne. Journal of the Mass Spectrometry Society of Japan 52, 230-232.

Ott, U., 2002. Noble gases in meteorites–trapped components, in: Porcelli, D., Ballentine, C.J., Wieler, R. (Eds.), Noble Gases in Geochemistry and Cosmochemistry. Reviews in Mineralogy and Geochemistry, pp. 71-100.

Ozaki, H., Ebihara, M., 2007. Determination of trace halogens in rock samples by radiochemical neutron activation analysis coupled with the k_0-standardization method. Analytica chimica acta 583, 384-391.

Ozima, M., 1975. Ar isotopes and Earth-atmosphere evolution models. Geochimica et Cosmochimica Acta 39, 1127-1134.

Ozima, M., Podosek, F.A., 2002. Noble gas geochemistry. Cambridge University Press.

Pagé, L., Hattori, K., de Hoog, J.C.M., Okay, A.I., 2016. Halogen (F, Cl, Br, I) behaviour in subducting slabs: A study of lawsonite blueschists in western Turkey. Earth and Planetary Science Letters 442, 133-142.

Pallister, J.S., Hoblitt, R.P., Reyes, A.G., 1992. A basalt trigger for the 1991 eruptions of Pinatubo Volcano? Nature 356, 426-428.

Palme, H., O'Neill, H.S.C., 2014. Cosmochemical estimates of mantle composition, in: Carlson, R.W. (Ed.), The Mantle and Core, 2 ed. Elsevier, pp. 1-39.

Parai, R., Mukhopadhyay, S., 2012. How large is the subducted water flux? New constraints on mantle regassing rates. Earth and Planetary Science Letters 317, 396-406.

Peacock, S.M., 2001. Are the lower planes of double seismic zones caused by serpentine dehydration in subducting oceanic mantle? Geology 29, 299-302.

Pearce, N.J.G., Perkins, W.T., Westgate, J.A., Gorton, M.P., Jackson, S.E., Neal, C.R., Chenery, S.P., 1997. A compilation of new and published major and trace element data for NIST SRM 610 and NIST SRM 612 glass reference materials. Geostandards newsletter 21, 115-144.

Pearson, D.G., Brenker, F.E., Nestola, F., McNeill, J., Nasdala, L., Hutchison, M.T., Matveev, S., Mather, K., Silversmit, G., Schmitz, S., 2014. Hydrous mantle transition zone indicated by ringwoodite included within diamond. Nature 507, 221-224.

Pitzer, K.S., Sterner, S.M., 1994. Equations of state valid continuously from zero to extreme pressures for H_2O and CO_2. The Journal of chemical physics 101, 3111-3116.

Porcelli, D., Ballentine, C.J., 2002. Models for distribution of terrestrial noble gases and evolution of the atmosphere, in: Porcelli, D., Ballentine, C.J., Wieler, R. (Eds.), Noble Gases in Geochemistry and Cosmochemistry. Reviews in Mineralogy and Geochemistry, pp. 411-480.

Porcelli, D., Ballentine, C.J., Wieler, R., 2002. An overview of noble gas geochemistry and cosmochemistry, in: Porcelli, D., Ballentine, C.J., Wieler, R. (Eds.), Noble Gases in Geochemistry and Cosmochemistry. Reviews in Mineralogy and Geochemistry, pp. 1-19.

Porcelli, D.R., O'Nions, R.K., Galer, S.J.G., Cohen, A.S., Mattey, D.P., 1992. Isotopic relationships of volatile and lithophile trace elements in continental ultramafic xenoliths. Contributions to Mineralogy and Petrology 110, 528-538.

Portnyagin, M., Hoernle, K., Plechov, P., Mironov, N., Khubunaya, S., 2007. Constraints on mantle melting and composition and nature of slab components in volcanic arcs from volatiles (H_2O, S, Cl, F) and trace elements in melt inclusions from the Kamchatka Arc. Earth and Planetary Science Letters 255, 53-69.

Pyle, D.M., Mather, T.A., 2009. Halogens in igneous processes and their fluxes to the atmosphere and oceans from volcanic activity: A review. Chemical Geology 263, 110-121.

Rüpke, L.H., Morgan, J.P., Hort, M., Connolly, J.A.D., 2004. Serpentine and the subduction zone water cycle. Earth and Planetary Science Letters 223, 17-34.

Ranero, C.R., Morgan, J.P., McIntosh, K., Reichert, C., 2003. Bending-related faulting

and mantle serpentinization at the Middle America trench. Nature 425, 367-373.

Richter, F.M., Rowley, D.B., DePaolo, D.J., 1992. Sr isotope evolution of seawater: the role of tectonics. Earth and Planetary Science Letters 109, 11-23.

Ritter, J.R.R., Jordan, M., Christensen, U.R., Achauer, U., 2001. A mantle plume below the Eifel volcanic fields, Germany. Earth and Planetary Science Letters 186, 7-14.

Roberge, M., Bureau, H., Bolfan-Casanova, N., Frost, D.J., Raepsaet, C., Surble, S., Khodja, H., Auzende, A.-L., Fiquet, G., 2015. Is the transition zone a deep reservoir for fluorine? Earth and Planetary Science Letters 429, 25-32.

Roddick, J.C., 1983. High precision intercalibration of ^{40}Ar-^{39}Ar standards. Geochimica et Cosmochimica Acta 47, 887-898.

Rollinson, H.R., 1993. Using geochemical data: evaluation, presentation, interpretation. Longman Scientific & Technical.

Rudnick, R.L., Gao, S., 2014. Composition of the continental crust, in: Rudnick, R.L. (Ed.), The Crust, 2 ed, pp. 1-51.

Ruzié-Hamilton, L., Clay, P.L., Burgess, R., Joachim, B., Ballentine, C.J., Turner, G., 2016. Determination of halogen abundances in terrestrial and extraterrestrial samples by the analysis of noble gases produced by neutron irradiation. Chemical Geology 437, 77-87.

Ryan, W.B.F., Carbotte, S.M., Coplan, J.O., O'Hara, S., Melkonian, A., Arko, R., Weissel, R.A., Ferrini, V., Goodwillie, A., Nitsche, F., Bonczkowski, J., Zemsky, R., 2009. Global multi-resolution topography synthesis. Geochemistry, Geophysics, Geosystems 10, Q03014.

Saal, A.E., Hauri, E.H., Langmuir, C.H., Perfit, M.R., 2002. Vapour undersaturation in primitive mid-ocean-ridge basalt and the volatile content of Earth's upper mantle. Nature 419, 451-455.

Sadofsky, S.J., Portnyagin, M., Hoernle, K., van den Bogaard, P., 2008. Subduction cycling of volatiles and trace elements through the Central American volcanic arc: evidence from melt inclusions. Contributions to Mineralogy and Petrology 155, 433-456.

Sakuyama, M., Koyaguchi, T., 1984. Magma mixing in mantle xenolith-bearing calc-alkalic ejecta, Ichinomegata volcano, northeastern Japan. Journal of volcanology and geothermal research 22, 199-224.

Salters, V.J.M., Stracke, A., 2004. Composition of the depleted mantle. Geochemistry, Geophysics, Geosystems 5, Q05B07.

Sarda, P., Staudacher, T., Allègre, C.J., 1988. Neon isotopes in submarine basalts. Earth and Planetary Science Letters 91, 73-88.

Scarsi, P., 2000. Fractional extraction of helium by crushing of olivine and clinopyroxene phenocrysts: effects on the $^{3}He/^{4}He$ measured ratio. Geochimica et Cosmochimica Acta 64, 3751-3762.

Schilling, J.-G., Unni, C.K., Bender, M.L., 1978. Origin of chlorine and bromine in the oceans. Nature 273, 631-636.

Schmincke, H.-U., 2004. Volcanism. Springer Science & Business Media.

Shannon, R.D., Prewitt, C.T., 1969. Effective ionic radii in oxides and fluorides. Acta Crystallographica Section B: Structural Crystallography and Crystal Chemistry 25, 925-946.

Sharp, Z.D., Barnes, J.D., 2004. Water-soluble chlorides in massive seafloor serpentinites: a source of chloride in subduction zones. Earth and Planetary Science Letters 226, 243-254.

Shibata, K., Iwamoto, O., Nakagawa, T., Iwamoto, N., Ichihara, A., Kunieda, S., Chiba, S., Furutaka, K., Otuka, N., Ohasawa, T., 2011. JENDL-4.0: a new library for nuclear science and engineering. Journal of Nuclear Science and Technology 48, 1-30.

Shimizu, A., 2007. Noble gas geochemistry of the Izu-Ogasawara subduction system. Ph. D thesis of The University of Tokyo, Japan.

Shinonaga, T., Ebihara, M., Nakahara, H., Tomura, K., Heumann, K.G., 1994. Cl, Br and I in igneous standard rocks. Chemical Geology 115, 213-225.

Shirasaka, M., Arai, S., Ishimaru, S., Ishida, Y., Shimizu, Y., Morishita, T., 2004. The solution introduction ICP-MS technique to trace element analysis of rocks. Science Report of Kanazawa University 48, 43-71.

Singh, B., 1992. Nuclear data sheets update for A= 80. Nuclear Data Sheets 66, 623-703.

Snyder, G.T., Fehn, U., 2002. Origin of iodine in volcanic fluids: ^{129}I results from the Central American Volcanic Arc. Geochimica et Cosmochimica Acta 66, 3827-3838.

Snyder, G.T., Fehn, U., Goff, F., 2002. Iodine isotope ratios and halide concentrations in fluids of the Satsuma Iwojima volcano, Japan. Earth, Planets and Space 54, 265-274.

Spilliaert, N., Métrich, N., Allard, P., 2006. S–Cl–F degassing pattern of water-rich alkali basalt: Modelling and relationship with eruption styles on Mount Etna volcano. Earth and Planetary Science Letters 248, 772-786.

Stachel, T., Brey, G.P., Harris, J.W., 2005. Inclusions in sublithospheric diamonds: glimpses of deep Earth. Elements 1, 73-78.

Staudacher, T., Allègre, C.J., 1988. Recycling of oceanic crust and sediments: the noble gas subduction barrier. Earth and Planetary Science Letters 89, 173-183.

Staudacher, T., Kurz, M.D., Allègre, C.J., 1986. New noble-gas data on glass samples from Loihi Seamount and Hualalai and on dunite samples from Loihi and Reunion Island. Chemical geology 56, 193-205.

Steiger, R.H., Jäger, E., 1977. Subcommission on geochronology: Convention on use of decay constants in geochronology and cosmochronology. Earth and Planetary Science

Letters 36, 359-362.

Stern, R.J., Leybourne, M.I., Tsujimori, T., 2016. Kimberlites and the start of plate tectonics. Geology 44, 799-802.

Stosch, H.-G., Seck, H.A., 1980. Geochemistry and mineralogy of two spinel peridotite suites from Dreiser Weiher, West Germany. Geochimica et Cosmochimica Acta 44, 457-470.

Straub, S.M., Layne, G.D., 2003. The systematics of chlorine, fluorine, and water in Izu arc front volcanic rocks: Implications for volatile recycling in subduction zones. Geochimica et Cosmochimica Acta 67, 4179-4203.

Stuart, F., Turner, G., Taylor, R., 1994. He-Ar isotope systematics of fluid inclusions: resolving mantle and crustal contributions to hydrothermal fluids, in: Matsuda, J. (Ed.), Noble Gas Geochemistry and Cosmochemistry, pp. 261-277.

Sumino, H., 2001. Origin of alkaline basalt volcanism inferred from noble gas isotopic systematics: implications for mantle dynamics in back arc region of subduction zone. Ph. D thesis of The University of Tokyo, Japan.

Sumino, H., 2012. Subduction of volatiles into the Earth's mantle. Chikyukagaku (Geochemistry) 46, 149-170. (in Japanese with English abstract)

Sumino, H., 2015. History and current status of noble gas mass spectrometry to develop new idea based on study on the past. Journal of the Mass Spectrometry Society of Japan 63, 1-30. (in Japanese with English abstract)

Sumino, H., Ballentine, C.J., Burgess, R., Endo, S., Yoshida, K., Mizukami, T., Holland, G., Wallis, S.R., Hirajima, T., 2011. Slab-derived halogens and noble gases with a marine pore-fluid signature. Mineralogical Magagine 75, 163-172.

Sumino, H., Burgess, R., Mizukami, T., Wallis, S.R., Holland, G., Ballentine, C.J., 2010. Seawater-derived noble gases and halogens preserved in exhumed mantle wedge

peridotite. Earth and Planetary Science Letters 294, 163-172.

Sumino, H., Kaneoka, I., Matsufuji, K., Sobolev, A.V., 2006. Deep mantle origin of kimberlite magmas revealed by neon isotopes. Geophysical research letters 33, L16318.

Sumino, H., Kim, K.H., Kagi, H., Nagao, K., Notsu, K., 2004. Subduction-related metasomatic signature in noble gases in mantle derived xenoliths from Cheju Island, Korea. Geochimica et Cosmochimica Acta 68, A616.

Sumino, H., Nagao, K., Notsu, K., 2001. Highly sensitive and precise measurement of helium isotopes using a mass spectrometer with double collector system. Journal of the Mass Spectrometry Society of Japan 49, 61-68.

Sumino, H., Nakai, S.i., Nagao, K., Notsu, K., 2000. High $^{3}He/^{4}He$ ratio in xenoliths from Takashima: Evidence for plume type volcanism in southwestern Japan. Geophysical Research Letters 27, 1211-1214.

Sumino, H., Yamamoto, J., Kumagai, H., 2005. Noble gas studies of mantle-derived xenoliths: mantle metasomatism revealed by a noble gas isotopes—a review. Japanese Magazine of Mineralogical and Petrological Sciences 34, 173-185. (in Japanese with English abstract)

Svensen, H., Jamtveit, B., Banks, D.A., Austrheim, H., 2001. Halogen contents of eclogite facies fluid inclusions and minerals: Caledonides, western Norway. Journal of Metamorphic Geology 19, 165-178.

Takahashi, E., 1978. Petrologic model of the crust and upper mantle of the Japanese island arcs. Bulletin Volcanologique 41, 529-547.

Takahashi, E., 1980. Thermal history of iherzolite xenoliths—I. Petrology of lherzolite xenoliths from the Ichinomegata crater, Oga peninsula, northeast Japan. Geochimica et Cosmochimica Acta 44, 1643-1658.

Takahashi, E., 1986. Genesis of calc-alkali andesite magma in a hydrous mantle-crust

boundary: Petrology of lherzolite xenoliths from the Ichinomegata crater, Oga peninsula, northeast Japan, part II. Journal of Volcanology and Geothermal Research 29, 355-395.

Takazawa, E., Okayasu, T., Satoh, K., 2003. Geochemistry and origin of the basal lherzolites from the northern Oman ophiolite (northern Fizh block). Geochemistry, Geophysics, Geosystems 4, 1021.

Tanaka, T., Togashi, S., Kamioka, H., Amakawa, H., Kagami, H., Hamamoto, T., Yuhara, M., Orihashi, Y., Yoneda, S., Shimizu, H., Kunimaru, T., Takahashi, K., Yanagi, S., Nakano, T., Fujimaki, H., Shinjo, R., Asahara, Y., Tanimizu, M., Dragusanu, C., 2000. JNdi-1: a neodymium isotopic reference in consistency with LaJolla neodymium. Chemical Geology 168, 279-281.

Taran, Y.A., Hedenquist, J.W., Korzhinsky, M.A., Tkachenko, S.I., Shmulovich, K.I., 1995. Geochemistry of magmatic gases from Kudryavy volcano, Iturup, Kuril Islands. Geochimica et Cosmochimica Acta 59, 1749-1761.

Tatsumi, Y., 1989. Migration of fluid phases and genesis of basalt magmas in subduction zones. Journal of Geophysical Research 94, 4697-4707.

Tatsumi, Y., Sato, K., Sano, T., Arai, R., Prikhodko, V.S., 2000. Transition from arc to intraplate magmatism associated with backarc rifting: evolution of the Sikhote Alin volcanism. Geophysical research letters 27, 1587-1590.

Tatsumi, Y., Shukuno, H., Yoshikawa, M., Chang, Q., Sato, K., Lee, M.W., 2005. The petrology and geochemistry of volcanic rocks on Jeju Island: plume magmatism along the Asian continental margin. Journal of Petrology 46, 523-553.

Tomaru, H., Ohsawa, S., Amita, K., Lu, Z., Fehn, U., 2007. Influence of subduction zone settings on the origin of forearc fluids: Halogen concentrations and $^{129}I/I$ ratios in waters from Kyushu, Japan. Applied Geochemistry 22, 676-691.

Trieloff, M., Kunz, J., Clague, D.A., Harrison, D., Allègre, C.J., 2000. The nature of

pristine noble gases in mantle plumes. Science 288, 1036-1038.

Tsay, A., Zajacz, Z., Sanchez-Valle, C., 2014. Efficient mobilization and fractionation of rare-earth elements by aqueous fluids upon slab dehydration. Earth and Planetary Science Letters 398, 101-112.

Tsujimori, T., Sisson, V.B., Liou, J.G., Harlow, G.E., Sorensen, S.S., 2006. Very-low-temperature record of the subduction process: a review of worldwide lawsonite eclogites. Lithos 92, 609-624.

Turner, G., 1965. Extinct iodine 129 and trace elements in chondrites. Journal of Geophysical Research 70, 5433-5445.

Turner, G., Huneke, J.C., Podosek, F.A., Wasserburg, G.J., 1971. ^{40}Ar-^{39}Ar ages and cosmic ray exposure ages of Apollo 14 samples. Earth and Planetary Science Letters 12, 19-35.

Turner, S., Rushmer, T., Reagan, M., Moyen, J.-F., 2014. Heading down early on? Start of subduction on Earth. Geology 42, 139-142.

Uto, K., Takahashi, E., Nakamura, E., Kaneoka, I., 1994. Geochronology of alkali volcanism in Oki-Dogo Island, Southwest Japan: Geochemical evolution of basalts related to the opening of the Japan Sea. Geochemical Journal 28, 431-449.

van der Hilst, R.D., 1995. Complex morphology of subducted lithosphere in the mantle beneath the Tonga trench. Nature 374, 154-157.

van der Hilst, R.D., Widiyantoro, S., Engdahl, E.R., 1997. Evidence for deep mantle circulation from global tomography. Nature 386, 578-584.

van Keken, P.E., Hacker, B.R., Syracuse, E.M., Abers, G.A., 2011. Subduction factory: 4. Depth‐dependent flux of H_2O from subducting slabs worldwide. Journal of Geophysical Research 116, B01401.

Villemant, B., Mouatt, J., Michel, A., 2008. Andesitic magma degassing investigated through H_2O vapour–melt partitioning of halogens at Soufrière Hills Volcano, Montserrat (Lesser Antilles). Earth and Planetary Science Letters 269, 212-229.

Wada, I., Behn, M.D., Shaw, A.M., 2012. Effects of heterogeneous hydration in the incoming plate, slab rehydration, and mantle wedge hydration on slab-derived H_2O flux in subduction zones. Earth and Planetary Science Letters 353-354, 60-71.

Wade, J.A., Plank, T., Melson, W.G., Soto, G.J., Hauri, E.H., 2006. The volatile content of magmas from Arenal volcano, Costa Rica. Journal of Volcanology and Geothermal Research 157, 94-120.

Wallace, P.J., 2005. Volatiles in subduction zone magmas: concentrations and fluxes based on melt inclusion and volcanic gas data. Journal of Volcanology and Geothermal Research 140, 217-240.

Wedepohl, K.H., Gohn, E., Hartmann, G., 1994. Cenozoic alkali basaltic magmas of western Germany and their products of differentiation. Contributions to Mineralogy and Petrology 115, 253-278.

Wetherill, G.W., 1954. Variations in the isotopic abundances of neon and argon extracted from radioactive minerals. Physical Review 96, 679-683.

Wieler, R., 2002b. Cosmic-ray-produced noble gases in meteorites, in: Porcelli, D., Ballentine, C.J., Wieler, R. (Eds.), Noble Gases in Geochemistry and Cosmochemistry. Reviews in Mineralogy and geochemistry, pp. 125-170.

Wieler, R., 2002a. Noble gases in the solar system, in: Porcelli, D., Ballentine, C.J., Wieler, R. (Eds.), Noble Gases in Geochemistry and Cosmochemistry. Reviews in Mineralogy and Geochemistry, pp. 21-70.

Wilson, J.T., 1965. Evidence from ocean islands suggesting movement in the earth. Philosophical Transactions of the Royal Society of London A: Mathematical, Physical

and Engineering Sciences 258, 145-167.

Wilson, M., Patterson, R., 2001. Intraplate magmatism related to short-wavelength convective instabilities in the upper mantle: Evidence from the Tertiary-Quaternary volcanic province of western and central Europe. Special Papers-Geological Society of America, 37-58.

Wilson, S.A., 1997. Data compilation for USGS reference material BHVO-2, Hawaiian Basalt. U.S. Geological Survey Open-File Report.

Witt-Eickschen, G., Seck, H.A., Mezger, K., Eggins, S.M., Altherr, R., 2003. Lithospheric mantle evolution beneath the Eifel (Germany): Constraints from Sr–Nd–Pb isotopes and trace element abundances in spinel peridotite and pyroxenite xenoliths. Journal of Petrology 44, 1077-1095.

Woo, Y., Yang, K., Kil, Y., Yun, S.-H., Arai, S., 2014. Silica-and LREE-enriched spinel peridotite xenoliths from the Quaternary intraplate alkali basalt, Jeju Island, South Korea: Old subarc fragments? Lithos 208, 312-323.

Workman, R.K., Hart, S.R., 2005. Major and trace element composition of the depleted MORB mantle (DMM). Earth and Planetary Science Letters 231, 53-72.

Wu, S.C., 2001. Nuclear Data Sheets for A= 83. Nuclear Data Sheets 92, 893-1028.

Wysoczanski, R.J., Wright, I.C., Gamble, J.A., Hauri, E.H., Luhr, J.F., Eggins, S.M., Handler, M.R., 2006. Volatile contents of Kermadec Arc–Havre Trough pillow glasses: fingerprinting slab-derived aqueous fluids in the mantle sources of arc and back-arc lavas. Journal of Volcanology and Geothermal Research 152, 51-73.

Yamamoto, J., Ishibashi, H., Kawakami, Y., Kagi, H., 2005. Raman spectroscopic geobarometer applicable to mantle xenolith. Japanese Magazine of Mineralogical and Petrological Sciences 34, 159-172. (in Japanese with English abstract)

Yamamoto, J., Kagi, H., 2006. Extended micro-Raman densimeter for CO_2 applicable to

mantle-originated fluid inclusions. Chemistry Letters 35, 610-611.

Yamamoto, J., Kagi, H., Kaneoka, I., Lai, Y., Prikhod'ko, V.S., Arai, S., 2002. Fossil pressures of fluid inclusions in mantle xenoliths exhibiting rheology of mantle minerals: implications for the geobarometry of mantle minerals using micro-Raman spectroscopy. Earth and Planetary Science Letters 198, 511-519.

Yamamoto, J., Kagi, H., Kawakami, Y., Hirano, N., Nakamura, M., 2007. Paleo-Moho depth determined from the pressure of CO_2 fluid inclusions: Raman spectroscopic barometry of mantle-and crust-derived rocks. Earth and Planetary Science Letters 253, 369-377.

Yamamoto, J., Kaneoka, I., Nakai, S.i., Kagi, H., Prikhod'ko, V.S., Arai, S., 2004. Evidence for subduction-related components in the subcontinental mantle from low $^{3}He/^{4}He$ and $^{40}Ar/^{36}Ar$ ratio in mantle xenoliths from Far Eastern Russia. Chemical Geology 207, 237-259.

Yamamoto, J., Nakai, S.i., Nishimura, K., Kaneoka, I., Kagi, H., Sato, K., Okumura, T., Prikhod'ko, V.S., Arai, S., 2009a. Intergranular trace elements in mantle xenoliths from Russian Far East: Example for mantle metasomatism by hydrous melt. Island Arc 18, 225-241.

Yamamoto, J., Nishimura, K., Sugimoto, T., Takemura, K., Takahata, N., Sano, Y., 2009b. Diffusive fractionation of noble gases in mantle with magma channels: origin of low He/Ar in mantle-derived rocks. Earth and Planetary Science Letters 280, 167-174.

Yamamoto, M., Kagami, H., Narita, A., Maruyama, T., Kondo, A., Abe, S., Takeda, R., 2013. Sr and Nd isotopic compositions of mafic xenoliths and volcanic rocks from the Oga Peninsula, Northeast Japan Arc: Genetic relationship between lower crust and arc magmas. Lithos 162, 88-106.

Yardley, B.W.D., 1997. The evolution of fluids through the metamorphic cycle, in: Jamtveit, B., Yardley, B.W.D. (Eds.), Fluid flow and transport in rocks. Springer, pp. 99-

121.

Yatsevich, I., Honda, M., 1997. Production of nucleogenic neon in the Earth from natural radioactive decay. Journal of Geophysical Research: Solid Earth (1978–2012) 102, 10291-10298.

Yokochi, R., Marty, B., Pik, R., Burnard, P., 2005. High $^{3}He/^{4}He$ ratios in peridotite xenoliths from SW Japan revisited: evidence for cosmogenic ^{3}He released by vacuum crushing. Geochemistry, Geophysics, Geosystems 6, Q01004.

Yoo, H.J., Herrmann, R.B., Cho, K.H., Lee, K., 2007. Imaging the three-dimensional crust of the Korean Peninsula by joint inversion of surface-wave dispersion and teleseismic receiver functions. Bulletin of the Seismological Society of America 97, 1002-1011.

Yoshida, K., Hirajima, T., 2012. Annular fluid inclusions from a quartz vein intercalated with metapelites from the Besshi area of the Sanbagawa belt, SW Japan. Journal of Mineralogical and Petrological Sciences 107, 50-55.

Yoshida, M., Takahashi, K., Yonehara, N., Ozawa, T., Iwasaki, I., 1971. The fluorine, chlorine, bromine, and iodine contents of volcanic rocks in Japan. Bulletin of the Chemical Society of Japan 44, 1844-1850.

Yoshikawa, M., Tamura, A., Arai, S., Kawamoto, T., Payot, B.D., Rivera, D.J., Bariso, E.B., Mirabueno, M.H.T., Okuno, M., Kobayashi, T., 2016. Aqueous fluids and sedimentary melts as agents for mantle wedge metasomatism, as inferred from peridotite xenoliths at Pinatubo and Iraya volcanoes, Luzon arc, Philippines. Lithos 262, 355-368.

Zhao, D., Hasegawa, A., 1993. P wave tomographic imaging of the crust and upper mantle beneath the Japan Islands. Journal of Geophysical Research: Solid Earth 98, 4333-4353.

Zhao, D., Horiuchi, S., Hasegawa, A., 1992. Seismic velocity structure of the crust beneath the Japan Islands. Tectonophysics 212, 289-301.

Appendix A. Density of CO_2 fluid inclusions and the depth origin of mantle xenoliths

本章については、５年以内に雑誌等で刊行予定のため、非公開。

This chapter is not published because it is scheduled to be published in journals or other publications within five years.

Appendix B. EPMA data of cpx separates from the Ichinomegata mantle xenoliths

本章については、５年以内に雑誌等で刊行予定のため、非公開。

This chapter is not published because it is scheduled to be published in journals or other publications within five years.

Appendix C. Trace element data of cpx separates from the Ichinomegata mantle xenoliths

本章については、５年以内に雑誌等で刊行予定のため、非公開。

This chapter is not published because it is scheduled to be published in journals or other publications within five years.